OPTIMUM FLOWSHEET SYNTHESIS FOR THE INTEGRATED GASIFICATION COMBINED CYCLE USING MATHEMATICAL MODELLING

Jude Kwaku Bonsu (1562787)

A thesis submitted in fulfilment of the requirements for the degree

Of

Doctor of Philosophy (Chemical Engineering)

Submitted to
School of Chemical and Metallurgical Engineering, Faculty of Engineering and the Built Environment, University of Witwatersrand, Johannesburg, South Africa.

DECLARATION

I declare that this thesis is my unaided work. It is being submitted for Doctor of Philosophy in Chemical Engineering to the University of the Witwatersrand, Johannesburg. It has not been submitted before for any other degree or examination in any other University.

……

Jude Kwaku Bonsu

On the 25th day of October 2021 at Johannesburg

ACKNOWLEDGEMENTS

I wish to express my gratitude to my supervisor Prof. T. Majozi for his support throughout this study. I would also like to sincerely thank the National Research Foundation (NRF) of South Africa for funding this project.

My special love goes to my father, Reverend O. Mensah-Bonsu and my mother, Mrs Katherine Bonsu. I could not have gone through this journey without you. To my siblings, Rachel Osaa-Bonsu, Obed Nana Osei-Tutu Bonsu, Jerome Antwi-Boasiako and Gladys Mensah-Bonsu, thank you for your support and prayers.

Finally, to my colleagues in the Sustainable Process Engineering research group, for the teamwork and making the environment conducive throughout the research period.

SUMMARY

The Integrated Gasification Combined Cycle (IGCC) is one of the most promising coal-based electrical power-producing technologies. The gas-side of the IGCC plays an important role in the efficiency of the process. This is because the gas turbine generates 60% of the gross power produced, while the air separation unit is the highest consumer of power in the IGCC plant. The gasifier is also responsible for the generation of the fuel-gas, which is the main source of energy for the combined cycle. Hence, optimizing the gas-side of the IGCC will lead to an improvement in the efficiency of the entire plant. Consequently, this work focused on the optimal flowsheet synthesis of the gas-side of the IGCC process.

The first step in achieving this included developing a novel optimization technique for the synthesis and design of an optimal entrained flow gasifier. The developed technique was then applied to three examples taken from literature. The first example studied was the optimal synthesis and design of a dry, nitrogen-fed entrained flow gasifier. The objective function for this example was the maximization of the cold gas efficiency of the gasifier. In this example, an improvement of 6% in the objective function relative to the base case was achieved. The optimal gasifier design for this example was a continuous stirred tank reactor followed by a plug flow reactor. Other findings included higher steam to coal ratio but a lower oxygen to coal ratio relative to the base case. The results also showed that although all the oxygen enters the reactor network through the first reactor, part of the total steam fed enters through the second reactor.

The second example under this section was the synthesis and design of a dry, carbon dioxide-fed entrained flow gasifier. The objective function for this example was the maximization of the higher heating value of the produced fuel-gas. The optimal solution for this example led to an improvement of 6.2% in the objective function relative to the base case. The optimal gasifier design was a plug flow reactor with a side stream. For this example, the optimal feeding

condition had higher steam to coal ratio but a lower oxygen to steam ratio relative to the base case.

The final example under this section was the synthesis and design of a slurry-fed entrained flow gasifier. The objective function for this example was the lower heating value of the fuel-gas product. The results showed an increase of 13.3% of the objective function relative to the base case. The optimal gasifier design was a plug flow reactor with a side stream followed by a continuous stirred tank reactor. The oxygen to coal ratio for the optimal design was lower than that of the base case. It was observed that the optimal feed distribution was 70% of the coal fed at the entrance of the plug flow reactor and the remaining 30% fed as a side stream.

The second step in this study involved the synthesis of an optimal flowsheet of the gas-side of the IGCC process. This was achieved by integrating the developed gasifier model into an IGCC framework. The developed model was applied to two examples. Example 1 was an IGCC plant with a dry-fed entrained flow gasifier. Example 2 was an IGCC plant with a slurry-fed entrained flow gasifier. Three scenarios were explored in each example. The base case or scenario 1 for each example is the simulation of a standard IGCC plant. The second scenario is the synthesis and design of an optimal gasifier with a background IGCC process. The decision variables in scenario 2 were the gasifier volume, reactor configuration, steam to coal ratio and the oxygen to coal ratio. The third scenario is the determination of the optimal flowsheet path for the IGCC process. In addition to the decision variables in scenario 2, scenario 3 also determined the optimal integration between the air separation unit and the gas turbine. In each of these examples, scenarios 2 and 3 were compared to the base case. The objective function of both examples was the thermal efficiency of the IGCC plant.

In example 1, an improvement of 6.79% and 10.96% in the objective function relative to the base case was achieved for scenario 2 and scenario 3 respectively. For both scenarios, the

optimal gasifier design was a CSTR followed by a PFR. This agreed with the results from the optimization of the standalone gasifier in the first step. Both scenarios also had higher steam to coal ratio relative to the base case, which agreed with results in the first step. However, the optimal oxygen to coal ratio for both scenarios were high relative to the base case. This deviated from the results in the first step.

In example 2, an improvement of 11% and 15.8% in the objective function relative to the base case was achieved for scenarios 2 and 3 respectively. For both scenarios, the optimal gasifier is a plug flow reactor with a side stream. The optimal oxygen to coal ratios for both scenarios were higher relative to the base case, which was different from the optimization of the standalone gasifier.

This study shows that a superstructure optimization technique is an effective tool for the design of standalone gasifiers and the synthesis of the optimal flowsheet of an IGCC plant. The differences in the optimal oxygen flowrates for the gasifier either as standalone or as part of an IGCC plant show the need for the simultaneous optimization of multiple units in a process instead of sequential optimization.

TABLE OF CONTENTS

LIST OF TABLES

LIST OF FIGURES

NOMENCLATURE

A. Reactor superstructure

i. Sets

m =Chemical reactions

n', n =Reactor compartments

i =set of chemical components

j =set of chemical reactions

d =heterogeneous reactions

ii. Continuous Variables

F_n^{in}	Mass flowrate of the total feed into a reactor compartment *n*	kg/s
f_n^{Coal}	Mass flowrate of the coal feed into a reactor compartment *n*	kg/s
$f_n^{O_2}$	Mass flowrate of the oxygen feed into a reactor compartment *n*	kg/s
$f_n^{H_2O}$	Mass flowrate of the steam feed into a reactor compartment *n*	kg/s
$f_{n',n}^{R,in}$	Mass flowrate from other compartments into compartment *n*	kg/s
F_n^{Out}	Mass flowrate of the product out of a reactor compartment *n*	kg/s
$f_n^{P,out}$	Mass flowrate of the stream from reactor compartment *n* to the final product	kg/s
$f_{n,n'}^{R,\mathrm{Out}}$	Mass flowrate of the stream from reactor compartment *n* to other reactor compartments	kg/s
$f_{solid,CSTR}^{In}$	Mass flowrate of a solid stream into a CSTR	kg/s
$f_{solid,CSTR}^{Out}$	Mass flowrate of the solid stream out of a CSTR	kg/s
$f_{gas,CSTR}^{Out}$	Mass flowrate of the gas stream out of a CSTR	kg/s
$f_{gas,CSTR}^{In}$	Mass flowrate of the gas stream into a CSTR	kg/s
$f_{i,CSTR}^{out}$	Mass flowrate of a chemical species *i* into a CSTR	kg/s
$f_{i,CSTR}^{in}$	Mass flowrate of a chemical species *i* into a CSTR	kg/s
$f_{i,PFR}$	Mass flowrate of component i into the PFR	kg/s
F^P	Mass flowrate of the total fuel-gas product	kg/s
w_{char}^{Pyro}	Mass fraction of the char in the pyrolysis product	kg/kg
w_i^{Pyro}	Mass fraction of pyrolysis product component *i*	kg/kg
$w_{F,i,n}^{In}$	Mass fraction of feed component *i* into a reactor compartment *n*	kg/kg
w_{Gas}^{Pyro}	Mass fraction of the gas in the pyrolysis product	kg/kg

$w_{CSTR,i,n}^{In}$	Mass fraction of feed component *i* into the CSTR of reactor compartment *n*	kg/kg
$w_{PFR,i,n}^{In}$	Mass fraction of feed component *i* into the PFR of reactor compartment *n*	kg/kg
$w_{F,i,n}^{Out}$	Mass fraction of product component *i* leaving reactor compartment *n*	kg/kg
$w_{i,n}^{P,Out}$	Mass fraction of component *i* in the stream moving from reactor compartment *n* to the final product	kg/kg
$w_{i,n.,n'}^{R,Out}$	Mass fraction of component *i* in the stream moving from reactor compartment *n* to other reactor compartments	kg/kg
$w_{CSTR,i,n}^{Out}$	Mass fraction of product component *i* out of the CSTR of reactor compartment *n*	kg/kg
$w_{PFR,i,n}^{Out}$	Mass fraction of product component *i* out of the PFR of reactor compartment *n*	kg/kg
w_i^P	Mass fraction of fuel-gas product component *i*	kg/kg
ξ	Normalized volume	m^3/m^3
V_R	The volume of a CSTR or PFR	m^3
r_j	Rate of reaction *j*	$kmol/m^3s$
X_{Char}	Conversion of char	kg/kg
r_d	Rate of heterogeneous reaction *d*	$kmol/m^3s$
k_d	The reaction rate constant for heterogeneous reaction *d*	Pa^{δ}
C_{Char}	Concentration of char	$kmol/m^3$
P_d	The partial pressure of gasification agent in heterogeneous reaction *d*	Pa
T	Gasifier temperature	K
H^{Out}	Rate of enthalpy flow out of a reactor	J/s
H^{In}	Rate of enthalpy flow into a reactor	J/s
$h_{gas,CSTR}^{Out}$	Specific enthalpy of the gaseous stream out of a CSTR	J/kg
$h_{gas,CSTR}^{In}$	Specific enthalpy of the gaseous stream into a CSTR	J/kg
β_{H_2O}	Steam to coal ratio	kg/kg
β_{O_2}	Oxygen to coal ratio	kg/kg
θ^{Coal}	Coal split ratio	kg/kg

iii. Binary variables

$y_{CSTR,n}$	Binary variable for the existence of a CSTR in reactor compartment *n*
$y_{PFR,n}$	Binary variable for the existence of a PFR in reactor compartment *n*

iii. Parameters

F^{Coal}	The mass flowrate of coal	kg/s
w_{VM}^{Coal}	Mass fraction of the volatile matter in the coal feed	kg/kg
w_{e}^{Coal}	Mass fraction of the element e in the coal feed	kg/kg
$P_{Gasifier}$	Gasification pressure	Pa or Bar
Mw_i	The molecular weight of chemical component *i*	kg/kmol
v_{ij}	Stoichiometric coefficient of chemical component *i* in reaction *j*	
ψ_d	Particle pore structural diameter of heterogeneous reaction *d*	
δ_d	Order of heterogeneous reaction *d*	
Q_{Loss}	Heat loss in a reactor	J/s
HHV^{Coal}	The higher heating value of coal	J/kg
HHV_i	Higher of the heating value of chemical component *i*	J/kg
R	Ideal gas constant	J/molK
Ea	Activation energy	J/mol
Δh_j^{rxn}	Enthalpy of reaction *j*	J/mol

iv. Abbreviations

ROM	Reduced Order Modelling
CGE	Cold Gas Efficiency
EFG	Entrained flow gasifier
PFR	Plug flow reactor
CSTR	Continuous stirred tank reactor
U	Upper bound

B. IGCC superstructure

i. Sets

m =Chemical reactions occurring in the combustion chamber of the gas turbine

h =Hot streams

c =Cold streams

t =Steam turbines

b =compressors

p =pumps

ii. Continuous Variables

F_{Air}^{ASU}	The flowrate of air into the ASU	kmol/s or kg/s
$F^{O_2,rich}$	The flowrate of oxygen-rich stream	kmol/s or kg/s
$F^{N_2,rich}$	Flowrate of nitrogen-rich stream	kmol/s or kg/s
F_{Air}^{MAC}	The flowrate of air supplied by the main air compressor	kmol/s or kg/s
F_{Air}^{GT-ASU}	The flowrate of air supplied by the compressor of the gas turbine	kmol/s or kg/s
$F_{Gasifier}^{N_2}$	The flowrate of nitrogen supplied to the gasifier	kmol/s or kg/s
$F_{GT}^{N_2}$	The flowrate of nitrogen supplied to the gas turbine	kmol/s or kg/s
$F_{Waste}^{N_2}$	The flowrate of waste nitrogen stream	kmol/s or kg/s
F_{FG}	The flowrate of the fuel gas into the gas turbine	kmol/s or kg/s
F_{Comp}	The flowrate of the feed into a compressor	kmol/s or kg/s
F_{Air}^{CC}	The flowrate of air into the combustion chamber	kmol/s or kg/s
F_H	The flowrate of hot streams into a HEN	kmol/s or kg/s
F_C	The flowrate of cold streams into a HEN	kmol/s or kg/s
F_{CE}	Flowrate out of the stream out of the combustion chamber of the gas turbine	kmol/s or kg/s
F_{BFW}	The flowrate of the boiler feedwater	kmol/s or kg/s
F_{Comp}	The flowrate of the feed into a compressor	kmol/s or kg/s
$\dot{W}_{Isen,Comp}$	Isentropic work input of a compressor	J/s
$\dot{W}_{Isen,Exp}$	Isentropic work output by the expander of the gas turbine	J/s
$\dot{W}_{Actual,Comp}$	Actual work input of the compressor	J/s
$\dot{W}_{Actual,Exp}$	Actual work output by the expander of the gas turbine	J/s
$\dot{W}_{Isen,ST}$	The isentropic work output of a steam turbine	J/s
$\dot{W}_{Actual,ST}$	The actual work output of a steam turbine	J/s
$\in_m$	Extent of reaction	kmol/s
$\dot{W}_{Isen,ST}$	The isentropic work output of a steam turbine	J/s
$\dot{W}_{Actual,ST}$	The actual work output of a steam turbine	J/s
$\in_m$	Extent of reaction	kmol/s
T_{Comb}	Temperature of the exhaust stream leaving the combustion chamber of the gas turbine	K
$T_{Out,Exp}$	The actual temperature of a stream leaving an expander	K
$T_{Out,Isen}$	The isentropic temperature of a stream leaving an expander	K
h_{Out}	Specific enthalpy of steam exiting a steam turbine	J/kg
h_{In}	Specific enthalpy of the steam entering a steam turbine	J/kg
θ_{N_2}	Nitrogen split ratio	kmol/kmol
$\theta_{Air,ASU}$	Air split ratio	kmol/kmol

$\dot{V}_p$	Volumetric flowrate of boiler feed water through pump, *p*	m^3/s
h_{Out}	Specific enthalpy of steam exiting a steam turbine	J/kg
h_{Air}	Specific enthalpy of air entering the gas turbine	J/kg
h_{FG}	Specific enthalpy of the fuel-gas stream entering the gas turbine	J/kg
h_{N_2}	Specific enthalpy of the nitrogen stream entering the gas turbine	J/kg
S_{In}	Specific entropy of steam entering turbine, *t*	J/kgK
S_{Out}	Specific entropy of steam leaving a turbine, *t*	J/kgK
x_{In}	Quality of steam entering turbine, *t*	kg/kg
x_{In}	Quality of steam leaving a turbine, *t*	kg/kg

iii. Parameters

$Y_{Air,i}$	Composition of air	kmol/kmol
$w_{H_2O,Slurry}$	Weight fraction of water in a coal slurry	kg/kg
P_{Out}	The pressure of a stream entering a compressor or turbine	Pascal or Bar
P_{In}	The pressure of air stream exiting c the MAC	Pascal or Bar
Cp_{CE}	Specific heat capacity of exhaust gas from the expander	J/molK
T_{Evap}^{App}	Approach temperature	K
T_{Evap}^{Sat}	Saturation temperature of the evaporator	K
$\eta_{Isen,b}$	Isentropic efficiency of compressor *b*	
$\eta_{Isen,t}$	Isentropic efficiency of steam turbine *t*	
$\eta_{Isen,\mathrm{Exp}}$	Isentropic efficiency of the gas turbine expander	
η_p^{Pump}	Efficiency of water pump	
ΔT_{Pinch}	Pinch temperature of evaporators	K
Cp_{CE}	Specific heat capacity of exhaust gas from the expander	J/molK
P_{Column}	The pressure of the ASU column	Pascal or Bar

iv. Abbreviations

ASU	Air separation unit
MAC	Main air compressor
CC	Combustion chamber
ST	Steam turbine

ASU	Air separation unit
MAC	Main air compressor
CC	Combustion chamber
HP	High pressure
IP	Intermediate pressure
LP	Low pressure
WH	Water heater
Pyro	Pyrolysis
Comp	Compressor
Exp	Expander
Cond	Condenser
Econ	Economiser
Evap	Evaporator
Sat	Saturated
LHV	Low Heating Value
CS	Compression stages

1. INTRODUCTION

1.1 Background

Access to modern energy has a close relationship with human development due to its effect on national productivities, quality healthcare, quality education, production of safe drinking water, agriculture, and modern communication services (Pîrlogea, 2012; Gaye, 2008). Figure 1.1 is a chart showing the total global primary energy supply. From Figure 1.1, it is observed that there has been a steady increase in the global consumption of energy. This could be due to countries striving to provide better lives for their citizens.

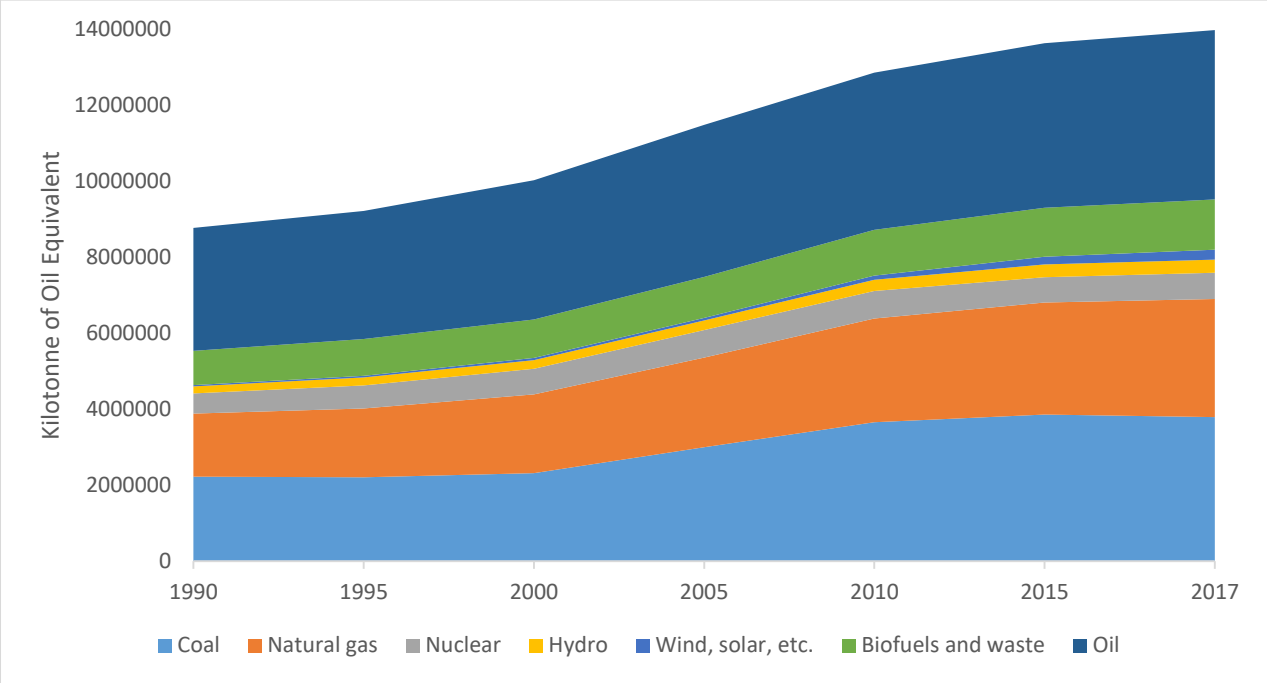

Figure 1.1. Total global primary energy supply (Data from IEA, 2019)

Although there has been a steady increase in energy consumption, there are wide variations in consumption levels between industrialised countries and developing countries. Figure 1.2 shows that the global energy consumption in the year 2017 for North America is about 10 times that of Africa. For developing countries to achieve their developmental goals, they must have access to reliable and affordable energy.

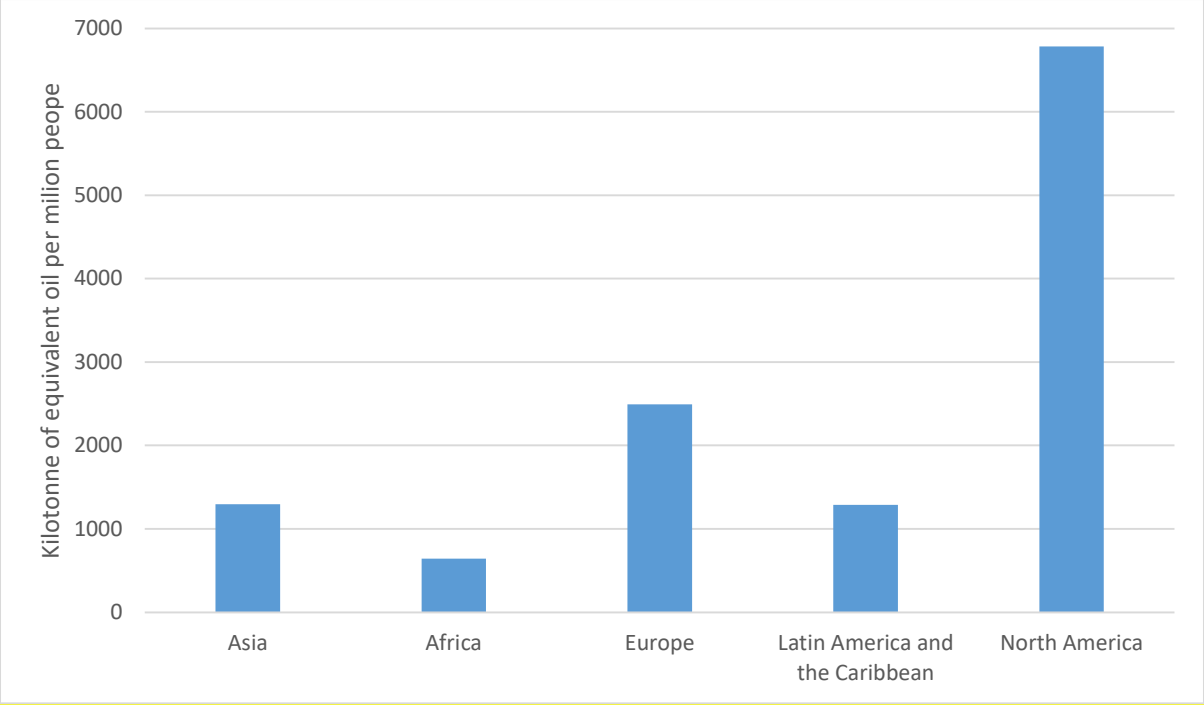

Figure 1.2. Per capita energy consumption for select regions, 2017 (Data from Enerdata, 2021)

Electricity is the most useful form of energy in the modern world. Thus, efficient conversion of primary energy sources to electricity is critical for human civilization (Majoumerd et al., 2012). Coal is one of the most widely used fossil fuels for electricity generation. Figure 1.3 shows that coal is used to generate approximately 40% of the world's electricity. However, the environmental impact of coal combustion for electrical power generation is significant. The combustion process produces a range of pollutants such as nitrous oxides, sulphur oxides, fly ash, and heavy metals. In addition to the pollutants above, coal combustion is also a significant contributor to climate change. Coal combustion contributes to over a third of global carbon dioxide production (see Figure 1.4). Another challenge posed by coal combustion for electricity generation is that the process requires a large amount of water input thereby stressing global water resources.

Notwithstanding the enumerated challenges associated with coal use, it will continue to play an essential role in meeting energy demands. This is because coal has a high reserves-to-

production ratio; it is a geographically distributed natural resource and a relatively inexpensive fuel compared to other fossil fuels (Higman and van der Burgt, 2003). Hence, there is a need for research into cleaner and more efficient ways of generating electricity from coal.

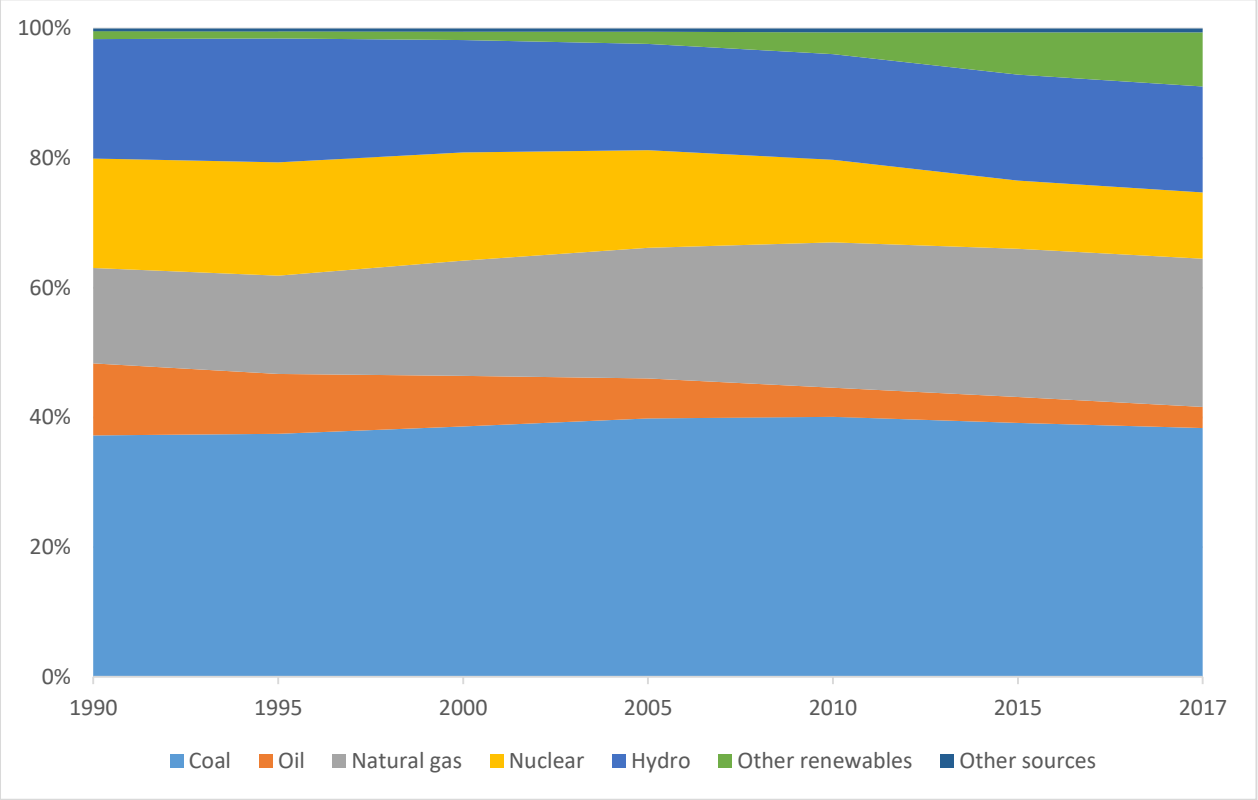

Figure 1.3. Global electricity generation by source (Data from IEA, 2019)

The Integrated Gasification Combined Cycle (IGCC) plant is an alternative way of generating electricity from coal. The technology combines two technologies, which are gasification and the combined cycle. IGCC power plants have several advantages over conventional coal-fired power plants. Major advantages of the IGCC over competing technologies include higher thermal efficiency, low pollutant emission, less water consumption, and less solid-waste generation (Ratafia-Brown, 2002; NETL, 2010). Figure 1.5 shows that IGCC plants have lower nitrous oxides (NO_x), sulphur dioxide (SO_2) and particulate matter (PM) emissions relative to pulverised coal (PC) power plants. Figure 1.6 shows the water consumption for different coal-based thermal power-producing plants and a natural gas combined cycle (NGCC) plant. Figure

1.6 also shows that the different IGCC plants, i.e. E-Gas, Shell and GE, have a lower water consumption per megawatts hours of electricity compared to sub and super-critical PC plants.

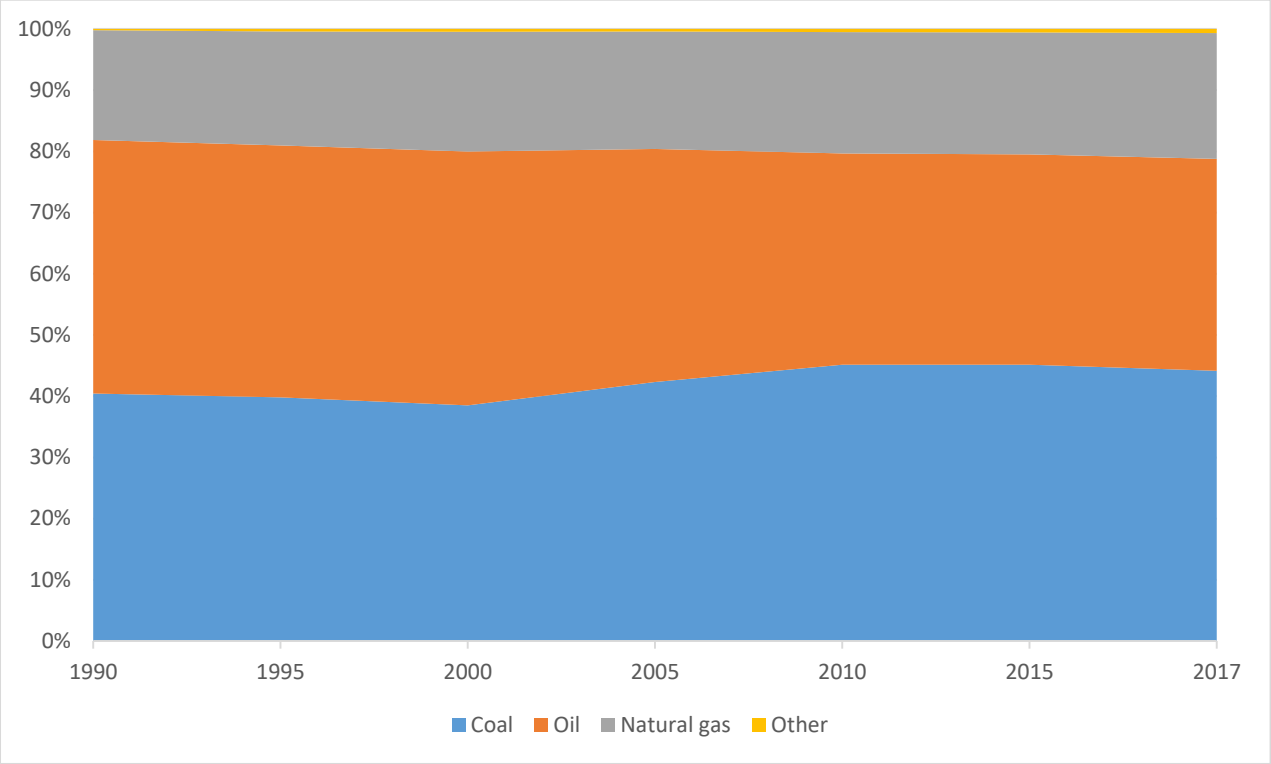

Figure 1.4. Global carbon dioxide emissions by energy source (Data from IEA, 2019)

Another advantage of IGCC over conventional power plants is its ability to mitigate global warming. This is due to the possibility of pre-combustion carbon capture in IGCC plants, which is made possible by converting the carbon monoxide in the fuel-gas to carbon dioxide and hydrogen through the water-gas shift reaction. Majoumerd et al. (2012) reported that pre-combustion carbon capture is an easier process compared to the post-combustion carbon capture possible in conventional coal power plants. This is because the small fraction of carbon dioxide in the flue gas after combustion, which is mixed with atmospheric nitrogen, is difficult to capture compared to the high fraction of carbon dioxide in the gaseous stream after the water-gas shift reactor.

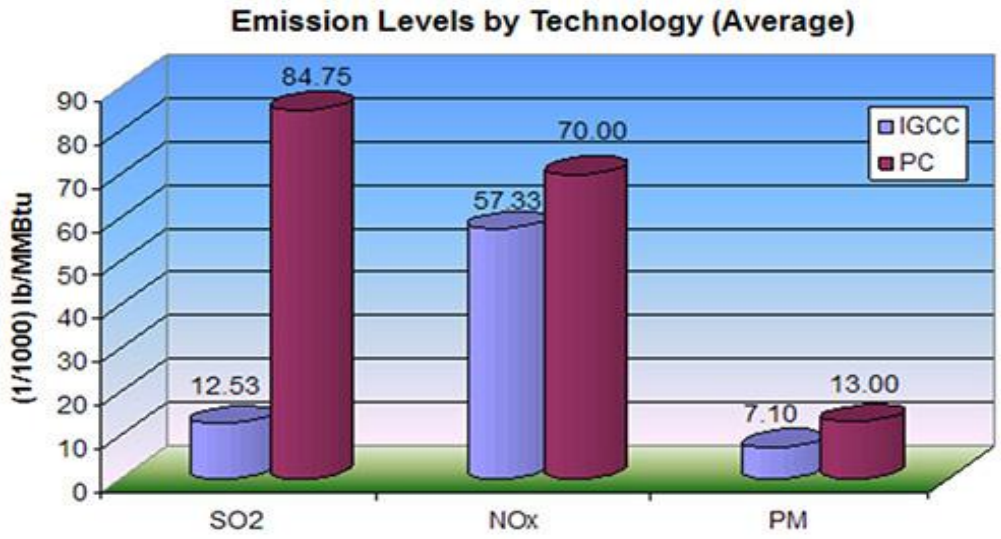

Figure 1.5. Average emissions comparison between IGCC and pulverized coal (NETL,2010).

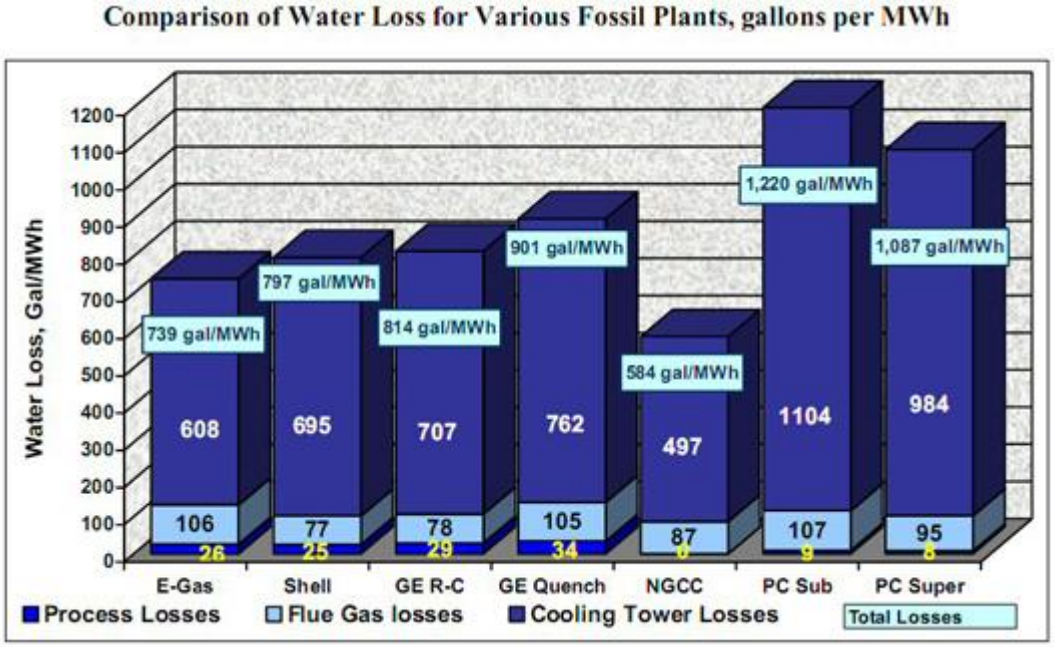

Figure 1.6. Comparison of water loss for various fossil plants, gallons per MWh (Klett et al.,2005)

The IGCC technology is still undergoing full commercialization, and further improvement of its efficiency will expedite the commercialization process. The efficiency of the IGCC process depends mainly on the performance of its components; hence, optimizing these units will increase the thermal efficiency of the entire process. The major units of the IGCC process include the gasifier, a gas-cleaning unit (GCU), the heat recovery steam generator (HRSG), a

cryogenic air separation unit (ASU), a gas turbine and a steam turbine. The gasifier, CGU, ASU and gas turbine together forms the gas side of the IGCC (Jiang et al., 2002). The gas-side of the IGCC plays an important role in the efficiency of the process. This is because the gas turbine generates 60% of the gross power produced, while the ASU is the highest consumer of power in the IGCC plant (Majoumerd et al., 2012). The gasifier is also responsible for the generation of the fuel-gas, which is the main source of energy for the combined cycle. Hence, optimizing the gas-side of the IGCC will improve the efficiency of the entire plant.

Figure 1.7 shows a common approach in optimising the gas-side of the IGCC, which is the feeding of part of the nitrogen product from the ASU to the gas turbine, and the extraction of air from the gas turbine into the ASU. Several studies have explored the interconnectivity between these units using sensitivity analysis (Anand et al., 1996; Frey and Zhu, 2006; Lee et al., 2007) and nonlinear programming (Wang et al., 2016).

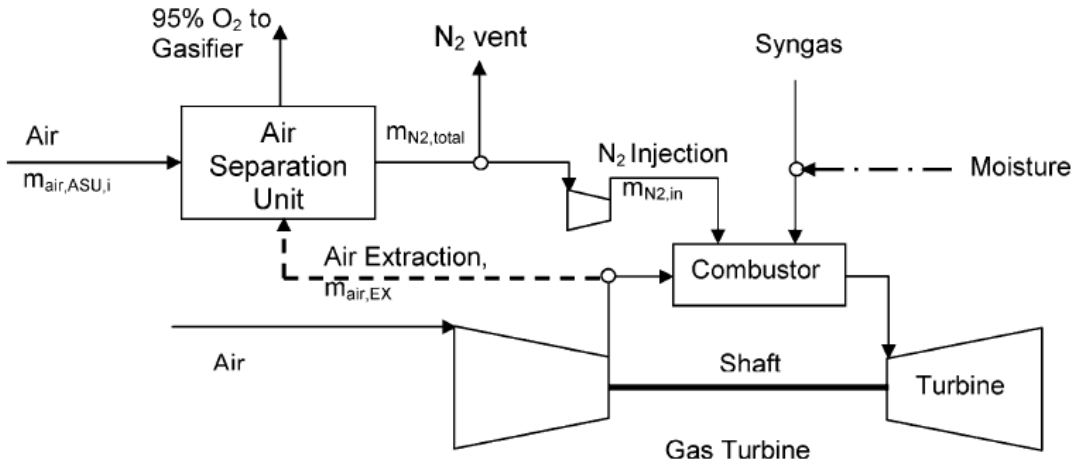

Figure 1.7. Conceptual diagram of integration of the air separation unit and gas turbine (Frey and Zhu, 2006)

What these studies have excluded is the effect of gasifier optimization on the flowsheet of the gas-side of the IGCC. Hence, this study focuses on exploring the effect of gasifier optimization on the gas side of the IGCC plant and the overall efficiency of the plant.

Although there are different gasification technologies (see Table 1.1), the entrained flow gasifier (EFG) has several advantages over other gasifiers due to its ability to handle various types of coal, its high carbon conversion, high throughput capacity and high-quality of fuel-gas

Table 1.1. Types of gasification technology (Higman and van der Burgt, 2003)

Gasifier type	**Fixed bed**	**Fluidized bed**	**Entrained flow**
Outlet temperature	Low (425 -600^{o}C)	Moderate (900 -1050^{o}C)	High (1250 -1600^{o}C)
Operating pressure	1-27 Atm	1-68 Atm	1-82 Atm
Oxidant demand	Low	Moderate	High
Steam demand	High	Moderate	Low
Ash conditions	Dry ash or slagging	Dry ash or agglomerating	Slagging
Size of coal feed	6-50 mm	6-10 mm	<100μm
Tolerance of fines	Limited	Good	Unlimited
Applications	Synfuel, chemicals	IGCC, chemicals	IGCC, synfuel and chemicals

Approximately 75% of existing and planned IGCC plants worldwide use EFG technology (Minchener, 2005). Hence, this study focuses on the synthesis and design of an EFG with a background IGCC process. The decision variables of interest in this study include the feed conditions of the gasifier, the configuration of the gasifier and the degree of integration between the gas turbine and the ASU. This will lead to the synthesis of the optimal flowsheet for the gas-side of the IGCC process.

1.2 Motivation

The first motivation is the need to develop an optimal gasifier synthesis method. Gasification is a critical process in many technologies. These include IGCC plants; transportation fuel production and other chemical industries such as ammonia production plants. However, there are few studies aimed at the scientific optimization of gasification technology. Some studies have used sensitivity analysis to assess the effect of the amount of oxygen and steam on the cold gas efficiency of the EFG (Lee et al., 2010; Ju and Lee, 2017). There has also been limited use of non-linear programming to optimize an EFG (Lang et al., 2011; Mvelase, 2016). These studies focused on the effect of feed conditions on the performance of a gasifier. Limiting the decision variables to gasifier input conditions places a constraint on the extent of the improvement that can be achieved. Figure 1.8 shows the heating value for the syngas produced by various EFG designs for mostly bituminous coal feed. The observed differences may be due to the variation in the design of these EFGs. However, there has not been an attempt to scientifically determine the best design for an EFG. Hence, this study uses a detailed reactor synthesis technique in the design and synthesis of an EFG.

The second motivation behind this study is the need to investigate the effect of EFG optimization on the overall IGCC process efficiency. There have been many studies focusing on the effect of other units on the IGCC process efficiency (Jiang et al., 2002; Frey and Zhu, 2006; Lee et al., 2007). There has also been the study of the effect of gasifier feeding conditions on the performance of the IGCC (Emun et al., 2010; Lang et al., 2011). However, there has not been any study that comprehensively assesses the effect of EFG design on the efficiency of the IGCC process. Hence, this study investigated the effect of EFG synthesis and design on the efficiency of the IGCC process.

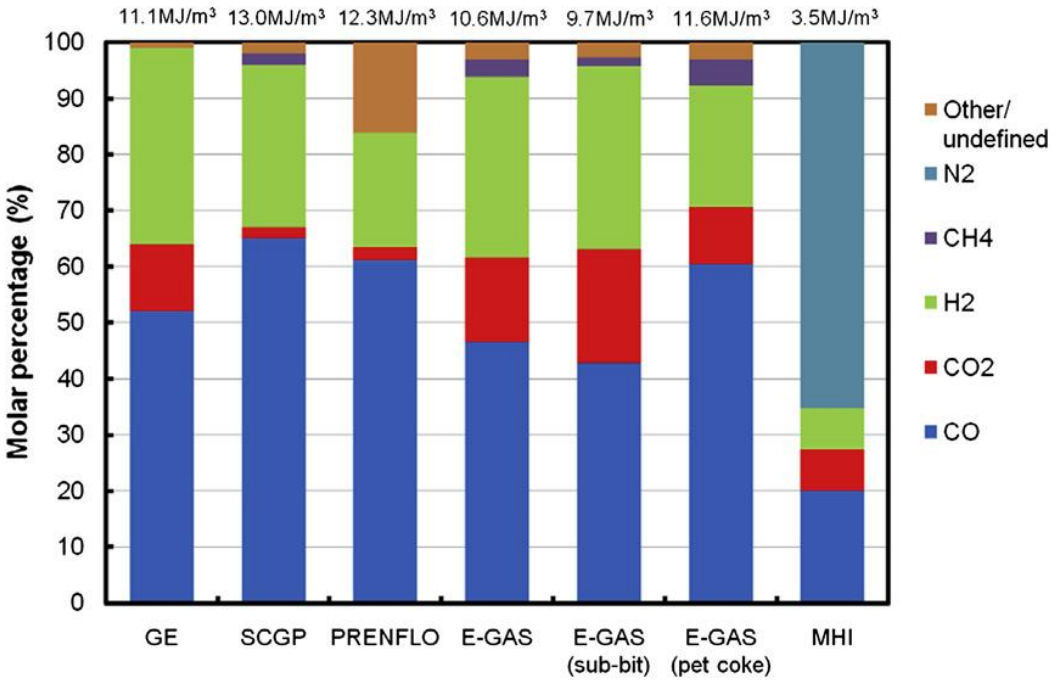

Figure 1.8. Heating values of different EFG (Monaghan and Ghoniem, 2012)

The third motivation behind this work is the need to investigate the effect of the simultaneous optimization of multiple IGCC sub-units on the overall process efficiency. Most of the previous studies have focused on only one sub-unit. Hence, the interactive effects of the variables in these subunits are unknown. No study has focused on simultaneously optimizing the gasifier and exploring integration options between the ASU and the gas turbine.

1.3 Research objectives

The objectives of this research are as follows:

(i) To develop a mathematical model with the ability to synthesize and design an optimal EFG

(ii) To use the developed mathematical model to simultaneously determine the optimal reactor network, reactor volumes, operating conditions and feeding strategy that optimizes the performance of the gasifier

(iii) To develop and integrate the sub-units of the IGCC process to simulate a base case IGCC process.

(iv) To use an integrated reactor superstructure model with a background IGCC process to synthesize and design an optimal EFG.

(v) To determine the optimal flowsheet for an IGCC plant with a known coal flowrate and composition.

1.4 Thesis structure

Chapter 2 provides a comprehensive review of the literature concerning the IGCC, gasifiers, gasifier modelling, and reactor synthesis. The review ends by identifying the gaps in the literature. Chapter 3 explains the model development steps implemented in developing the novel technique for the optimization of the EFG. The modelling platform used in this study is also described. Chapter 4 describes the use of the developed mathematical framework for the synthesis and design of an optimal EFG. The robustness of the model developed in chapter 3 is also proved by simulating examples of the EFG from different literature sources. Chapter 5 describes the development of a mathematical model for the synthesis of an optimal IGCC flowsheet. In Chapter 6, the model developed in Chapter 5 is applied in the synthesis of an optimal flowsheet for two illustrative examples. The recommendations and conclusions are discussed in Chapter 7.

1.5 Summary of the major contribution

The major contributions of the study are listed below:

(i) This study presents a novel mathematical modelling technique for the optimization of entrained flow gasifiers. The technique expands the optimization variables considered in previous studies to include reactor configuration, reactor volume and feed staging.

(ii) The study also explores the effect of gasifier design and conditions on the overall thermal efficiencies of an IGCC plant.

(iii) Finally, the study develops a superstructure with the ability to determine the optimal flowsheet of the gas-side of an IGCC plant. The technique expands the variables which have been previously explored by incorporating gasification variables with ASU-gas turbine integration.

References

Anand, A. K., Cook, C. S., Corman, J. C., Smith, A. R., 1996. New Technology Trends for Improved IGCC System Performance. *Journal of Engineering for Gas Turbines and Power*, 118, pp.732–736.

Emun, F., Gadallaa, M., Majozi, T. and Boer, D., 2010. Integrated gasification combined cycle (IGCC) process simulation and optimization. *Computers and Chemical Engineering*, 34(3), pp. 331–338

Enerdata., 2021.Global Energy Statistical Yearbook. Available online at http:// https://yearbook.enerdata.net/total-energy/world-consumption-statistics.html

Frey, H. C., Zhu, Y., 2006. Improved System Integration for Integrated Gasification Combined Cycle (IGCC) Systems. *Environmental Science and Technology*, February, 40(5), pp. 1693–1699.

Gaye, A., 2008. Access to Energy and Human Development. Human Development Report Office Occasional Paper. Available online at http://hdr.undp.org/en/content/access-energy-and-human-development [Accessed 20th May 2020]

Higman, C., van der Burgt, M., 2003. Gasification. Elsevier Science, pp. 47-48.

IEA., 2019. World Energy Balances 2019. Available online at https://www.iea.org/subscribe-to-data-services/world-energy-balances-and-statistics [Accessed 3rd March 2020]

IEA., 2019. CO2 Emissions from Fuel Combustion. Available online at https://www.iea.org/subscribe-to-data-services/co2-emissions-statistics [Accessed 3rd March 2020]

IEA., 2019. Electricity Information 2019. Available online at https://www.iea.org/subscribe-to-data-services/electricity-statistics [Accessed 3rd March 2020]

Jiang, L., Lin R., Jin, H., Cai, R., Liu, Z., 2002. Study on Thermodynamic Characteristics and Optimization of Steam Cycle System in IGCC. *Energy Conversion and Management,* 43, pp. 1339-1348.

Ju, Y., Lee, C.H., 2017. Evaluation of the Energy Efficiency of the Shell Coal Gasification Process. *Energy Conversion and Management,* 143, pp. 123–136.

Klett M. G., Kuehn N. J., Schoff R. L., Vaysman V., White J. S., 2005. Power Plant Water Usage and Loss Study. Technical Report (Pittsburgh, PA: US Department of Energy, National Energy Technology Laboratory)

Lang, Y., Zitney, S. E. and Biegler, L. T., 2011. Optimization of IGCC Process with Reduced Oder CFD Models. *Computers and Chemical Engineering*, 35, pp. 1705-1717.

Lee, C., Lee, S. J. and Yun, Y., 2007. Effect of Air Separation Unit Integration on Integrated Gasification Combined Cycle Performance and NOx Emission Characteristics. *Korean Journal of Chemical Engineering*, 24(2), pp. 368-373.

Lee Lee, H., Choi, S., Paek, M., 2010. A Simple Process Modelling for a Dry-feeding Entrained Bed Coal Gasifier. *Proc.IMechE Part A: J Power and Energy,* 225, pp. 74-84.

Majoumerd, M. M., De, S., Assadi, M., Brehaus, P., 2012. An EU Initiative for Future Generation of IGCC Power Plants Using Hydrogen-rich Syngas: Simulation Results for the Baseline Configuration. *Applied Energy*, 99, pp. 280-290.

Minchener, J., 2005. Coal Gasification for Advanced Power Generation. *Fuel*, 84, pp. 2222–2235.

Monaghan, R. F. D., Ghoniem, A. F., 2012. A Dynamic Reduced Order Model for Simulating Entrained Flow Gasifiers: Part I: Model Development and Description. *Fuel*, 91(1), pp. 61-80.

Mvelase, B. E., 2016. Optimization of the Integrated Gasification Combined Cycle Using Mathematical Modelling (PhD Thesis). Johannesburg: University of the Witwatersrand.

NETL, 2005. Water Usage in Coal to Power Applications. Available online https://netl.doe.gov/research/Coal/energy-systems/gasification/gasifipedia/water-usage [Accessed 1 July 2020]

NETL, 2010. Cost and Performance Baseline for Fossil Energy Plants Volume 1: Bituminous Coal and Natural Gas to Electricity. Available online at https://www.netl.doe.gov/sites/default/files/netl-file/BitBase_FinRep_Rev2.pdf [Accesed 1st October 2020]

Pîrlogea, C., 2012. Human development Relies on Energy. Panel Data Evidence. *Procedia Economics and Finance*, *3*, pp. 496-501

Ratafia-Brown, J.A., Manfredo, L.M., Hoffmann, J.W., Ramezan, M., Stiegel G.J., 2002. An Environmental Assessment of IGCC Power Systems. Nineteenth Annual Pittsburgh Coal Conference, September 23 – 27, 2002

Wang, M., Liu, G., Hui, C. W., 2016. Simultaneous Optimization and Integration of Gas Turbine and Air. *Energy*, 116, pp. 1294-1301.

2. LITERATURE REVIEW

2.1 The IGCC process review

The application of gasification for power generation forms part of the broader clean coal initiative promoted by governments worldwide. The most well-known clean coal technology is the IGCC process. The advantages of IGCC technology over other coal-based generation plants have already been enumerated. However, there are still avenues for improvement. A thorough understanding of the entire process is required to help identify these avenues of improvement. This section focuses on the IGCC processes, the competing IGCC technologies, and explores options for optimising the plant.

2.1.1 IGCC Process description

IGCC plants differ in their exact details but follow the same principle. Figure 2.1 shows an IGCC plant with a slurry-fed gasifier. In such a plant, the coal feed is milled and fed to the gasifier in a slurry form. In the gasifier, the coal reacts with high purity oxygen from the ASU and steam from the HRSG. The oxidants react with char and the gaseous pyrolysis products to produce fuel-gas. The gasifier's high temperature ensures that the ash in the coal melts into a liquid slag with low viscosity so that it smoothly flows out of the gasifier. The raw fuel-gas leaves the gasifier at 1500–1600^{o}C. The temperature of the fuel-gas product is reduced to 900^{o}C through either radiant coolers or mixing with cooled fuel-gas. The fuel-gas is cooled further to 300 ^{o}C to generate high and medium pressure steam. The cooled syngas is passed through filters to remove solid particles from them. After the filtration, the fuel-gas is cooled further before feeding it to a Venturi scrubber, which uses water to remove HCL, NH_3 and any remaining particulates. Following this, the fuel-gas enters a carbonyl sulphide (COS) hydrolyser where the carbonyl sulphide reacts with steam to form carbon dioxide and hydrogen sulphide. The fuel-gas enters a scrubber from the COS hydrolyser, which uses methyl di-ethanolamine to remove the hydrogen sulphide. The cleaned fuel-gas is burnt in the gas turbine combustor to

generate high-temperature gas. The hot gas is expanded in the gas turbine to generate electricity. Heat is recovered from the exhaust of the gas turbine in the HRSG to superheat the high and intermediate pressure steam and generate low-pressure steam.

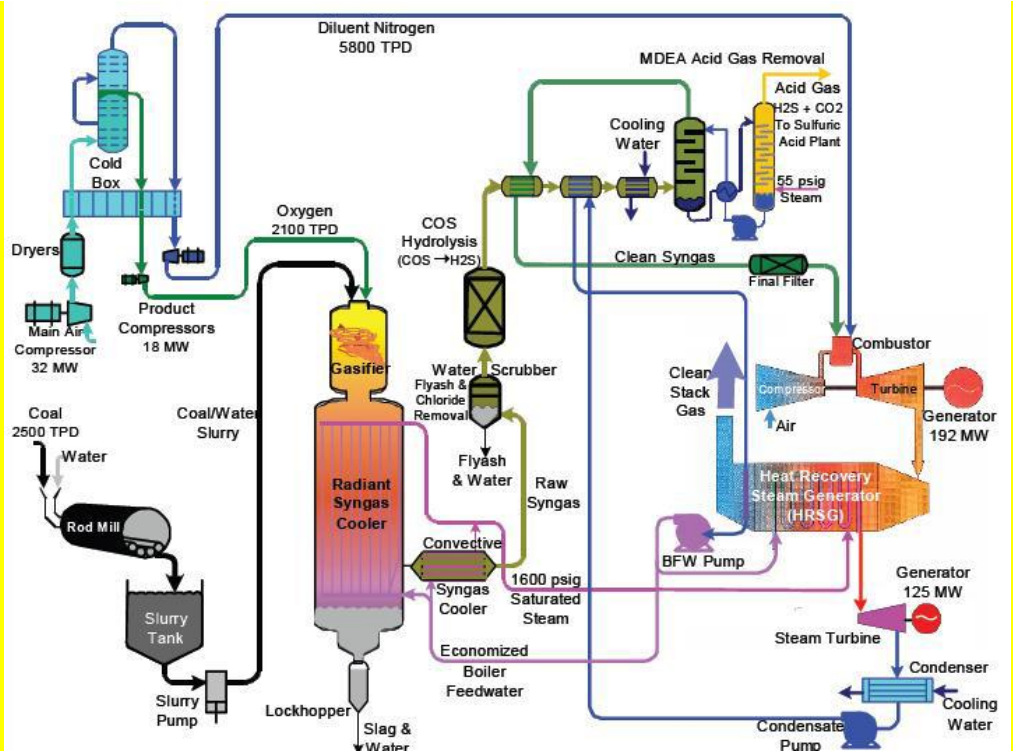

Figure 2.1. A simplified IGCC plant (McDaniel, 2002)

2.1.2 IGCC Technologies

There are several IGCC plants globally; these plants differ in gasification technologies, type of feedstock and plant efficiencies. IGCC plants usually take the name of the provider of gasification technology. For example, a GE-IGCC is a plant with the gasification technology supplied by General Electric (GE). These plants are in Europe, Asia and North America. Table 2.1 summarizes the different IGCC plants across the globe (Maurstad, 2005; Sahraei, 2017). There are other IGCC plants such as Duke Energy (Zupan, 2009) in the USA and Green Gen project in China (Xu, 2014). These plants are still under development; hence, their complete data are not readily available.

Table 2.1. Commercial IGCC plants (Sahraei, 2017)

Plant	Gasifier	Feedstock	Net Power	Efficiency
Tampa Electric (USA)	GE	Coal, Petcoke	250 MW	38.2%
Nuon Power (Netherlands)	Shell	Coal, biomass	253 MW	43%
Elcogas (Spain)	Prenflo	Coal, Petcoke	317.7 MW	47.12%
Wabash River (USA)	E-Gas	Coal, Petcoke	262 MW	40%
Nakoso (Japan)	MHI	Coal	250 MW	42%
Vresova (Czech Republic)	HTW	Lignite	400 MW	42.2%

Table 2.1 shows that some IGCC designs are more competitive than others in terms of their efficiency. The differences in efficiency are mostly due to gasification technology, gas cleaning, gas turbine, and process integration. These differences are discussed in the next section.

2.1.1.1 Gasification technologies

The EFG is the technology of choice for commercial IGCC plants due to its ability to utilize various types of coal, high throughput capacity, tar-free fuel-gas product and high carbon conversion (Lee et al., 2014). All EFGs are of the slagging type, which implies that the operating temperature is above the ash melting point. Nonetheless, there are also significant differences in the design of these competing technologies. Table 2.2 shows the differences in design which include the nature of the feed, the flow direction of the feed, the number of stages, the feed injection and the type of injection (Monaghan and Ghoniem, 2012). These enumerated differences are primarily responsible for the variations in the efficiencies observed in the different IGCC plants.

Table 2.2. Types of Entrained Flow gasifiers (Monaghan and Ghoniem, 2012)

	Stages	Feed	Flow	Oxidant	Syngas cooling	Injectors
SCGP	1	Dry	Up	Oxygen	Quench	Radial
Prenflo	1	Dry	Up	Oxygen	Radiant+ Quench	Radial
Siemens	1	Dry	Down	Oxygen	Quench	Axial
GE Energy	1	Slurry	Down	Oxygen	Radian+ Quench	Axial
E-gas	2	Slurry	Up	Oxygen	Quench	Opposed
MHI	2	Dry	Up	Air	Quench	Radial

Maurstad et al. (2006) investigated the impact of EFG technologies on the performance of IGCC for different coal qualities. The study showed that IGCC plants with dry-fed gasifiers have higher efficiencies than those with slurry-fed gasifiers. This is because slurry-fed gasifiers require a higher oxygen consumption than dry-fed ones. The excess oxygen goes into the combustion of a portion of the coal to generate the energy needed for the evaporation of the slurry water. The increase in oxygen consumption leads to a rise in ASU power consumption, leading to decreased overall plant's net power consumption. Another reason for the lower performance of the slurry-fed gasifiers relative to the dry ones is the higher concentration of carbon dioxide and water in the syngas, giving it a lower heating value. Giuffrida et al. (2011) showed that a conceptual IGCC plant with an air-blown gasifier has a higher thermal efficiency than a plant with an oxygen-blown gasifier. This is due to the reduction in auxiliary power consumption resulting from the decrease in the ASU power consumption resulting from air use by the gasifier.

2.1.1.2 Other IGCC technologies

Other competing IGCC technologies include the type of gas cleaning technology and the design of the HRSG units. The choice between a cold or hot gas cleaning technology for an IGCC

plant affects its net efficiency. Giuffrida et al. (2013) did a thermodynamic analysis of two IGCC plants with a different gas cleaning technology. The study showed that an IGCC plant with hot gas cleaning technology has a 2.58 percentage point higher efficiency than cold gas cleaning. There has also been a pilot testing of the operability of hot gas cleaning technology at the Tampa electric IGCC plant (US-DOE, 2011). There have also been studies showing that other variations such as the number of pressure levels of the HRSG (Jiang et al., 2002) and the inlet temperature of the gas turbine technology (Anand et al., 1996) affect the efficiency of the IGCC process. The study of Jiang et al. (2002) showed increasing the pressure level of the HRSG increases the overall efficiency of IGCC. Anand et al. (1996) also showed that increasing the gas turbine's inlet temperature improves the overall efficiency of the IGCC.

2.1.3 Optimization of the IGCC process

There have been several studies optimizing different parts of the IGCC process. Optimization used in this context broadly refers to any attempt to improve the IGCC plant's performance and is not limited to mathematical programming.

Bhattacharyya et al. (2011) investigated the effects of the carbon capture units on an IGCC plant's overall performance with pre-combustion carbon capture. The gasification technology for this plant was a slurry-fed EFG. The study applied a three-tier sequential optimization process. The first step involved using sensitivity analysis to determine the optimal carbon monoxide conversion in the water gas shift reactor and its corresponding carbon dioxide capture. Based on the result from the first step, the optimal carbon capture configuration was determined in step 1. This was achieved by comparing a single and multi-staged unit. The study showed that a multi-stage stage unit led to a further increase in net power production by reducing auxiliary power consumption. The final optimization step involved the determination of operating variables and parameters for the multi-stage carbon capture unit. Using sensitivity analysis and factorial design, they determined the optimal flow rate of the stripping gas and the

multi-stage units' operating pressures. The study was useful in highlighting variables affecting the carbon capture unit; the technique used does not achieve the true optimal due to its sequential nature.

Anand et al. (1996) presented an analysis of IGCC performance at different degrees of air extraction between the gas turbine and the ASU. The study showed that partial air extraction between the ASU and gas turbine leads to an increase in the thermal efficiency of the IGCC process. This finding was contradicted by the study of Frey and Zhu (2006), which reported that any degree of air extraction leads to a reduction in the overall efficiency of the IGCC process. The reason given for this observation was that the compressor of the ASU has a higher efficiency than that of the gas turbine; hence, there was no net benefit in extracting air from the compressor of the gas turbine. However, most studies (Jones et al., 2011; Wang et al. 2015) have contradicted the claim by Frey and Zhu (2006); hence, the consensus remains that the gas turbine's compressor has a higher efficiency than that of the ASU. The study of Frey and Zhu (2006) also evaluated the effect of injecting nitrogen produced from the ASU into a gas turbine on the thermal efficiency of the IGCC process. This investigation was done on low and high-pressure ASU. The study reported that nitrogen injection leads to an increase in the thermal efficiency of the IGCC for both low and high-pressure ASU. This finding has been confirmed by the studies of Lee et al. (2007), Emun et al. (2010), and Jones et al. (2011). All these studies employed sensitive analysis. Wang et al. (2016) used a nonlinear programming (NLP) formulation to study the effect of ASU-gas turbine integration on the thermal efficiency of an IGCC process. The Generalized Reduced Gradient (GRG-2) code was used in determining the optimal air extraction and nitrogen injection for an IGCC plant.

The availability of heat sources and sinks in the IGCC process makes heat integration a means of optimization. Hence, another approach in optimizing the IGCC process is the use of pinch technology. Madzivhandila et al. (2009) used pinch analysis in the optimization of the IGCC

process. The study showed that by process-to-process heat integration, the steam turbine's output could increase, leading to an overall increase in IGCC efficiency. This technique was applied to the Elcogas plant and reported an increase in efficiency from 47% to 51.6%. The study of Emun et al. (2010) used process-to-process heat integration to optimise an IGCC plant. The study used sensitivity analysis to study the effect of integration between the gas turbine combustor and the gasifier on the IGCC process's efficiency. Their results showed a peak integration point after which further integration leads to a decrease in IGCC efficiency.

These studies have mostly ignored the effect of the gasifier on the efficiency of the IGCC. This study is focused on the effect of EFG. The next section will be dedicated to the review of optimization studies on the EFG.

2.1.4 Optimal EFG design

The studies on the optimization of the EFG is influenced by the different competing manufacturers on the market. Hence, a lot of research is aimed at a specific type of EFG technology. One common approach is the use of sensitivity analysis. Wen and Chaung (1979) evaluated the effect of oxygen and steam-to-coal ratios on char conversion in a slurry-fed EFG. The study showed that high ratios of oxygen and steam-to-coal increases carbon conversion. However, it was also reported that the steam-coal ratio has a negative effect on conversion after a peak value is exceeded. These results were corroborated by the study of Lee et al. (2010) for a commercial-scale dry-fed EFG. However, there was no peak value for the steam-coal ratio as reported by Wen and Chaung (1979). In addition to these, the study of Lee et al. (2010) reported that the CGE of a gasifier is favoured by a low steam-to-coal ratio. Vamvuka et al. (1995) used sensitivity analysis to evaluate the effect of operating parameters on a pilot-scale, dry-fed gasifier's performance. The results suggested that gasification's most critical parameters are oxygen-to-coal ratio, steam-to-coal ratio, and gasifier pressure. The study concluded low oxygen and steam to coal ratio improves the gasifier’s heating value. The study of Emun et al.

(2010) evaluated a slurry-fed gasifier's performance as part of an IGCC plant. The results show that increasing the oxygen-coal ratio decreases both the CGE of the gasifier and the thermal efficiency of the IGCC plant. Ju and Lee (2017) expanded the sensitivity analysis to study the effects of oxygen, and steam-to-coal ratios on the CGE of a commercial scale dry-fed EFG for five different coal feeds. They reported that the optimal ratio of oxygen-to-coal ratio flow for the maximum CGE varied from 0.70 to 0.87 depending on the type of coal. The study also showed that while steam addition improved the CGEs of bituminous coals, the CGE of sub-bituminous coals showed no improvement upon steam addition. The advantage of using sensitivity analysis is that it helps identify the critical parameters for optimal gasifier operation. The main drawback of using sensitivity is that its sequential nature means interactive effects between variables are excluded. Hence, the optimal operation points, which may exist at a trade-off position, cannot be determined. However, sensitivity analysis serves as a pre-processing technique for mathematical optimization.

The use of NLP or MINLP optimization addresses the limitations of sensitivity analysis. This approach addresses the limitations of sensitivity analysis due to the simultaneous evaluation of all variables. Lang et al. (2011) used an NLP optimization to determine the optimal operating conditions of a slurry-fed EFG. The aforementioned study applied NLP optimization to a two-stage slurry fed gasifier. The final gasifier model used in the study was an artificial neural network model. Using an NLP formulation, the developed models were solved to determine the input variables for the optimal cost of syngas and the net power produced.

Mvelase (2016) applied NLP optimization to a dry-fed EFG with a pre-defined configuration. Using a kinetic-based model, the study used an NLP optimization model to determine the optimal operating temperature for an EFG. The results showed that low operating temperatures improve the gasifier's CGE but occur at a penalty of low carbon conversion.

Limiting the options to gasifier input conditions limits the extent of the improvement that can be achieved. The analyses of different EFG by Monaghan and Ghoniem (2012) and Majoumerd et al. (2014) showed that different designs lead to different gasifier performance under similar operating conditions. However, there is no evidence in literature proving the optimality of any of these designs. Maurstad (2005) suggested that new gasifier designs must be explored to achieve improvements in the current levels of gasifier performance.

Since this research aims to explore the potential of reactor design to synthesize an optimal IGCC flowsheet, there must also be a fundamental understanding of both flowsheet synthesis and reactor synthesis and design. Hence the next section focuses on IGCC process flowsheet synthesis.

2.1.5 IGCC process flowsheet synthesis

Process synthesis comprises the systematic generation of alternate process flowsheets and the selection of a design whose configuration and parameters optimize a given objective function (Grossmann and Daichendt, 1995). Hence, this review will focus on any attempt to find alternative routes for the IGCC process. Due to the number of units, all attempts to synthesize an optimal IGCC process route focuses on, synthesizing a part of the IGCC plant.

Diwekar et al. (1992) used an MINLP formulation to determine an optimal IGCC flowsheet under environmental control. The authors achieved this by employing an ASPEN program with MINLP process synthesis capabilities as a result of the incorporation of FORTRAN coding. The developed mathematical programming was used to determine the gas cleaning technology that led to the minimal cost.

Using the reaction configuration obtained by Diwekar et al. (1992), Rubin and Diwekar (1997) used the stochastic annealing method to determine the perform a superstructure optimization of an IGCC power plant under uncertainties. The decision variables in the superstructure were

the type of coal and the oxidation agent. The stud focused on 6 coal samples and two types of oxidants. They reported that using air as the oxidant leads to the lowest IGCC plant cost.

Madzivhandila et al. (2009) redesigned the steam side of the IGCC process using pinch analysis. The authors extracted from heat sinks and source data the Elcogas IGCC flowsheet. They then used the table algorithm to compute the net heat available for steam generation, after the heating load of the plant is satisfied. The authors reported an increase in the thermal efficiency from 47% to 51.6%. Using the Super Target software package, the new flowsheet in Figure 2.2 was obtained.

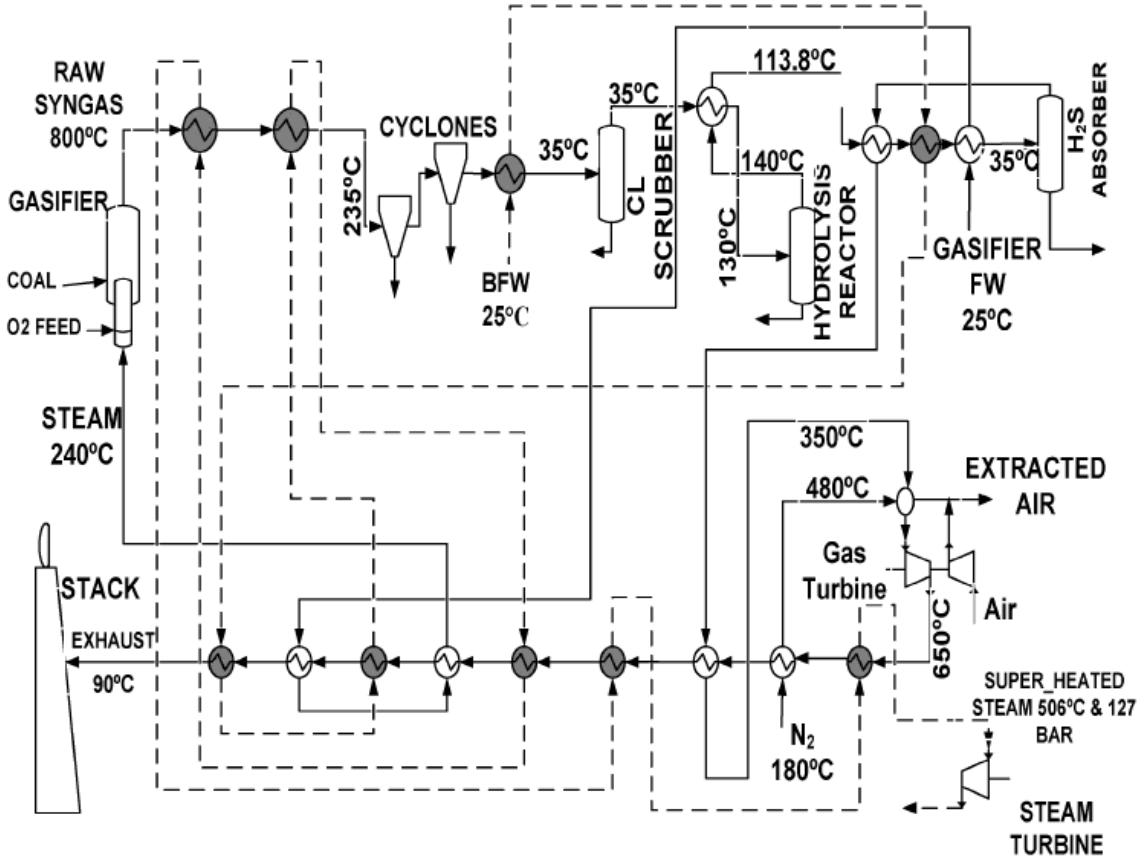

Figure 2.2. The new design of the Elcogas IGCC plant (Madzivhandila et al., 2009)

A summary of these studies shows that a change in the flowsheet of the IGCC plant can lead to improvements in its performance. However, none of these studies focuses on the design of the gasifier. Hence, this study closes that gap by exploring the effect of EFG design on the efficiency of the IGCC process. This requires that there the integration of a gasifier design technique in a background IGCC process. However, the review of EFG optimization techniques showed that none of the existing techniques focuses on gasifier synthesis and design. Hence another objective of this study is to develop a novel EFG optimization technique that explores the effect of both reactor configuration and operating conditions.

To be able to do is, there must be a fundamental understanding of gasification and reactor synthesis techniques to develop this optimization technique. Hence, this study aims to develop a novel EFG optimization technique that explores the effect of both reactor configuration and operating conditions. Hence, the remainder of the literature review focuses on the fundamentals of the gasification process and explores the possible techniques to be used in the synthesis and design.

2.2 Fundamentals of gasification

Gasification is converting a solid or liquid carbonaceous feed into a combustible gaseous product, through the sub-stoichiometric reaction of the feed with oxidants (Majoumerd et al., 2014). The process is a complex interaction of several sub-processes. These sub-processes include particle dispersion, gas mixing, particle heating, mass transfer, gas and particle reaction, recirculating and swirling fluid mechanics, heat transfer, and phase transformation of mineral matter, and pollutant formation and destruction. Notwithstanding these complexities, the entire process can be grouped into two stages, namely pyrolysis and chemical reactions.

2.2.1 Pyrolysis

Pyrolysis is the thermal decomposition of solid carbonaceous fuel under high temperature to light gases, water, tar and char. This decomposition is a fast process consisting of other sub-processes. The process starts with the weakest bonds' breakage at low temperatures to produce light hydrocarbons and tar. This process is primary pyrolysis. As the heating is increased, further bonds are broken for the evolution of secondary volatile matter (Eisermann et al., 1980; Solomon et al., 1988). Other processes that may occur during the pyrolysis of coal include the plasticization of coal and the annealing of char (Smith, 1982; Maffei, 2013). The pyrolysis of coal depends on a wide range of factors such as structure and composition of coal and reactor conditions such as heating rate, residence time, temperature, particle sizes, and pressure (Lee et al., 2014). The main products from the pyrolysis of feedstock are char, hydrocarbons, hydrogen, carbon monoxide, carbon dioxide and pollutants such as hydrogen sulphide, ammonia, carbonyl sulphide and nitrogen.

2.2.2 Reactions

This stage is the actual gasification process. It involves several homogeneous and heterogeneous reactions. Examples of homogeneous reactions are hydrocarbon and hydrogen combustion, carbon monoxide oxidation and the water gas shift reaction (Table 2.3). These reactions are mostly exothermic and are generally responsible for the high temperatures observed during gasification. Another critical reaction occurring in the gasifier is the water gas shift reaction. This is one of the gasifier's controlling reactions (Lee et al., 2014). The gasifier's heterogeneous reactions occur between the char and gases such as oxygen, steam, carbon dioxide, and hydrogen. Except for the char-oxygen reaction, all the other heterogeneous reactions are endothermic, requiring the energy generated by the homogeneous and exothermic reactions. Some authors have grouped the reactions occurring in a gasifier as combustion and gasification reactions based on this knowledge. Under this classification, the oxidation and

exothermic reactions are classified as combustion reactions, while the remaining reactions are classified as gasification reactions (Perez-Fortes et al., 2009).

Table 2.3. Homogeneous gasification reaction

	Reaction	**Heat of reaction (KJ/mol)**
Reaction 1	$C_XH_Y+(0.5X)O_2 \rightarrow XCO+(0.5Y)H_2$	N/A
Reaction 2	$C_XH_Y+ (0.5X+0.5Y)O_2 \rightarrow XCO_2+(0.5Y)H_2O$	N/A
Reaction 3	$H_2+0.5O_2 \rightarrow H_2O$	-242
Reaction 4	$CO+0.5O_2 \rightarrow CO_2$	-283.1
Reaction 5	$CO +H_2O \leftrightarrow CO_2+H_2$	-41.2

2.2.3 Gasification feedstock

The feedstock for gasification includes coal, petcoke, biomass and some other liquid and gaseous fuels. The availability of standards methods of feed classification is essential in the final analysis of the gasification process. The standard techniques of classifying feedstock include proximate and ultimate analysis and heating value. The proximate analysis provides information on the percentage of moisture, volatile matter, ash and fixed carbon in the feed. The analysis is essentially a practical tool providing an initial indication of the feed quality and type. The ultimate analysis provides information on the percentages of carbon, hydrogen, oxygen, sulfur and nitrogen in the feedstock. It is used in calculating the heating value in the absence of measured data (Higman and Van de Burgt, 2003). The ultimate analysis is presented under different frameworks such as "As received", "dry basis" and "dry-ash free basis". An analysis reported as "As received" means the composition of feed was computed with both the moisture content and ash content included. An analysis presented as "dry basis" means the composition was computed without taking into consideration the moisture content. Analysis

moisture and ash content. Based on these standards, the different feedstock differs in quality and reactivity. For example, the reactivity of petcoke is lower than coal, and hence a higher temperature or a longer reactor residence time is required. The use of biomass also faces high moisture content and relatively low heating value (Rubiera et al., 2011). Figure 2.3 shows that coal remains a dominant feedstock for the production of synthetic gases. Hence, this study focuses primarily on coal gasification. Synthetic gas or fuel-gas is the main product of gasification.

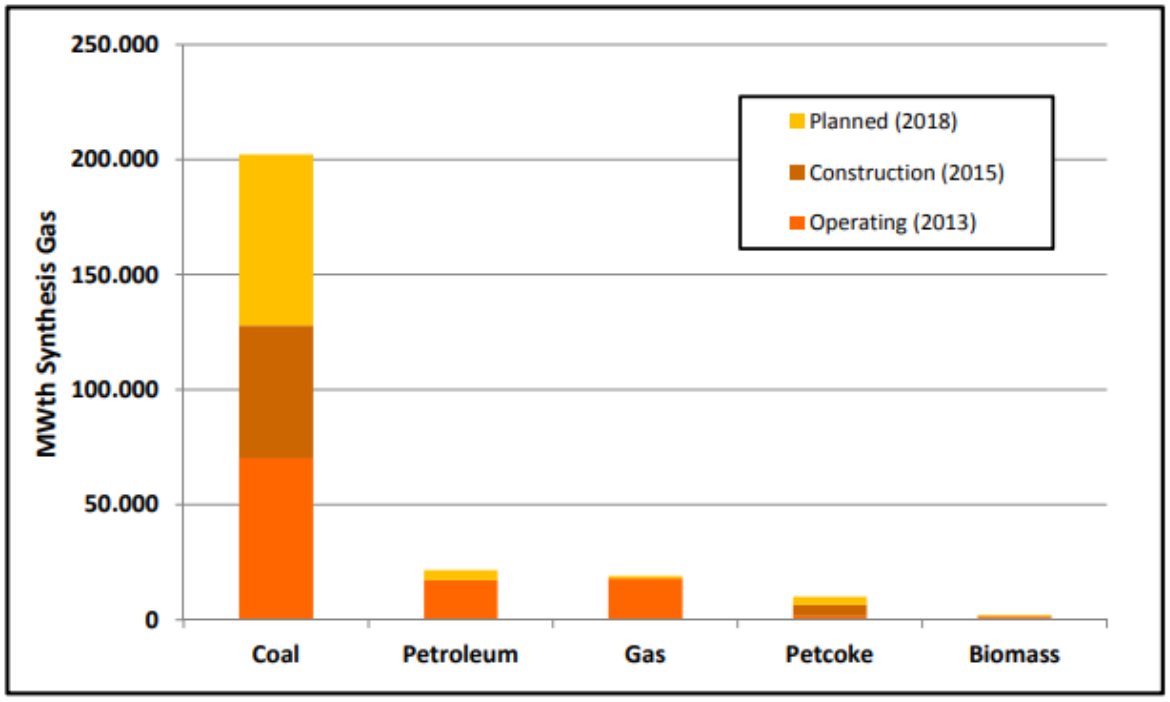

Figure 2.3. Gasification by Primary Feedstock (Higman, 2013)

2.3 Gasification Models

Mathematical modelling plays a vital role in the research and development of an EFG. Mathematical models are necessary for gaining insights into the influence of design variables, feed materials, and processing conditions on gasifier performance. Furthermore, such models will be essential and powerful tools in optimising, scaling up and designing gasifiers.

There are different gasifier models. The choice of a gasification model is determined by the research objectives. Gasification efficiency and reactor operability are the two main objectives in gasification related research (Monaghan, 2010). While gasification efficiency is concerned with improving feedstock conversion and syngas quality, operability focuses on improving the gasifier's reliability and availability. This study focuses on improving and optimizing the chemical efficiency of the EFG. For this study, gasification models will be classified as either, equilibrium-based, kinetic-based, computational fluid dynamics, reactor network modelling and artificial neural networks models.

2.3.1Equilibrium-based models

Equilibrium models assume that gasifiers operate under equilibrium conditions. This assumption eliminates the need for chemical rate laws and hence simplify the simulation process. Equilibrium models have advantages such as a simple and quick method that gives satisfactory reliability and accuracy for syngas composition. The study of Gazzani et al., (2013) showed that simple equilibrium models are as accurate as a detailed gasifier model in predicting syngas composition. There are two types of equilibrium models, namely stoichiometric and non-stoichiometric.

The stoichiometric equilibrium model requires a defined reaction mechanism, incorporating all chemical reactions and species concerned. The model features include atomic balances, Dalton equation, heat balance and equilibrium constants (Wang et al., 2017). The non-stoichiometric equilibrium model is based on minimising Gibb's free energy of the gasifier constituents for a given temperature and pressure. The model depends on the principle that reactions achieve equilibrium at low energy levels. This approach uses an NLP minimization to determine the final composition of the syngas.

Although equilibrium-based models have been used in the simulation of all the gasifier types, this review will focus on instances used in modelling EFGs.

Watkinson et al., (1991) applied a stoichiometric equilibrium model to simulate syngas composition of Shell and Texaco EFGs for different feedstock. The results showed a reasonable agreement between model outputs and industrial data. Ni and Williams (1995) applied a multivariable model involving equilibrium, mass balance and energy balance to simulate the Shell EFG. The model was solved as a constrained NLP problem. The study reported simulated syngas composition which was very close to the actual plant data. Yuehong et al., (2006) applied the Gibb's minimization technique as a tool for the equilibrium modelling of the co-gasification process with coal and coke. The modelling of this co-gasification process was performed using Gibb's reactor module (RGIBBS) in the ASPEN Plus process simulator. The performance of the developed model was analysed in terms of its ability to predict the produced syngas composition. The simulation results are in good agreement with the laboratory scale experimental data. Wang et al. (2017) developed an IGCC gasification unit based on a novel simplified equilibrium model in the simulation of a generic dry-EFG. The authors reported good agreement between syngas composition and experimental data.

However, whilst this approach is suitable for a preliminary study, it is not ideal for process optimization procedures. Biagini et al. (2009) analysed the features of equilibrium models that make them inadequate in optimization studies:

(i) The gasification temperature is independent of other operating conditions.

(ii) Char conversion is fixed in the equilibrium model.

These assumptions are suitable for a fixed-point simulation problem where char conversion and gasifier operating pressure are known. However, in an optimization problem, the operating conditions and reactor configuration are varied. Hence, the gasification temperature and char

conversion cannot be treated as a constant. Consequently, equilibrium modelling is unsuitable for the optimization model that is to be developed in this study.

2.3.2 Kinetics-based models

These models incorporate the kinetic equations of occurring chemical reactions in predicting the operation of the gasifier. Kinetics-based models apply the design equations of different reactor types, mass and energy balances to predict the performance of a gasifier at specified reactor designs and operating conditions. Consequently, kinetic-based models are suitable for the optimization of the CGE of an EFG. This study applies kinetic-based models in the development of a novel EFG optimization technique. There are no examples of using such techniques in the synthesis and design of an EFG hence the review will focus on the use of reaction-based models for simulation.

Ubhayakar et al. (1977) modelled a generic single-stage dry fed EFG as a 1-dimensional PFR. The developed model comprised sub-models such as pyrolysis, volatile cracking, gas-phase reactions, heat balance and mixing. Wen and Chaung (1979) modelled a single-stage down-flow Texaco (GE) gasifier as a steady-state CSTR in series with a PFR. In the study, the gasification process was divided into three stages. The three stages were pyrolysis and volatile combustion, char combustion and gasification. Mass, momentum and energy balances were performed on each of these stages. Govind and Sha (1984) used a slightly different approach to model the GE gasifier. Based on a calculated low dispersion factor, the Texaco gasifier was modelled as a PFR. The authors also included a momentum balance for the solid-phase instead of the Stoke equations used by Wen and Chaung (1979). Based on a prior experimental study of coal gasification, Vamvuka et al. (1995) rejected the division of the gasifier into three stages claiming the zones were indistinguishable. The authors used a 1-dimensional PFR in modelling a lab-scale dry-feed EFG with all gasification stages co-occurring. Valero and Uson (2006) employed two isothermal CSTR in series to model a Pressurized Entrained Flow (Prenflo)

gasifier. This reflected the near-perfect conditions of mixing observed in Prenflo gasifiers (Higman and van de Burgt, 2003). The model also employed the stages-based gasification approach proposed by Wen and Chaung (1979). Pérez-Fortes et al. (2009) used two CSTR in series followed by an equilibrium reactor to model the Prenflo gasifier. They use Gibb's minimization reactor to model the equilibrium stage. Lee et al. (2010) developed a simple 1-dimensional PFR model to study a Shell coal gasifier with diametrical burners. The main components of the model were mass and energy balance. Kasule et al. (2012) revisited the 1-dimensional PFR modelling of Texaco slurry-fed gasifiers with some significant modifications. One of the main modifications includes product recirculation, which accounts for deviations from pure PFR conditions. The model formulation also included the detailed accounting of heat flow through the gasifier wall. Lee et al. (2014) revisited the modelling of Shell gasifiers with diametrical injector configuration using a 1-dimensional PFR. The model included axial dispersion to account for deviation from ideal PFR due to upward flow. The study also used an equation of state software in estimating gas properties. Most of the previous studies assumed ideal gas behaviour.

In general, all these studies obtained good agreement between simulated and experimental data for syngas composition and carbon conversion, syngas exit temperature. Most of these models generated temperature and velocity profiles in which there was no way to validate it since such data is usually not available. Although it is difficult in comparing these studies due to the difference in operating and feed conditions, it can be deduced that the different mixing conditions, i.e. perfect and no axial mixing can be achieved in the EFG. It can also be deduced that kinetic-based models take as inputs feeding conditions and reactor configuration and produce as outputs carbon conversion, syngas composition, and syngas temperature. Consequently, these models are suitable for sensitivity analysis and gasifier optimization studies. However, kinetic-based models are not able to simulate the hydrodynamics, the

temperature distribution, and the near-wall temperature profile of the gasifier adequately (Yang et al., 2011; Monaghan and Ghoniem, 2012). All these variables have a significant impact on slag flow behaviour. Hence, if a study aims to include details such as injector temperature, wall temperature profile, and slag development in a gasifier, other types of models are more useful. Such models include computational fluid dynamics (CFD) and reactor network modelling.

2.3.3 Computational Fluid Dynamics (CFD) models

CFD models include equations that describe detailed fluid mechanics in the gasifier as part of its mathematical formulation. There are two types of CFD models: the Eulerian-Eulerian model (EEM) and the Eulerian-Lagrangian model (ELM). While the EEM treats both the gas and solid phase as a continuum, the ELM treats the gas phase as a continuum while modelling the solid phase using discrete element modelling. CFD models can produce a more accurate internal temperature distribution for a gasifier used in estimating the thickness of the slag layer. (Gomez-Barea and Leckner, 2010; Xie et al., 2013). The use of CFD simulation in the simulation of EFGs started with Smooth et al. (1984) who developed one and two-dimensional models for entrained coal combustion. The model assumed a constant elemental composition and heating value for the coal off-gas for the coal at all points in the gasifier. Other CFD models have been used in the simulation of two-staged air-blown EFG (Chen et al., 2000; Watanabe and Otaka,2006), single-stage EFG (Bockelie et al., 2002), slurry-fed bench-scale EFG (Choi et al., 2001; Liu et al., 2001) and two-stage slurry-fed EFG (Jeong et al., 2014). CFD models are mostly employed for operability studies. They provide data such as slag profile, temperature hot spots, and wall temperature profile not provided by kinetic-based models. However, such detailed nature of CFD models leads to difficulty in integration with IGCC or poly-generation plant flowsheets (Monaghan and Ghoniem, 2012). CFD models also require detailed information on gasifier geometry (Lang et al., 2011) and cannot be used in preliminary design. Hence, CFD models are not suitable for developing an optimization model.

2.3.4 Reactor Network Modelling (RNM)

These techniques are a unique form of kinetic-based models. Based on the pioneering work of Pedersen et al., (1997; 1998), it was revealed through the analysis of the residence time distribution of pulverised entrained coal combustors, a reactor network detailing the modelling the mixing complexities could be proposed. The use of RNM eliminates the need for CFD modelling. In RNM models, most of these reactors have no reactions but are included to achieve the desired mixing and hydrodynamics. RNM was first used to model EFGs in the study of Monaghan and Ghoniem (2012). The studies applied RNM to simulate the performance of four different EFGs. The authors reported temperature and slag profiles comparable to CFD modelling. RMN has been used in the modelling of oxygen-staged EFG (Yang et al., 2011; 2013), carbon dioxide-fed EFG (Gazzani et al., 2013), and the modelling of laboratory-scale EFG (Sahraei, 2017). The advantage of using this technique is similar to using a CFD model. Data such as slag thickness and hot spots in the gasifier can be obtained with a reduced computational effort compared to CFD modelling. Sahraei et al. (2015) reported that the convergence time for a single simulation of a gasifier for an RNM is 2.5 min, whereas CFD simulations require 7–10 days. Figure 2.4 shows the RNM for an oxygen-staged reactor. In this diagram, the authors used the alternate name for a CSTR, the well-stirred reactor (WSR). It must be stated that the RNM used in other studies is different from the one shown in Figure 2.4. Ideally, an RNM for the EFG must be developed from CFD simulations. Hence, an RNM as a technique to prevent the computationally expensive CFD is not absolute since CFD modelling must occur before an accurate RNM can be determined. RNM can be used in a sensitivity analysis. It has been argued that they are computationally expensive for mathematical optimization (Wang et al., 2019). The reactor network resulting from this model is not optimal but deemed suitable in depicting the hydrodynamics and temperature profile in an EFG.

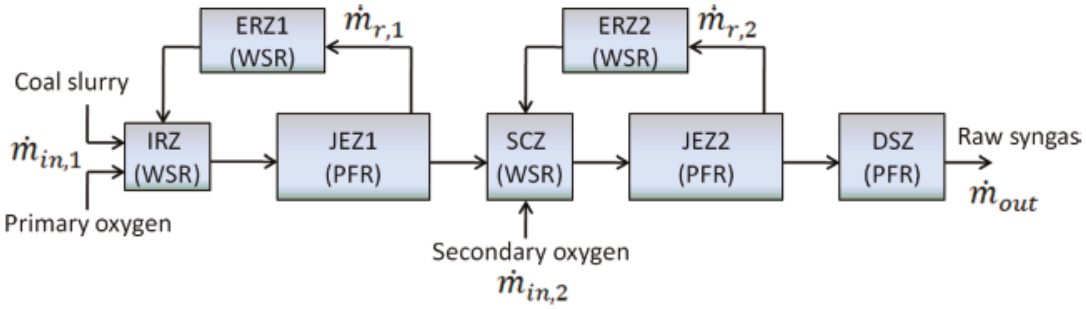

Figure 2.4. RNM for oxygen staged reactor (Yang et al., 2011)

2.3.5 Artificial Neural Networks (ANN) model

Artificial neural networks (ANNs) are an alternative modelling method in simulating the performance of the gasification unit in IGCCs at reduced computational costs. The biological neural networks in the human brain inspire the concept of the ANN. An ANN consist of several layers of simple computing nodes called neurons. The architecture of an ANN model includes several layers of hidden neurons and an input and output layer. The hidden layer of the ANN determines the relationship between the inputs and the outputs. The values calculated by the hidden layer neurons are transmitted to the next layer. A linear transfer function maps the final hidden layer outputs onto the range of the desired output parameters in the output layer. The first step in developing is to decide the number of input variables to be investigated. After the input parameters are determined, the next step is to determine the optimal number of hidden layers and neurons in each hidden layer. This is determined on a trial-and-error basis, based on the criteria of minimizing the error between the model output and the actual data. Each of the neurons in the hidden layers has weights for its input values and a bias and a transfer or activation function. To ensure that the developed ANN model predicts accurately, the right weights and biases must be determined. This is achieved by the training of the developed model using a backpropagation technique. The list of available backpropagation techniques can be found in the study of Wang et al. (2019). Figure 2.5 shows an example of an ANN architecture

for the modelling of a gasifier. The ANN model for Figure 2.5 consists of eight sub-models. Each sub-model will predict one of the output variables. The study of Puig-Arnavat et al. (2013) developed an ANN model for the gasification of biomass in a fluidized bed gasifier. The obtained results show that the ANN successfully predicted the composition and yield of the syngas. There has also been the study of a developed ANN model for steady (Wang et al., 2019) and dynamic state (Wang and Ricardez-Sandoval, 2020) operation of a pilot-scale EFG.

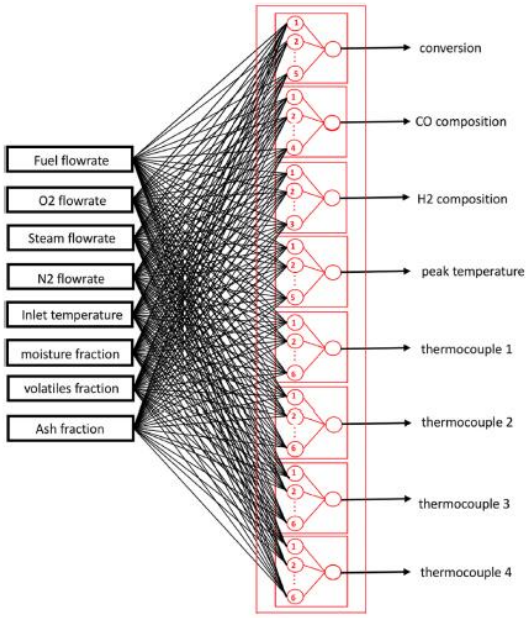

Figure 2.5. An optimal ANN architecture for the modelling of a gasifier (Wang et al., 2019)

The main advantage of using ANN to model gasification is that one can model a system without fully understanding the system. In addition, the final model is simple mathematically. For example, if all the activation functions in the hidden neurons of an ANN are tan-sigmoid functions, equation (2.1) predicts the output variable, O_j using and the nominal value, P_m, for an input variable, m, with weights, $IW_{m,z}$ and bias b_z for hidden neuron z and weight $OW_{j,z}$ output neuron and bias b_j for the output neuron, j.

$$O_j = \sum_{z=1}^{Z} OW_{j,z} \left(\frac{2}{1+\exp\left(-2\left(\sum_{m=1}^{M}\left(IW_{m,z}.P_m\right)\right)+b_z\right)} - 1 \right) + b_j \quad (2.1)$$

Equation (2.1) shows that the relationship between an output such as yield and all the inputs has been reduced to a simple logistic equation. The main limitation of using the ANN is that a large amount of data is needed to train the model. Hence, it is not suitable in a situation where there is not enough data. Another limitation in using the ANN approach is that the final model is opaque. The nature of the equation between two outputs (e.g. exit temperature and hydrogen content) and the input variables can be the same. It can also be argued that ANN models developed are not generic but specific to the dataset used in developing the model.

2.4 Structure of a gasifier model

Most gasifier models have sub-models describing different aspects of the gasification process. These include pyrolysis, reactor, heat transfer, slag development, and momentum sub-models. The number of sub-models incorporated into a gasifier model depends on the level of details required. For example, while a CFD gasifier model will include all the sub-models, a kinetic-based model may incorporate just the pyrolysis and reactor sub-models.

2.4.1 Pyrolysis models

The pyrolysis sub-model converts the feed data into molecular species that can serve as input variables to the reactor sub-model. This study reviews the existing pyrolysis models and their suitability for EFG modelling. Pyrolysis models can generally be grouped into kinetic models and Feed-based models.

2.4.1.1 Kinetic models

Kinetic models predict the rates and yields of the species released during pyrolysis based using differential equations. Equation (2.2) is an example of a kinetic model for the pyrolysis of coal (Bazoich and Hawksley, 1970). Equation (2.2) states that the volatiles evolution rate is directly

proportional to the amount of volatile content remaining in the coal. The amount of coal remaining equals the difference between the equilibrium amount, V^*, and *V*, which is the cumulative amount that has evolved at time t.

$$\frac{dV}{dt} = k(V^* - V) \tag{2.2}$$

This kind of model does not provide data on the composition of the final evolved product. Hence, an atomic balance is needed to estimate the final composition of the evolved gases. Govind and Shah (1984) augmented the kinetic model with a model developed by Loison and Chauvin (1964). There are other kinetic models describing pyrolysis as a parallel process instead of a single step (Ubhayakar et al., 1977).

2.4.1.2 Composition-based models

These refer to any model that is dependent on the properties of the feed. Some of these models are based on the chemical structure and the function of the parent coal. Examples of such models are the Flashchain model (Niksa and Kerstein, 1991), and the chemical percolation devolatilization model (Grant et al., 1989). These models' primary defects are the composition of the gas released during pyrolysis are not predicted as they provide output results related only to the average molecular weight of the mixture of light gases. Other models use the ultimate analysis or the proximate analysis data of the coal or both to predict the pyrolysis product's composition. An example of composition models is the empirical correlations proposed by Loison and Chauvin (1964) in estimating the mass fraction of the most critical gaseous products in coal pyrolysis. The model requires only the proximate coal data. Another example of composition-based models is one proposed by Merrick (1983). The model uses both proximal analysis and ultimate analysis data to predict the products of pyrolysis. The primary defect of composition-based models is the fact that it ignores the possible effect of operating conditions on the effect of pyrolysis.

2.4.2 Homogeneous reactions models

There are two approaches to modelling homogeneous reactions. These are based on either global reactions or elementary kinetic steps (Monaghan, 2010; Mvelase, 2016). The elementary kinetic reactions generally have a limitation in modeling because not all the intermediate chemical reaction steps are always readily available (Mvelase, 2016). Hence, this study adopts models based on global reactions. The global reaction models are based on the power-law approach.

2.4.3 Heterogeneous reaction models

Kinetic models representing heterogeneous reactions can be classified as black-box, semi-global and global.

2.4.3.1 Black-box models

These are models derived solely from experimental results. They are usually regression models defining the relationship between the output and input variable(s). These models may be more accurate than global and semi-global models because they are developed for the coal or feed under investigation. However, they may be inapplicable to other coal species. An example of such a model was employed in the work of Sahraei et al. (2015). In the study, the equation (2.3) is used to compute the rate of char consumption, R_i, which is a function of the decay parameter, υ, pre-exponential, A_i, the activation, Ea_i, the partial pressure of the gasification component on the particle surface, P, the reaction temperature T, the universal gas constant, R_G, and the order of the reaction, n_i. Equation 2.4 is used to compute the decay parameter which is a function of the char conversion, X_{Char}. The decay parameter ensures that the reaction rate slows down as the conversion increase.

$$R_i = \upsilon A_i \exp\left(-\frac{Ea_i}{R_G T}\right) P_{i,S}^{n_i} \quad (2.3)$$

$$\upsilon = (-2E-08)X_{Char}^{5} + (5E-06)X_{Char}^{4} - 0.0005X_{Char}^{3} + 0.0244X_{Char}^{2} - 0.5489X_{Char} + 6.7283 \quad (2.4)$$

The decay rate coefficients have been calculated by fitting reaction data.

2.4.3.2 Semi-global kinetic models

These models incorporate adsorption, reaction, and desorption steps in the modelling of solid fuel gasification because they reflect the physiochemical processes that occur during heterogeneous chemical reactions more accurately. The rate of reactions, for the Boudard reaction is given by equation (2.5) (Mahinpey and Gomez, 2016).

$$r = \frac{k_{ii} P_{CO_2}}{1 + k_{ij} P_{CO_2} + k_{iz} P_{CO}} \quad (2.5)$$

Monaghan (2010) did an extensive review of the available existing semi-global mechanism-based models. The main conclusion is that the semi-global mechanisms are not yet at the required level of maturity for EFG simulations. Most mechanisms were found not to have been validated over wide ranges of temperature, pressure, and gas composition to be applicable for EFGs.

2.4.3.3 Global reactions models

These are simplified models representing the kinetic behaviour of gas-solid reactions when adsorption and desorption are ignored or treated as assumed as not limiting factors for the overall reaction. Global reaction models lump the effects of film diffusion, pore diffusion, and chemical kinetics into a single expression. Available global reactions models include the volumetric model, the shrinking core model, the integrated core, and the random pore model (Monaghan and Ghoniem, 2012; Mahinpey and Gomez, 2016). All these global reactions can be represented in a standard form depicted by equation (2.6). Equation (2.6) states that the rate

of change of char conversion, X , is proportional to the product of the unconverted char, and a function for the conversion, $f(X)$.

$$\frac{dX}{dt} = kf(X)(1-X) \tag{2.6}$$

Table 2.4 shows different char conversion functions for the various global models developed for char gasification. As shown in Table 2.4, these semi-global models differ in the parameters needed. These parameters are usually determined through empirical techniques. All these models are based on different assumptions of how different gasification agents react with the char product from pyrolysis. For example, while the volumetric model assumes that the reaction takes place uniformly within the particle's volume, the shrinking core model assumes that the reaction occurs only on the surface of a non-porous shrinking carbon core.

Global models are desired due to their broadly applicable nature. Hence this study uses global heterogeneous models in the modelling of the heterogeneous reactions. The random pore model is chosen because it can accurately describe the variation in reactivity as conversion increases (Lee et al., 2014).

2.5 Fundamentals of reactor synthesis

Reactor network synthesis is primarily concerned with determining the type, number, sizes of reactors and their interconnectivity that optimizes a chosen performance index for a set of reaction kinetic data (Hua et al., 2000). These decisions include discrete decisions such as the existence or non-existence of a particular reactor type and the choice of optimal values of continuous variables such as the reactor size. The techniques used in making these decisions can be graphical, mathematical, and a hybrid of methods.

Table 2.4. Semi-global models applied to the gasification of char

Model	f(X)	Reference(s)
Uniform conversion model	1	Adschiri et al. (1986)
Shrinking or grain model	$(1-X)^{-\frac{1}{3}}$	Kajitani et al., 2002
Random pore	$(1-\psi \ln(1-X))^{\frac{1}{2}}$	Bhatia and Perlmutter (1980)
Extended random pore	$(1-\psi \ln(1-X))^{\frac{1}{2}}\left(1+(cX)^{P}\right)$	Zhang et al. (2008)
Simons model	$(X+\alpha \ln(1-X))^{\frac{1}{2}}$	Simons (1980)
Johnson model	$(1-X)^{-\frac{1}{3}}\exp(\alpha X^{2})$	Gomez-Barea and Leckner (2010)
Gardner model	$\exp(\alpha X)$	Gardner et al. (1974)
Modified volumetric model	$a^{1/b}b[-\ln(1-X)]^{\frac{(b-1)}{b}}$	Kasaoka et al. (1985)
Empirical potential model	$(1-X)^{\alpha}$	Laurendeau (1978)
Polynomial model	$\sum_{i=1}^{n} a_i X(1-X)^{i}$	Ollero et al. (2003)

2.5.1 Types of ideal reactor

Ideal reactors serve as the building blocks for reactor synthesis techniques. These ideal reactors are chosen to represent the type of mixing in different sections of the reactor. A review of the literature shows different kinds of ideal reactors. Although these representations are different, all ideal reactors represent the two extremes of mixing that can occur. These are total axial mixing between the constituents of the reactor and no axial mixing. The ideal reactor regime used in reactor synthesis techniques includes axial dispersion reactor, recycle reactor, the two-

environment reactor model, and ideal CSTR and PFR (Ng and Rippin, 1965; Paynter and Haskins, 1970; Achenie and Biegler, 1990).

2.5.1.1 Axial dispersion reactor (ADR)

Paynter and Haskins (1970) introduced the use of axial dispersion reactor in reactor synthesis. Figure 2.6 shows that the axial dispersion reactor which is a PFR with the dispersion of materials in the axial direction.

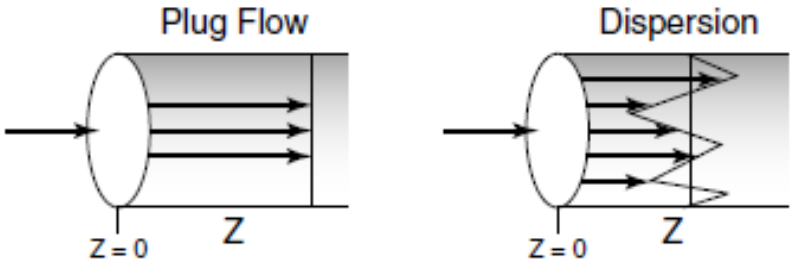

Figure 2.6. Concentration profile of a PFR with and without dispersion (Fogler, 2016)

Due to the dispersion above, there is mixing in the axial direction hence the deviation from ideal PFR. The design equation for the ADR is described by either equation (2.7) or (2.8). The authors defined a dimensionless dispersion coefficient, D_{sp} to account for the degree of mixing. Equation (2.9), also shows that the dispersion coefficient is the inverse of the Peclet number. The equation (2.8) shows that the dispersion coefficient, D_{sp}, can be used in transforming the AXR to either an ideal PFR (at zero dispersion) or an ideal CSTR (at very high dispersion).

$$D_i \frac{d^2C_i}{dz^2} - U\frac{dC_i}{dz} + r_i = 0, 0 \le z \le L \tag{2.7}$$

$$D_{sp} \frac{d^2C_i}{d\lambda^2} - \frac{dC_i}{d\lambda} + \frac{Lr_i}{U} = 0, 0 \le \lambda = \frac{z}{L} \le 1 \tag{2.8}$$

$$D_{sp} = \frac{D_i}{UL} \tag{2.9}$$

The main reason for using such a model is it helps in eliminating binary variables.

2.5.1.2 Recycle reactor

Achenie and Biegler (1990) introduced the use of the recycle reactor in reactor synthesis. At the conceptual level, the recycle reactor is a PFR with a recycle (Figure 2.7). Equations (2.10) and (2.11) state that the volumetric flowrate, Q, for a reaction system with constant density is constant. Equations (2.12) and (2.13) represent the overall and component balances respectively. Equation (2.14) determines the final concentration profile.

Figure 2.7. A recycle reactor (Achenie and Biegler, 1990)

$$Q_1 = Q_4 \tag{2.10}$$

$$Q_2 = Q_3 \tag{2.11}$$

$$Q_2 = Q_1 + RQ_4 = Q_1(R+1) \tag{2.12}$$

$$Q_2 C_{2,i} = Q_1 C_{1,i} + RQ_4 C_{3,i} \tag{2.13}$$

$$C_{2,i} = \frac{C_{1,i}}{R+1} + \frac{RC_{3,i}}{R+1} \tag{2.14}$$

In this reactor, the concentration profile between points 2 and 3 is used to determine the type of reactor. From equation (2.14), it can be seen that varying the recycle rate, R, from 0 to infinity changes the reactor from a PFR to CSTR respectively. For a CSTR, the molar concentration at points two and three are equal due to the complete mixing that occurs in the reactor. This is achieved at high R-values, which renders the first term on the right side of

equation (2.14) insignificant. For a PFR, the concentration at point 2 is equal to the concentration at point 1. This is achieved by small R-values, which renders the second term in equation (2.14) insignificant. The main advantage of using this model is that it helps eliminate the need for the use of binary variables.

2.5.1.3 The two-environment model

The two-environment model was introduced by the study of Ng and Rippin (1965). Conceptually, the two-environment model comprises a reactor with two different types of mixing. These are the segregated environment and the maximum mixed environment (Figure 2.8). In the segregated environment (SEG), molecules of different age do not mix hence is analogous to PFR with multiple product streams. In the maximum mixed environment (MAX), molecules of different ages are allowed to mix hence is analogous to a PFR with multiple feed streams approximating a CSTR (Fogler, 2016). Figure 2.8 shows that the fresh feed enters the framework through the segregated environment. The two-environment model uses a transfer coefficient, *h*, to achieve either a CSTR to a PFR. The transfer coefficient, *h*, is the fraction of molecules transferred from the segregated environment to the maximum mixed. When the transfer coefficient, *h*, is varied from zero to infinity, ideal PFR and CSTRs are simulated. The study of Achenie and Biegler (1988) provided instances of how the two-environment model becomes a PFR. Figure 2.9a shows that the intermediate mixed model becomes a PFR when there is no transfer from the segregated section to the maximum mixedness section. Figure 2.9b shows that the intermediate model is converted to a CSTR when the feed spends no time in the segregated environment but all of it is sent to the maximum mixedness environment. Similar to the use of axial dispersion or recycle reactors, the two-environmental models help in avoiding the use of binary variables.

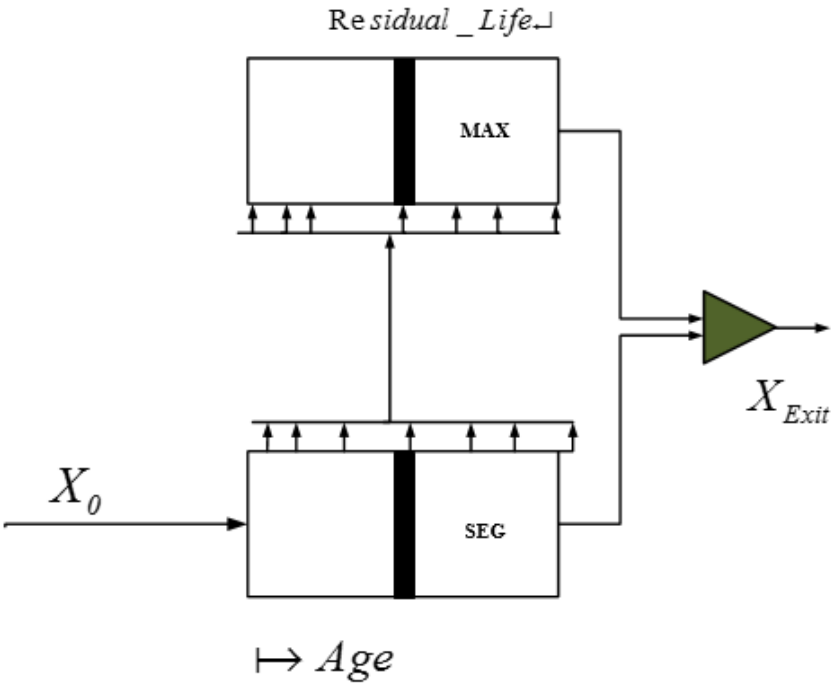

Figure 2.8. The intermediate mixed model (Achenie and Biegler, 1988)

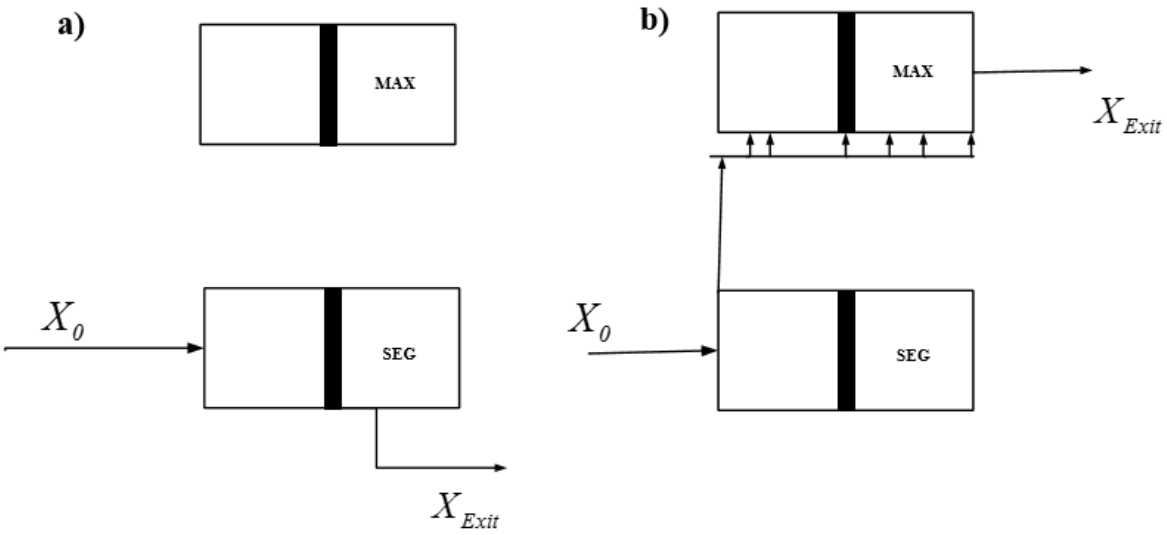

Figure 2.9. A conversion of the intermediate model into a) A PFR b) A CSTR (Achenie and Biegler, 1988)

2.5.1.4 Ideal CSTR and PFR

The main reasons for the development of the aforementioned reactor representation are to avoid the need for discrete decisions in creating CSTR or PFR mixing. If the need to create discrete decisions is accepted, ideal CSTR and PFR can be used as the ideal reactor. Ideal CSTRs and PFRs have been implemented in different reactor synthesis techniques (Glasser et al., 1987; Kokossis and Floudas, 1990). Other studies use CSTR together with generalized forms of a PFR, examples of such are distributed side-stream reactor (Lakshmanan and Biegler, 1996) or a cross-flow reactor (Schweiger and Floudas, 1999).

2.5.2 Choice of reactor synthesis techniques

Reactor network synthesis can be classified as insight-based techniques, constructive approach, and superstructure optimization. Several factors are considered in the choosing or development of a reactor synthesis technique. These factors include simplicity, rigorousness, generality/robustness, tractability, and the ability to interpret results. The strength and weaknesses of these techniques will be analysed based on the aforementioned criteria. Although a single technique cannot incorporate all these factors, the chosen synthesis technique should incorporate as many of these factors as possible. Simple synthesis techniques are desired because they are easy to understand and easy to apply by many users. Such techniques are usually graphical or rule-based. However, this simplicity is usually achieved at the expense of generality. Hence, most simple and elegant techniques are limited in terms of the type of problems that can be solved. Generality or robustness is desired if the purpose of the developed technique is to be applied to as many different types of problems as possible. For example, techniques developed to synthesize non-isothermal reaction systems can also tackle isothermal problems but the converse is not true. Tractability is also an important factor to consider when developing or choosing a reactor synthesis technique. This is especially important in mathematical optimization-based synthesis techniques. The final mathematical formulation

must be solvable by existing optimization solvers. As already stated, a reactor synthesis technique aims to arrive at an optimal design. Hence, rigorousness is a desirable property of the reactor synthesis technique. Rigorousness is the ability of a chosen technique to adequately evaluate all available options.

2.5.3 Insight based techniques

Insight-based techniques are the names ascribed to any synthesis technique that is based on an understanding of the fundamental processes that determine the outcome of chemical reactions. This heuristics approach applies rules-of-thumb that are based on engineering judgment, experience, and a 'wish list' in choosing or determining the final reactor design. This review is limited to the synthesis and design of multiphase reactor design. Krishna and Sie (1994) developed a three-tier hierarchical technique to deduce the reactor configuration that most closely meets the requirement for a multiphase reaction. The performance index for the technique includes multiple objective criteria encompassing yield, operability, safety, the feasibility of scale-up, and capital and operation cost. Figure 2.10 shows that the reactor design stages include catalyst design strategy, feed injection and product dispersion, and choice of the hydrodynamic or mixing regime.

The limitation to the approach implemented here is that it serves as a general guideline rather than arriving at final designs. It also leads to a choice between existing conventional designs but can never generate new designs. There is also no clear criterion on how to deal with conflicting goals if they should exist. The advantage with heuristics is that they allow quick location of reactor designs that often are "near" optimal solutions.

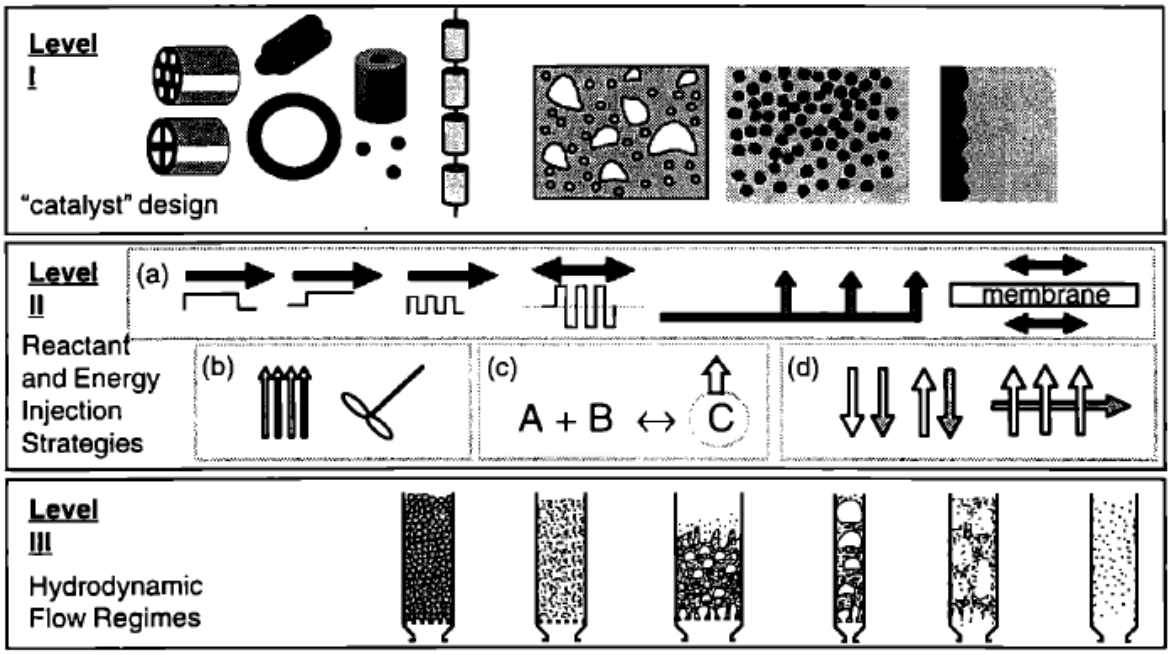

Figure 2.10. Three-level strategy for multi-phase reaction design (Krishna and Sie, 1994)

2.5.4 Constructive approach

This term is used to designate techniques based on the taking of standardized discrete steps to achieve an optimal reactor design. These discrete steps are aimed at either generating the universal set of concentration space or continuously improving the chosen performance index. Because of the stated goal and approach, these techniques need a termination criterion. The two main constructive-based techniques are Attainable Region-based techniques and constructive targeting networks.

2.5.4.1 Attainable Region-based techniques

These techniques are based on the concept of "Attainable region (AR)" by Horn (1964). The Attainable region is the set of all possible concentration points that can be achieved from a given feed point. The idea originated from the work of Horn (1964). However, the study of Glasser et al. (1987) developed the geometric concepts needed for achieving the convex hull of concentrations from a known feed point. This was achieved by reaction and mixing. Figure 2.11 demonstrates the developed geometric technique. The process includes drawing alternate

PFR and CSTR trajectories to cover the attainable region and derive an optimal reactor network. These structures define the boundary of the entire set of all possible achievable states in a system. Objective functions may be overlaid onto the same space and intersection points of the line and the AR boundary can then be determined if certain conditions are satisfied. This intersection points hence act as solutions to the optimisation problem under consideration. There are other geometric techniques such as shrink and wrap (Manousiouthakis et al., 2004) and bounding hyperplanes (Abraham and Feinberg, 2004; Ming et al., 2016).

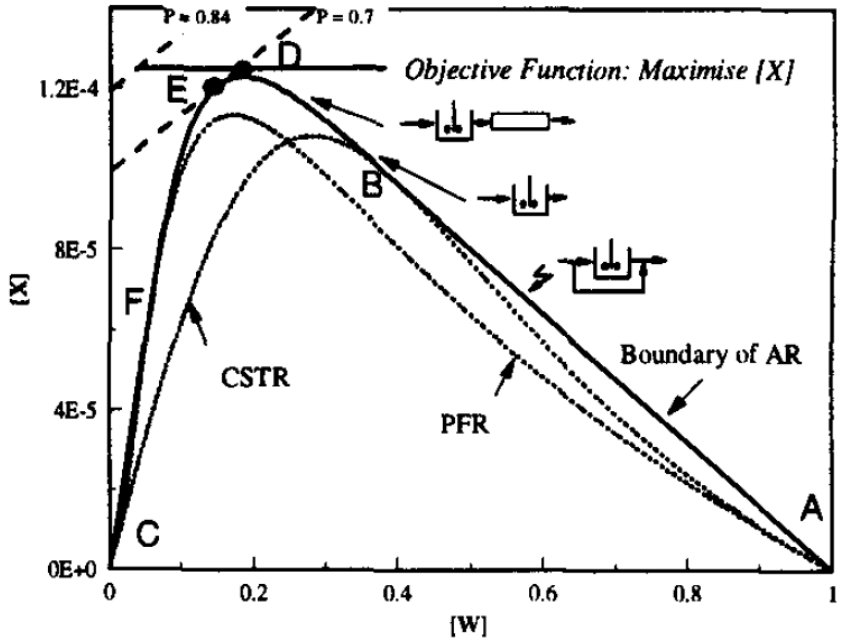

Figure 2.11. AR technique for the synthesis of an optimal reactor system (Glasser and Hildebrandt, 1997)

The advantage of this method is its simplicity and elegance, which usually accompanies graphical techniques. The weaknesses of the graphical technique by Glasser et al. (1987) include difficulty to apply beyond three dimensions, applicable to isothermal problems, and suitable constant density problems. The problem of applicability was solved in the number of mathematical-based AR techniques. The dimensionality challenges faced by geometric techniques are addressed by mathematical-based AR techniques. For example, the study of

Kauchali et al. (2002) developed a linear programming formulation for the generation of the attainable region. This approach loses the simplicity advantage of geometric AR techniques. The study derived stronger conditions for achieving a candidate attainable region. Another mathematical technique that addresses the dimensionality challenge by geometric techniques includes the study of Burri et al. (2002). The study used a novel Infinite Dimensional State-Space (IDEAS) approach for the construction of the AR for a constant density, isothermal reaction system. This technique can construct the AR of a higher-dimensional reactor synthesis problem without the need to visualize. The approach also has the potential of finding a reactor network that delivers the maximum concentration of a component without having to construct the AR. The limitation of the IDEAS technique to constant density systems was addressed in the study of Zhou and Manousiouthakis (2007). This was achieved by replacing the volumetric flowrate used in earlier studies with mass flowrate and molar concentration with the mass fraction. The limitation of the IDEAS technique was also addressed in the study of Zhou and Manousiouthakis (2009) and applied to problems where a constant heat capacity assumption is valid.

In summary, techniques based on the achieving of the AR has undergone a steady evolution to a point where it can be used to solve problems which are non-isothermal and are characterised by variable density fluids. However, there is still no proof that the true attainable region can be attained (Ming et al., 2016). The solved non-isothermal problems are still simplistic since it doesn't consider the effect of temperature on heat capacities, which means that the non-isothermal problems are limiting in scope. Also, the techniques that can handle some of these complexities loses the original simplicity. Another major challenge with the AR techniques is the incorporation of constraints such as minimum temperature or maximum concentration.

2.5.4.2 Constructive targeting techniques

This technique has its roots in a study by Achenie and Biegler (1988) applying the two-environment model of Ng and Rippin (1965). The study (Achenie and Biegler, 1988) comprised of a two-tier optimization technique where an optimal target was achieved using the two-environment model. This is followed by the determination of a reactor configuration to achieve the determined target. The study of Balakrishna and Biegler (1992a) extended the two compartments in Figure 2.8 to a multi-compartment model. Figure 2.12 shows that the multi-compartment mixing model consists of one segregation environment and multiple maximum mixed environments. This covers a vast array of mixing states compared to the two-compartment model when determining the optimal target for isothermal systems.

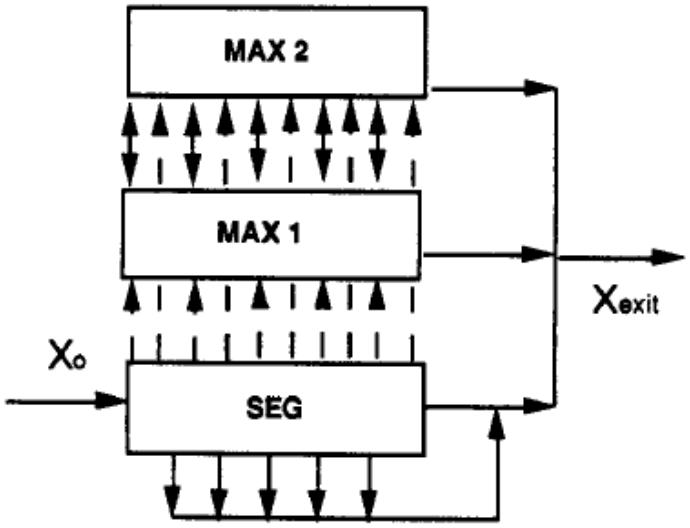

Figure 2.12. Multiple compartments mixing model (Balakrishna and Biegler, 1992)

However, the approach starts with a model containing only a segregated environment. The constructive procedure continues by adding subsequent maximum mixed compartments. Upon each addition, the set of equations is solved to see if there is an improvement in the target. If the objective is improved then the reactor extension was necessary for the network, else the optimal network has been achieved. This approach avoids the need to solve MINLP problems.

This technique was extended to the synthesis of non-isothermal reaction systems in the study of Balakrishna and Biegler (1992b). In the study, the authors used a crossflow reactor in place of the segregated reactor and successive additions of recycle-reactors as options to increase the concentration space. The main advantage of the constructive approach is the complexity of the problem is increased gradually; hence, it avoids the generation of very complex problems. However, this approach can only lead to an increase resulting from successive monotonic increases. This weakness was addressed in the study of Lakshmanan and Biegler (1996). The study developed a new constructive optimization-based technique, which considers multiple reactor paths at each stage as compared to solving the single reactor additions in the previous study. The technique starts with the establishment of a lower bound of the objective function by solving a model based on a segregated environment. After this step, a reactor model made up of a PFR/DSR and CSTR (Figure 2.13) is solved using the solution from the segregated model as initialization points. After the second step, the first reactor module is extended with additional reactor modules using the solution of the first reactor module as initial points. If this extension improves the objective, then further extensions need to be considered, else the optimal network is assumed to have been found. This makes it possible to arrive at optimal solutions with non-monotonic increases. The moves made in these studies (Balakrishna and Biegler, 992 a and b; Lakshmanan and Biegler, 1996) are aimed at creating and increasing the attainable region. However, it has not been proven that by the time the optimization techniques were terminated the attainable region had been achieved.

Rooney and Biegler (2000) revised the mathematical formulation presented by Lakshmanan and Biegler (1996) to enable it to cater for uncertainties associated with reactor synthesis. Formulating the synthesis problem as a multi-period optimization problem, the model was solved over different values of the given parameters. The other change in the study includes the introduction of recycle streams to the original reactor module developed by Lakshmanan

and Biegler (1996), which was intended at increasing the options provided by the reactor modules. The new reactor module can be seen in Figure 2.14.

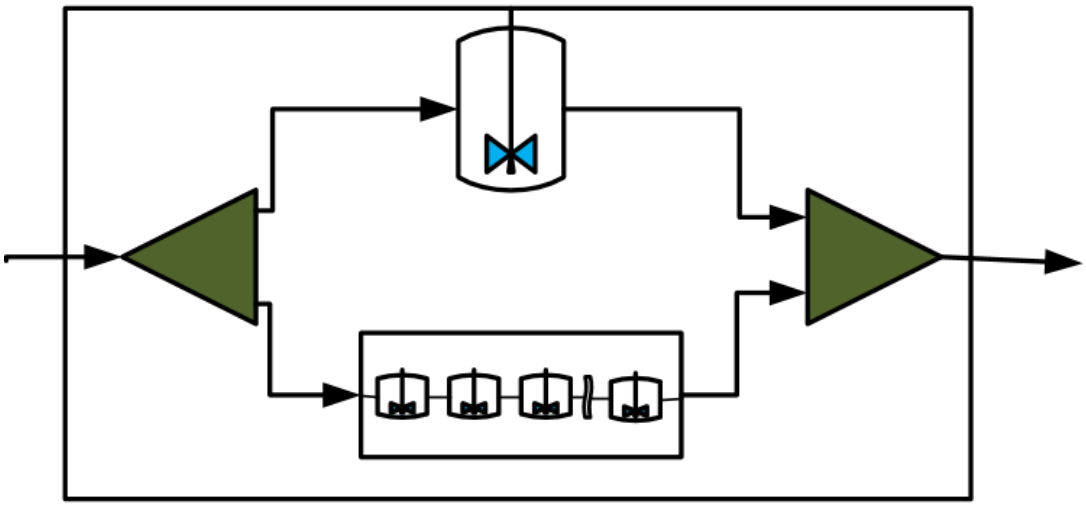

Figure 2.13. A reactor module (Lakshmanan and Biegler, 1996)

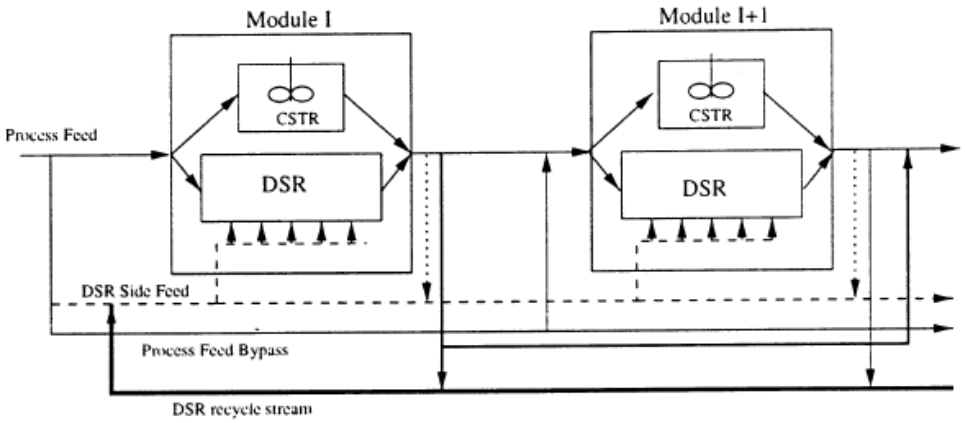

Figure 2.14. Reactor module with recycle streams (Rooney and Biegler, 2000)

Pahor et al. (2000) extended the supposed attainable region generated by the reactor modules during the successive process to enable it to cater to economic criteria such as profit. The study also used an accurate representation of differential-algebraic equations for the modelling of the PFR and Recycle-reactors in the reactor model.

In conclusion, constructive techniques which started with the two-environment models have moved into a hybrid technique that uses superstructure techniques for the direct design of reactors while applying attainable region principles. The main contribution of this technique is to avoid the solving of MINLP problems. The problems have been mostly restricted LP, NLP and very simple MINLP problems. However, the termination criterion for the problem is arbitrary.

2.5.5 Superstructure approach

A superstructure is a framework containing all the possible alternatives available in a reactor synthesis problem. In this technique, the optimal design is a subset of the options provided by the superstructure.

The basis of the use of superstructure optimization as a tool for reactor synthesis can be traced back to the work of Jackson (1968), where a superstructure made up of PFR connected by side streams was used to model the reaction path in a reactor. The study developed a set of algebraic equations that related changes in reactor performance to small changes in the mixing pattern, or flow configuration, of the system in which the reactions are carried out. However, the study did not include reactors with perfect mixing.

This was addressed in the study of Ravimohan (1971) which extended the work of Jackson (1968) by incorporating a single CSTR into the superstructure of PFRs. The developed mathematical formulation was applied to the Van de Vusse reaction scheme. The final mathematical model was solved manually. The main output of the formulation was determining the optimal location of the CSTR in the reactor network. However, in the formulation, the addition of a continuous stirred tank reactor (CSTR) to the network was a discrete decision and the optimization algorithm could not consider the CSTR volume automatically. To avoid this difficulty, Chitra and Govind (1981) replaced the CSTR in the study of Ravimohan (1971) with

a recycle-reactor. As explained in section 2.5.1.2, the recycle ratio of a recycle reactor can be used as a decision variable to achieve either a CSTR and a PFR.

The need to avoid discrete decisions was also achieved by Paynter and Haskins (1970) using an axial dispersion reactor model. As described in section 2.5.1.1, the dimensionless dispersion coefficient, D_{sp}, is a continuous function of position in the reactor. However, the authors used the values of the derivative of the dispersion coefficient in setting the bounds instead of the dispersion coefficient itself. This made it difficult for the dispersion coefficient to observe the right bounds.

To avoid some of the problems associated with the Paynter and Haskins (1970) formulation. Achenie and Biegler (1986) suggested a network of axial dispersion reactors in which a dispersion coefficient was used as the determinant of reactor type. In addition to ensuring that the dispersion coefficient, D_{sp}, observed the appropriate bounds, the formulation could account for non-isothermal effects. Although this formulation avoids the need for discrete variables, there is no universal way for the determination of bounds of the dispersion coefficient for all reaction systems. This technique is also challenged with the problem of deciding what type of reactor is to be used when the optimal dispersion coefficient falls in between the values for a CSTR and a PFR. In addition, the dispersion model may not be appropriate for all reacting systems. Some of the challenges enumerated in this study were addressed in the study of Achenie and Biegler (1990). In this, the authors replaced the axial dispersion reactor in the superstructure with the recycle-reactor. The recycle ratio, R, was the decision variable that determined the type of reactor. This eliminated the arbitrariness which comes with the use of the dispersion coefficient. As can be seen from Figure 2.15, the superstructure for the aforementioned study consists of recycle-reactors and heat exchangers. The use of the recycle-reactors ensures that the resulting mathematical formulation is an NLP.

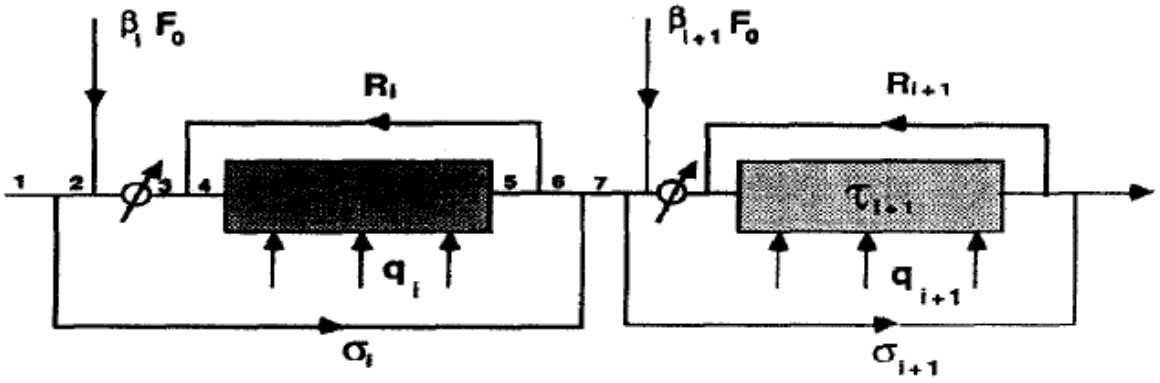

Figure 2.15. The recycle reactor superstructure (Achenie and Biegler, 1990)

This approach has the advantage of being more universally applied compared to the axial dispersion reactor. However, how to interpret which reactor configuration can be assigned to all values of the recycle ratio remains a challenge. Other minor limitations of this study include the development of the model based on a constant density system and the assumption of constant heat capacities.

The challenges faced in the choice of reactor configuration in the NLP-based reactor synthesis models (Achenie and Biegler, 1986, 1990) are addressed by using MINLP formulations. In such formulations, the potential existence of each reactor unit is achieved using binary variables. This eliminates the difficulties in the interpretation of results faced in interpreting final designs. An example of the application of such a technique is the work of Kokossis and Floudas (1990). In the study, a reactor network superstructure of CSTRs and PFRs was used. The study eliminated the need for differential-algebraic equations by modelling a PFR as a series of CSTRs. The mathematical formulation representing the proposed superstructure is an MINLP formulation. To be able to use the MINLP approach to synthesize non-isothermal reaction systems, the study of Kokossis and Floudas (1994) replaced the PFRs in the previous structure with a series of sub-PFRs units known as Basic Non-isothermal Unit (BNU). Figure 2.16 shows that a BNU is a series of CSTRs preceded by a heat exchanger enabling the direct

heating or cooling of that specific section of the PFR. There are also bypass streams enabling indirect heating and cooling along BNU.

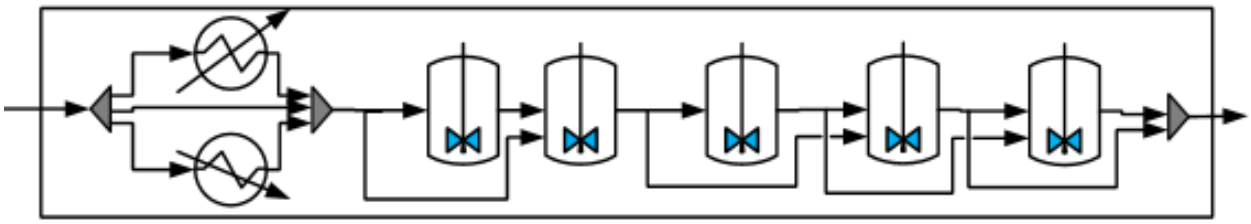

Figure 2.16. Temperature control in a BNU (Kokossis and Floudas, 1994)

To increase the options provided by the superstructure in an MINLP formulation in a compact manner, the study of Schweiger and Floudas (1999) replaced the PFRs in the study of Kokossis and Floudas (1990, 1994) with cross-flow reactors. The study also differed from the previous studies by modelling the differential reactors with differential-algebraic equations instead of approximating them with a series of the CSTRs. The solution methodology for the mathematical formulation was based on the discretization of selected parameters. These changes increase the options provided by the superstructure.

Although most of the non-isothermal techniques are also suitable for the synthesis of heterogeneous systems with radial mixing, the study of Mehta and Kokossis (1997, 1998) extended the existing techniques to the synthesis of the multi-phase systems involving the mass transfer between the existing phases. As shown in Figure 2.17, the developed superstructure involved two networks of reactor compartments. Each of the networks represents the two phases present. A shadow network exists to account for mass transfer between the phases. The mathematical formulation led to a very large MINLP which necessitated the use of stochastic optimization techniques.

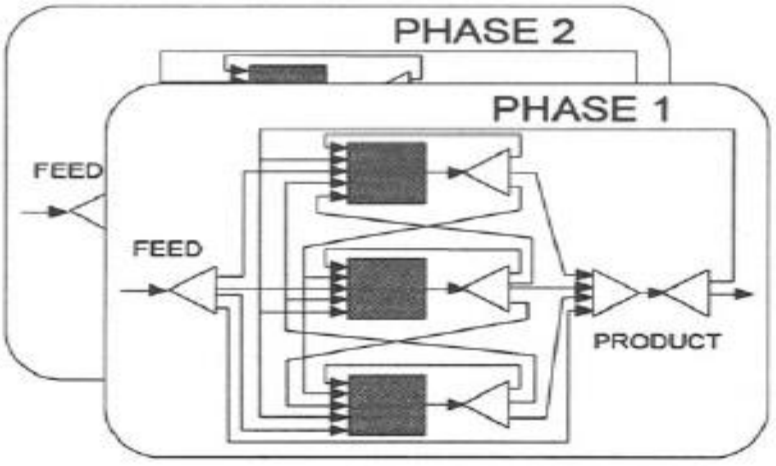

Figure 2.17. Multi-phase reactor network (Mehta and Kokossis, 1997)

Other studies (Kokossis and Floudas, 1991; Marcoulaki et al., 2001) have focused on the synthesis of a combined reactor and separation system.

Superstructure optimization is a very rigorous and robust technique. The method has the advantage of simultaneously generating reactor networks, sizes of reactors and flow rates of interconnecting streams while optimizing the performance index. There is also the ease of introducing new constraints to achieve specific objectives. The main criticism of the superstructure approach is the fact that the solutions are only as good as the richness of the original superstructure as compared to the constructive approaches, which are not restrained until further structure improvement cannot be obtained. However, it is the view of the author of this study that this criticism is of theoretical value. All practical optimization problems are of a constrained nature i.e. the optimal design is found subject to some conditions. These constraints are not only limited to mass and energy balances but also temperature ranges and maximum volumes allowed. Hence, the optimal being sought during a constrained optimization is not a theoretical one but a practical one, which lies in the search space defined by the mathematical formulation. During the development of mathematical equations, the constraints are set up such that final designs are practical and interpretable. Hence this study

chose the superstructure approach as the basis for developing a novel optimization technique for the synthesis and design of an EFG. The details of the technique are explained in Chapter 3.

The rest of the literature review focuses on the available solution techniques for the mathematical formulations resulting from setting up the optimization problems.

2.6 Solution techniques

Solution techniques is the term used in describing the algorithms that search the problem space in order to determine the optimal solutions. The mathematical formulation that will result from the modelling of the superstructure of ideal reactors will result in a multi-variable optimization problem. Solution techniques for multi-variable optimization are either stochastic or deterministic (Smith, 2005).

2.6.1Stochastic techniques

Stochastic or heuristic optimization techniques are methods that determine the solution of an optimization problem by iteratively trying to improve a candidate solution with regard to a given measure of quality. These techniques make few or no assumptions about the problem being optimized (Wang and Chen, 2013). Stochastic techniques mostly depend on the objective function. Stochastic techniques make improvement of the objective function an ultimate goal instead of an immediate goal. This helps reduce the probability of a search being trapped in a local solution (Smith, 2005). Stochastic techniques can search large spaces of candidate solutions toward finding optimal or near-optimal solutions at a reasonable computational cost without being able to guarantee either feasibility or optimality, or even in many cases to state how close to, optimality a particular feasible solution is.

These methods often try to mimic a natural or physical occurrence such as the annealing, genetic algorithms. Examples of stochastic techniques include Tabu search (TS), ant colonies, scatter search, simulated annealing, genetic and evolutionary algorithm. Of these, simulated annealing and genetic algorithm are two of the most popular stochastic algorithms. Stochastic optimization techniques have been used in the synthesis of reactor systems (Mehta and Kokossis, 1997). The major challenge in using a stochastic technique is the struggle faced in optimizing problems involving both continuous variables (e.g. temperature and pressure) and structural changes. These algorithms take finite steps for the continuous variables and do not necessarily find the exact value for the optimum setting. There is also the need to readapt stochastic algorithms for different optimization problems. This may also require the need for the researcher to have highly advanced coding skills.

2.6.2 Deterministic techniques

Deterministic or exact optimization techniques that find optimization based on theoretical techniques rooted in linear algebra, direct search methods and differentials. These techniques are designed to test for conditions of optimality (Smith, 2005). When the synthesis problem to be optimized contains both continuous and integer variables, the solution algorithms contains sub-techniques to solve LP, NLP and integer problems. Example of such methods includes Branch and Bound (BB) methods, cutting planes methods, Generalized Benders decomposition and the Outer-approximation method. The next sections will briefly elaborate on some of the most common solution algorithms.

2.6.2.1 Branch and Bound

The branch and bound technique is an approach based on the principle that the total set of solutions can be partitioned into a smaller subset of solutions, which can be evaluated until the best solution is found. This method starts by relaxing the integrality requirements of the binary variables, which leads to NLP or LP optimization problems. Because the relaxed solution is

less constrained than the true mixed integer solution it will, in general, give a better value for the objective function than the true mixed integer solution. This value then serves as either a lower bound (during minimization) or an upper bound (during maximization) to the true optimization problem. It then continues by performing a tree enumeration (branching) where a subset of the binary variables are successively fixed at each node. The solution of the corresponding NLP or LP at each node provides a lower bound for the optimal MINLP objective function value (Beale, 1977).

The branching can either take place through the depth-first approach or the breadth-first approach. The depth-first approach performs branching on the most recently created node within the tree. If no nodes are expanded, the method then backtracks to a node whose successor has not been examined. The breadth-first approach, however, selects a node with the best value at each level and then expands on all its successor nodes. The breadth-first approach requires examination of fewer nodes and backtracking is also not required. The depth-first approach, however, requires less storage and can find the optimal solution early in the enumeration procedure (Smith, 2005).

The major disadvantage of the branch and bound method is that it may require the solution of a relatively large number of NLP sub-problems which cannot be updated as readily as in the linear case where few pivot operations are required to update the LP solution of a new node. On the other hand, if the MINLP has a tight NLP relaxation the number of nodes to be enumerated may be modest. In the limiting case where the NLP relaxation exhibits 0-1 solution for the binary variables (convex hull formulation), only one single NLP problem needs to be solved (Grossman, 1990).

2.6.2.2 Generalized Benders Decomposition and Outer Approximation

The Generalized Benders Decomposition (GBD) and Outer-Approximation (OA) algorithm consist of solving at each major iteration as an NLP sub-problem (with all binary variables fixed) and a MILP master problem. The NLP sub-problems have the role of optimizing the continuous variables and providing an upper bound to the optimal MINLP solution. The MILP master problems have the role of predicting a lower bound to the MINLP as well as new 0-1 variable values for each major iteration. The predicted lower bounds increase monotonically as the cycle of major iterations proceeds, and the search is terminated when the predicted lower bound coincides or exceeds the current upper bound (Benders, 1967, Grossmann, 1990).

The main difference between the GBD and OA methods lies in the definition of the MILP master problem. In the case of GBD, it is given by a dual representation of the continuous space, while in the case of the OA it is given by a primal approximation (Duran and Grossman,1986).

2.7 Summary

There have been studies focusing on generating different IGCC flowsheets. These studies prove that flowsheet synthesis can improve the efficiency of the IGCC process. However, none of these studies achieved the flowsheet synthesis via EFG design. Hence, this study focused on using gasifier optimization as a means of generating new IGCC flowsheets. Hence a review on the optimization of entrained flow gasifiers was conducted. The studies show that there have been several attempts made at improving the performance of an Entrained flow gasifier. It has always started with the level of details in gasifier modelling. What can be concluded from these studies is the fact that kinetic, RNM and CFD models can account for the carbon conversion, gasifier exit temperature and final syngas composition from a given reactor feed to a fair degree of accuracy. However, until this research, the effect of gasifier configuration on its performance has not been explored. Given a specific coal feed, there is no standard technique or process to

determine what the gasifier design should be. This study elects to develop a superstructure optimization technique in the synthesis and design of an EFG. This is because the use of heuristic techniques does not guarantee the optimality of the final design and does not provide clear guidelines for the resolution of conflicting goals. The use of superstructure optimization involves the following major components: a graphical representation of the space of alternatives; formulation of optimization model and application of solution method. The use of this technique for reactor synthesis requires the choice of representation of the basic mixing units in the reactor. The existing representations of the type of mixing that exist in literature have been reviewed and the use of ideal CSTRs and PFRs have been selected due to its advantages over other types of representation. The final decision is the choice of a solution algorithm. The major choices for solution techniques are either stochastic or deterministic techniques. Both techniques have their strengths and weaknesses but the choice is constrained by the availability of commercial software codes for the solution algorithms. The software used in this study applies the OA technique.

References

Abraham T.K., Feinberg, M., 2004. Kinetic Bounds on Attainability in the Reactor Synthesis Problem. *Ind. Eng. Chem. Res***,** 43, pp. 449-457.

Achenie, L. E. K., Biegler, L. T. 1986. Algorithmic Synthesis of Chemical Reactor Networks Using Mathematical Programming. *Ind. Eng. Chem. Fundam.*, 25, pp. 621-627.

Achenie, L. E. K., Biegler, L. T. 1988. Developing Targets for the Performance Index of a Chemical Reactor Network. *Ind. Eng. Chem. Fundam.*, 27, pp.1811-1821.

Achenie, L. E. K., Biegler, L. T. 1990. Superstructure Based Approach to Chemical Reactor Network Synthesis. *Comput. Chem. Eng.*, 14, 1, pp. 23-40.

Adschiri T, Shiraha T, Kojima T, Furusawa T., 1986. Prediction of CO_2 Gasification Rate of Char in Fluidized-bed Gasifier. *Fuel*, 65, pp.1688–1693.

Anand, A. K., Cook, C. S., Corman, J. C., Smith, A. R., 1996. New Technology Trends for Improved IGCC System Performance. *Journal of Engineering for Gas Turbines and Power*,118, pp.732–736.

Balakrishna, S., Biegler, L. T., 1992. Constructive Targeting Approaches for the Synthesis of Chemical Reactor Networks. *Ind. Eng. Chem. Res.* , 31(1), pp. 300-312.

Balakrishna, S., Biegler, L. T., 1992. Targeting Strategies for Synthesis and Energy Integration of Nonisothermal Reactor Networks. *Ind. Eng. Chem. Res, 31* (9), pp. 2152-2164.

Badzioch, S., Hawksley, P.G.W., 1970. Kinetics of Thermal Decomposition of Pulverized Coal Particles. *Ind. Eng. Chem. Process Des. Develop*, 9(4), pp. 521-530

Beale, E.M.L., 1977. Integer Programming. The State of the Art in Numerical Analysis, *Academic Press*, pp. 409-448.

Benders, J.F., 1962. Partitioning Procedures for Solving Mixed-variables Programming Problems. *Numerische Mathematik*, 4, pp. 238-252.

Bhattacharyya, D., Turton, R., Zitney, S. E., 2011. Steady-State Simulation and Optimization of an Integrated Gasification Combined Cycle. *Ind. Eng. Chem. Res.*, 50, pp. 1674–1690.

Bhatia, S. K., Perlmutter, D. D., 1980. A Random Pore Model for Fluid-Solid Reactions: 1. Isothermal, Kinetic Control. *AIChE,* 26(3), pp. 379-385.

Bhatia, S. K., Perlmutter, P. D., 1981. A Random Pore Model for Fluid-Solid Reactions: II. Diffusion and Transport Effects. *AIChE Journal,* 27(2), pp. 247-254.

Bhatia, S. K., Vartak, B. J., 1996. Reaction of Microporous Solids: The Discrete Random Pore Model. *Carbon,* 34(11), pp. 1383-1391.

Biagini, E., Bardi, A., Pannocchia, G., Tognotti, L., 2009. Development of an Entrained Flow Gasifier Model for Process Optimization. *Ind. Eng. Chem. Res,* 48(19), pp. 9028-9033.

Bockelie, M.J., Denison, M.K., Chen, Z., Linjewile, T., Senior, C.L., Sarofim, A.F. Holt, N., 2002. CFD modelling for Entrained Flow Gasifiers. Proceedings of the Gasification Technologies Conference 2002, San Francisco, CA, Oct.28-30, 2002(e).

Burri, J. F., Wilson, S. D., Manousiouthakis, V. I., 2002. Infinite Dimensional State-space Approach to Reactor Network Synthesis: Application to Attainable Region Construction. *Computers and Chemical Engineering*, 26, pp. 849-862.

Chen, C., Horio, M., Kojima, T., 2000. Numerical Simulation of Entrained Flow Coal Gasifiers. Part I: Modelling of Coal Gasification in an Entrained Flow Gasifier. *Chemical Engineering Science,* 55, pp. 3861-3874.

Chitra, S.P., Govind, R. 1981. Yield Optimization for Complex Reactor Systems. *Chemical Engineering Science,* 36, pp. 1219-1225

Choi, Y. C. Li, X. Y., Park, T., Kim, J. H., Lee, J. G., 2001. Numerical Study of Coal Gasification Characteristics in an Entrained Flow Gasifier. *Fuel,* 80, pp. 2193-2201.

Daichendt M.M., Grossmann, I.E., 1997. Integration of Hierarchical Decomposition and Mathematical Programming for the Synthesis of Process Flowsheets. *Computers chem. Engng*, 22(1-2), pp. 147-175.

Diwekar, U.M., Frey, H.C., Rubin, E.S., 1992, Synthesizing optimal flowsheets: Applications to IGCC System Environmental Control, *Ind. Eng. Chem. Res.* , 31, pp. 1927-1936.

Duran, M.A. and Grossmann, I. E.,1986. An Outer-Approximation Algorithm for a Class of Mixed-Integer Nonlinear Programs. *Mathematical Programming*, 36, pp. 307-339.

Eisermann W., Johnson P., Conger W.L.,1980. Estimating Thermodynamic Properties of Coal, Char, Tar and Ash. *Fuel Processing Technology*, 3, pp.39-53

Emun, F., Gadallaa, M., Majozi, T. and Boer, D., 2010. Integrated Gasification Combined Cycle (IGCC) Process Simulation and Optimization. *Computers and Chemical Engineering*, 34(3), pp. 331–338.

Frey, H. C., Zhu, Y., 2006. Improved System Integration for Integrated Gasification Combined Cycle (IGCC) Systems. *Environmental Science and Technology*, February, 40(5), pp. 1693–1699.

Fogler, H. S., 2016. Elements of Chemical Reaction Engineering. Prentice-Hall International, Inc. Fifth Edition. pp. 767-883.

Gardner N., Samuels E., Wilks K., 1974. Catalysed Hydrogasification of Coal Chars. *Adv. Chem. Ser.*, 131 pp. 217–236.

Gazzani M, Manzolini G, Macchi E, Ghoniem A.F.2013. Reduced Order Modelling of the Shell–Prenflo Entrained Flow Gasifier. *Fuel*, 101, pp 822–837

Giuffrida, A., Romano, C. R., Lozza, G., 2011. Thermodynamic Analysis of Air-blown Gasification for IGCC Applications. *Applied Energy*, 88, pp. 3949–3958.

Giuffrida, A., Romano, M. C., Lozza, G., 2013. Efficiency enhancement in IGGC power plants with air-blown gasification and hot gas clean-up. *Energy*, 53, pp. 221-229.

Glasser, D., Hildebrandt, D. Crowe, C., 1987. A Geometric Approach to Steady Flow Reactors: The Attainable Region and Optimization in Concentration Space. *Ind. Eng. Chem. Res*., 9, pp. 26.

Glasser, D., Hildebrandt, D., 1997. Reactor and Process Synthesis. *Computers chem. Engng*, 21, Suppl. pp. 775-783

Grant, D.M., Pugmire R.J., Fletcher, T.H., Kerstein, A.R., 1989. Chemical Model of Coal Devolatilization Using Percolation Lattice Statistics. *Energy & Fuels*, 3, pp. 175-186

Gomez-Berea, A., Leckner, B., 2010. Modelling of Biomass Gasification in Fluidized Bed. *Progress in Energy and Combustion Science*, 36, pp. 444–509.

Govind R., Shah J., 1984. Modelling and Simulation of an Entrained Flow Gasifier. *AIChE Journal*, 33(1), pp. 79-92

Grossmann I. E. 1990, MINLP Optimization Strategies and Algorithms for Process Synthesis. Proceedings FOCAPD'89 Cot& pp. 105-132.

Gupta, O.K.,1980. Branch and Bound Experiments in Nonlinear Integer Programming. PhD. Thesis, Purdue University.

Hildebrandt, D., Glasser, D., Crowe, C., 1990. The Geometry of the Attainable Region Generated by Reaction and Mixing with and without Constraints. *Ind. Eng. Chem. Res.*, *29* (1), pp. 49-58.

Higman, C., van der Burgt, M., 2003. Gasification: Elsevier Science, pp. 50-52, 120-124

Higman, C., 2013. State of the Gasification Industry–the Updated Worldwide Gasification Database. Proceedings of International Pittsburgh Coal Conference, Beijing.

Horn, F. (1964). Attainable and Non-attainable Regions in Chemical Reaction Technique. Third European Symposium on Chemical Reaction Engineering. London: Pergamon Press. pp. 123–138.

Hua, K., Li, Y., Hu, S., She, J., 2000. Three-distribution-parameter General Model for Reactor Network Synthesis. *Computers and Chemical Engineering,* 24, pp. 217-223.

Jackson, R., 1968. Optimization of chemical Reactors with Respect to Flow Configuration. *Journal of Optimal Theory and Application,* 2(4), pp. 240-259

Jacobs, R., Jansweijer, W., 2000. A knowledge-based System for Reactor Selection. *Computers and Chemical Engineering,* 24, pp. 1781-1801.

Jeong, H. J., Seo, D. K., Hwang, J., 2014. CFD Modelling for Coal Size Effect on Coal Gasification in A Two-stage Commercial Entrained-bed Gasifier with an Improved Char Gasification Model. *Applied Energy*, 123, pp. 29-36.

Jiang, L., Lin R., Jin, H., Cai, R., Liu, Z., 2002. Study on Thermodynamic Characteristics and Optimization of Steam Cycle System in IGCC. *Energy Conversion and Management,* 43, pp. 1339-1348.

Johnson J. L., 1979. Kinetics of Coal Gasification. New York: Wiley

Jones, D., Bhattacharyya, D., Turton, R. and Zitney, S. E., 2011. Optimal Design and Integration of an Air Separation Unit (ASU) for an Integrated Gasification Combined Cycle (IGCC) Power Plant with CO2 Capture. *Fuel Processing Technology*, 92(9), pp. 1685–1695.

Ju, Y., Lee, C.H., 2017. Evaluation of the Energy Efficiency of the Shell Coal Gasification Process. *Energy Conversion and Management*, 143, pp. 123–136.

Kajitani, S., Hara, S., Matsuda, H., 2002. Gasification Rate Analysis of Coal Char with a Pressurized Drop Tube Furnace. *Fuel,* 81, pp. 539-546.

Kasaoka S, Sakata Y, Tong C., 1985. Kinetic Evaluation of the Reactivity of Various Coal Chars for Gasification with Carbon Dioxide in Comparison with Steam. *Int. Chem. Eng.*, 25, pp.160–175.

Kasule, J. S., Turton, R., Bhattacharyya, D., Zitney, S. E., 2012. Mathematical Modelling of a Single-stage, Down-firing, Entrained-flow Gasifier. *Industrial and Engineering chemistry research*, 51, pp. 6429-6440.

Kauchali, S., Rooney W.C., Biegler L.T., Glasser D., Hildebrandt, D., 2002. Linear Programming Formulations for Attainable Region Analysis. *Chemical Engineering Science*, 57, pp. 2015 – 2028.

Kokossis, A. C., Floudas, C. A., 1990. Optimization of Complex Reactor Networks-I. Isothermal Operations. *Chemical Engineering Science*, 45(3), pp. 595-614.

Kokossis A.C., Floudas, C.A., 1990. Synthesis of Isothermal Reactor-separator-recycle Streams. *Chemical Engineering Science,* 46 (516), pp. 1361-1383

Kokossis, A. C., Floudas, C. A., 1994. Optimization of Complex Reactor Networks-II. Non-isothermal Operation. *Chemical Engineering Science*, 49(7), pp. 1037-1051.

Krishna, R., Sie, S. T., 1994. Strategies for Multiphase Reactor Selection. *Chemical Engineering Science*, 49(24A), pp. 4029-4065.

Lakshmanan, A., Biegler, L. T., 1996. Synthesis of Optimal Chemical Reactor Networks. *Ind. Eng. Chem. Res.*, 35, pp. 1344-1353.

Lang Y. Zitney S.E. Biegler L.T., 2011. Optimization of IGCC Processes with Reduced order CFD models. *Computers and chemical engineering*, 35, pp. 1705– 1717.

Laurendeau N. M., 1978. Heterogeneous Kinetics of Coal Char Gasification and Combustion. *Prog. Energy Combust Sci.*, 4, pp. 221–270.

Lee, C., Lee, S. J., Yun, Y., 2007. Effect of Air Separation Unit Integration on Integrated Gasification Combined Cycle Performance and NOx Emission Characteristics. *Korean Journal of Chemical Engineering*, 24(2), pp. 368-373.

Lee, H., Choi, S., Paek, M., 2010. A Simple Process Modelling for a Dry-feeding Entrained Bed Coal Gasifier. *Proc.IMechE Part A: J Power and Energy,* 225, pp. 74-84.

Lee, H.H., Lee, J.C., Joo, Y.J., Oh M., Lee C.H., 2014. Dynamic Modelling of Shell Entrained Flow Gasifier in an Integrated Gasification Combined Cycle Process. *Applied Energy*,131. pp. 425–440

Lima, F. V., Daoutidis, P., Tsapatsis, M., 2016. Modelling, Optimization, and Cost Analysis of an IGCC plant with a Membrane Reactor for Carbon Capture. *AIChE Journal*, 62(5), pp. 1568-1580.

Liu, X. J., Zhang, W. R., Park, T. J., 2001. Modelling Coal Gasification in an Entrained flow. *Combust. Theory Modelling*, 5, pp. 595–608.

Loison, R., Chauvin, R., 1964. "Pyrolise Rapide du Charbon". *Chimie et Industrie,* 91, pp. 269.

Madzivhandila, V. A., Majozi, T., Zhelev, T. K., 2009. Process Integration as an Optimization tool in Clean Coal Technology. A Focus on IGCC. *Chemical Engineering Transactions*, 18, pp. 941-946.

Maffei, T., 2013. Kinetic Model for Coal Combustion. (PhD Thesis). Millan. Politecnico Di Milano.

Mahinpey, N., Gomez, A., 2016. Review of Gasification Fundamentals and New Findings: Reactors, Feedstock, and Kinetic Studies. *Chemical Engineering Science*, 148, pp. 14–31.

Majoumerd, M. M., De, S., Assadi, M., Brehaus, P., 2012. An EU Initiative for Future Generation of IGCC Power Plants Using Hydrogen-rich Syngas: Simulation Results for the Baseline Configuration. *Applied Energy*, 99, pp. 280-290.

Majoumerd, M. M., Raas, H., De, S. Assadi, M., 2014. Estimation of Performance Variation of Future Generation IGCC with Coal Quality and Gasification Process – Simulation Results of EU H_2-IGCC project. *Applied Energy*, 113, pp. 452–462.

Manousiouthakis, V.I., Justanieah, A.M. Taylor, L.A., 2004. The Shrink–Wrap Algorithm for the Construction of the Attainable Region: An Application of the IDEAS Framework. *Computers and Chemical Engineering*, 28, pp. 1563–1575.

Marcoulaki, E., Linke, P. and Kokossis, A., 2001. Design of Separation Trains and Reaction-Separation Networks Using Stochastic Optimization Methods. *Trans IChemE*, 79(Part A), pp. 25-32.

Maurstad, O. 2005. An Overview of Coal Based Integrated Gasification Combined Cycle (IGCC) Technology; MIT LFEE 2005-002 WP; Massachusetts Institute of Technology: Cambridge, MA.

Maurstad, O., Herzog H, Bolland O, Beér J., 2006. Impact of Coal Quality and Gasifier Technology on IGCC Performance. In: 8th international conference on greenhouse gas control technologies (GHGT8), Trondheim, Norway.

McDaniel, J., 2002. Tampa Electric Polk Power Station Integrated Gasification Combined Cycle Project. Final Technical Report. (Morgantown, WV: US Department of Energy Office of fossil energy, National Energy Technology Laboratory).

Mehta, V. L., Kokossis, A., 1997. Development of Novel Multiphase Reactors Using a Systematic Design Framework. *Computers chem. Engng*, 21, pp. S325-S330.

Mehta, V. L., Kokossis, A., 1998. New Generation Tools for Multiphase Reaction Systems: A Validated Systematic Methodology for Novelty and Design Automation. *Computers chem. Engng*., 22, pp. S119-S126.

Merrick, D., 1983. Mathematical models of the thermal decomposition of coal. *Fuel,* 62, pp. 534-539.

Ming, D., 2014. A Parallel Attainable Region Construction Method Suitable for Implementation on a Graphics Processing Unit (GPU). *Computers and Chemical Engineering,* 67, pp. 103–120.

Ming D., Glasser D., Hildebrandt D., Glasser B., Metzger M., 2016. Attainable Region Theory: An Introduction to Choosing an Optimal Reactor. Wiley.

Monaghan, R.F.D., 2010. Dynamic Reduced Order Modeling of Entrained Flow Gasifiers. (PhD thesis). Cambridge (MA): Massachusetts Institute of Technology.

Monaghan, R. F. D., Ghoniem, A. F., 2012. A Dynamic Reduced Order Model for Simulating Entrained Flow Gasifiers: Part I: Model Development and Description. *Fuel*, 91(1), pp. 61-80.

Monaghan, R. F. D., Ghoniem, A. F., 2012. A Dynamic Reduced-order Model for Simulating Entrained Flow Gasifiers: Part II: Model Validation and Sensitivity Analysis. *Fuel*, 94, pp.280-297.

Mvelase, B. E., 2016. Optimization of the Integrated Gasification Combined Cycle Using Mathematical Modelling. (PhD thesis) Johannesburg: University of the Witwatersrand.

Ng, D. Y. C., Rippin, D. W. T., 1965. The Effect of Incomplete Mixing on Conversion in Homogeneous Reactions. *Third Symposium on Chemical Reaction Engineering*, Pergamon.

Ni, Q., Williams, A., 1995. A Simulation Study on the Performance of an Entrained-flow Coal Gasifier. *Fuel,* 74(1), pp. 102-110.

Niksa, S., Kerstein, A.R., 1991. FLASHCHAIN Theory for Rapid Coal Devolatilization Kinetics. 1. Formulation. *Energy & Fuels*, 5, pp. 647-665

Ollero P., Serrera A., Arjona R., Alcantarilla S., 2003. The CO_2 Gasification kinetics of Olive Waste. *Biomass and Bioenergy*, 24, pp.151–61.

Pahor, B., Irsic, N., and Kravanja, Z., 2000. MINLP Synthesis and Modified Attainable Region Analysis of Reactor Networks in Overall Process Schemes Using More Compact Reactor Superstructure. *Computers and Chemical Engineering*, 24(2–6), pp. 1403–1408.

Paynter, J. D., Haskins, D. E., 1970. Determination of Optimal Reactor Type. *Chem. Eng. Sci.*, *25*, pp. 1415-1422.

Pedersen, L. S., Breithaptb, P., Dam-Johansen, K., Weber, R., 1997. Residence Time Distributions in Confined Swirling Flames. *Combustion Science and Technology*, 127, pp. 251-273.

Pedersen, L. S. Glarborg, P., Dam-Johansen, K., Hepburn, P. W., Hesselmann, G.,1998. A Chemical Engineering Model for Predicting NO Emissions and Burnout from Pulverised Coal Flames. *Combustion Science and Technology*, 132(1), pp. 251-314.

Perez-Fortes, M., Bojarski, A. D., Velo, E. and Nouges, J. M., 2009. Conceptual model and Evaluation of Generated Power and Emissions in an IGCC Plant. *Energy*, 34(10), pp. 1721-1732.

Puig-Arnavat, M., Hernández J.A., Bruno J.C., Coronas, A., 2013. Artificial Neural Network Models for Biomass Gasification in Fluidized Bed Gasifiers. *Biomass and Bioenergy*, 49, pp. 279-289

Rubiera, F., Pis, J.J., Pevida, C., 2011. Raw Materials, Selection, Preparation and Characterization. In Puigjaner, L. Syngas from waste. Emerging technologies. *Springer*. Pp. 11-22

Ravimohan, A. L., 1971. Optimization of Chemical Reactor Networks with Respect to Flow Configuration. *Journal of Optimization Theory and Applications*, 8(3), pp. 204-211.

Rooney W. C., Biegler L.T., 2000 Multiperiod Reactor Network Synthesis. *Computers and Chemical Engineering* 24. pp. 2055–2068.

Rubin, E.S., Diwekar, U.M., 1997. A New Approach for IGCC Process Synthesis Under Uncertainty. *International Joint Power Generation Conference*, American Society of Mechanical Engineers, pp.1-7.

Sahraei, H. M., Duchesne M.A., Yandoh R., Majeski A., Hughes R.W., Richardez-Sandoval., L.A., 2015. Reduced Order Modelling of a short-residence Time Gasifier. *Fuel*, 161, pp. 222–232.

Sahraei, M.H., 2017. Reduced Order Modeling and Scale-up of an Entrained Flow Gasifier (PhD Thesis). Ontario: University of Waterloo.

Schweiger, C. A., C. A. Floudas, 1999. Optimization Framework for the Synthesis of Chemical Reactor Networks. *Ind. Eng. Chem.* Res. 38, pp. 744-766

Seodigeng T., Hausberger B., Hildebrandt D., D. Glasser D. 2009. Recursive constant control Policy Algorithm for Attainable Regions Analysis. *Computers and Chemical Engineering*, 33, pp. 309–320

Shi, S., Zitney, S.E., Shahnam, M., Syamlal, M., Rogers, 2006. W.A., Modelling Coal Gasification with CFD and the Discrete Phase Method, *Journal of the Energy Institute*, 79 (4), pp. 217-221

Simons G. A., 1980. The Unified Coal-char Reaction. *Fuel*, 59, pp. 143–149.

Smith I.W., 1982. The combustion Rates of Coal Chars: A Review. Nineteenth Symposium (International) on Combustion. pp. 1045-1065

Smith, R., 2005. Chemical Process Design and Integration. 2nd ed. s.l.: John Wiley and Sons.

Smooth, L. D., Hedman, P. O., Smith, P. J., 1984. Pulverized-coal Combustion Research at Brigham Young University. *Prog. Energy Combust. Sci.,* 10, pp. 359-441.

Solomon, P. R. Hamblen, D. G., Carangelo, R. M., Serio, M. A., Deshpande, G. V., 1988. General Model of Coal Devolatilization. *Energy and Fuels,* 2, pp. 405-422.

Ubhayakar, S. K., Stickler, D. B., Von Rosenberg, C. W., Gannon, R. E., 1977. Rapid Devolatilization of Pulverized Coal in Hot Combustion Gases. *Symposium (International) on Combustion*, 16(1), pp. 427–436.

US-DOE., 2011. Final Environmental Assessment for RTI International Scale-up of High-Temperature Syngas Cleanup and Carbon Capture and Sequestration Technologies, Polk County, Florida. Available online at https://netl.doe.gov/sites/default/files/environmental-assessments/Final-EA-RTI-Syngas-CCS-Project-PDF_101711.pdf (Accessed on March 2019)

Vamvuka, D., Woodburn, E. T., Senior, P. R., 1995. Modelling of an Entrained Flow Coal Gasifier 1. Development of the Model and General Predictions. *Fuel,* 74(10), pp. 1452-1460.

Vamvuka, D., Woodburn, E. T. and Senior, P. R., 1995. Modelling of an Entrained Flow Coal Gasifier 2. Effect of Operating Conditions on Reactor Performance. *Fuel,* 74(10), pp. 1461-1465

van den Aarsen F. G., 1985. Fluidised Bed Wood Gasifier. Performance and modelling, PhD. dissertation, Twente University Publication, University of Twente.

Viswanathan, J., Grossmann, I.E. 1990. A Combined Penalty Function and Outer-Approximation Method for MINLP Optimization, *Computers and Chemical Engineering*, vol. 14(7), pp. 769-782.

Wang F.S., Chen L.H. 2013. Heuristic Optimization. In: Dubitzky W., Wolkenhauer O., Cho KH., Yokota H. (eds) *Encyclopedia of Systems Biology. Springer, New York, NY*. https://doi.org/10.1007/978-1-4419-9863-7_411

Wang H., Chaffart D., Ricardez-Sandoval, L. A., 2019 Modelling and Optimization of a Pilot-scale Entrained-flow gasifier Using Artificial Neural Networks, *Energy*, 188, pp. 1-14.

Wang H., Ricardez-Sandoval, L. A., 2020 Dynamic Optimization of a Pilot-scale Entrained-flow gasifier using artificial recurrent neural networks, *Fue*l, 272, pp. 1-14.

Wang, M., Liu, G., Hui, C. W., 2016. Simultaneous Optimization and Integration of Gas Turbine and Air. *Energy*, 116, pp. 1294-1301.

Wang, M., Guilian, L., Hui, C. W., 2017. Optimization of IGCC Gasification Unit Based on the Novel Simplified Equilibrium Reactor. *Clean Technologies and Environmental Policy*, 20(2), pp. 259-269.

Watanabe, H., Otaka, M., 2006. Numerical Simulation of Coal Gasification in Entrained Flow Coal Gasifier. *Fuel*, 85, pp. 1935–1943.

Watkinson, A. P., Lucas, J. P., Lim, C. J., 1991. A Prediction of Performance of Commercial Coal Gasifiers. *Fuel*, 70, pp. 519-527.

Wen, C. Y., Chaung, T. Z. 1979. Entrained coal gasification modelling. *Ind. Eng. Chem. Process Des. Dev*., 18 (4), pp. 684−695.

Xie, J. Zhong, W., Jin, B., Shao, Y. Huang, Y., 2013. Eulerian-Lagrangian Method for Three-dimensional Simulation of Fluidized Bed. *Advanced Powder Technology*, 24, pp. 382-392.

Xu, S., 2014. Moving Forward with the Huaneng GreenGen IGCC Demonstration, *Cornerstone*, 2(3), pp. 61–65.

Valero, A., Uson S., 2006. Oxy-co-gasification of Coal and Biomass in an Integrated Gasification Combined Cycle (IGCC) Power Plant. *Energy*, 31, pp. 1643–1655

Yang, Z., Wang, Z., Wu, Y., Wang, J., Lu, J., Li Z., Ni, W., 2011. Dynamic Model for an Oxygen-Staged Slagging Entrained Flow Gasifier. *Energy and Fuels,* 25, pp. 3646–3656.

Yang, Z., Wang, Z., Wu, Y., Li Z., Ni, W., 2013a. Use of a Reactor Network Model in the Design and Operation of a New Type of Membrane Wall Entrained Flow Gasifier. *Energy and Fuels*, 27, pp. 6322−6332.

Yang, Z., Xue, Y., Wu, Y., Li Z., 2013b. Modelling of an Oxygen-staged Membrane Wall Gasifier: Effects of Secondary Oxygen. *Chemical Engineering and Processing,* 74, pp. 131–141.

Yuehong, Z., Hao, W., Zhihong, X., 2006. Conceptual Design and Simulation Study of a Co-Gasification Technology. *Energy Conversion and Management,* 47, pp. 1416–1428.

Zhang Y., Ashizawa M., Kajitani S., Miura K., 2008. Proposal of a Semi-empirical Kinetic Model to Reconcile with Gasification Reactivity Profiles of Biomass Chars. *Fuel,* 87, pp. 475–81.

Zhou, W., Manousiouthakis, V. I., 2007. Variable Density Fluid Reactor Network Synthesis—Construction of the Attainable Region Through the IDEAS Approach. *Chemical Engineering Journal,* 129, pp. 91–103.

Zhou, W., Manousiouthakis, V. I., 2009. Automating the AR Construction for Non-isothermal Reactor Networks. *Computers and Chemical Engineering,* 33, pp. 176-180.

Zupan, D.M., 2009. Edwardsport IGCC - Moving Forward, Gasification Technologies Conference. Available online at https://netl.doe.gov/sites/default/files/netl-file/15ZUPAN.pdf

3. MODEL DEVELOPMENT FOR GASIFIER DESIGN

This chapter focuses on developing a novel mathematical model that can simultaneously determine the optimal reactor configuration and reactions conditions for an EFG. As stated in the literature review, this study adopted the use of superstructure optimization in achieving the goal. Hence, this chapter is focused on a detailed explanation of the developed superstructure technique. The main steps employed in developing a model for the optimal synthesis of the gasification reactor are choice of basic reactor unit, superstructure development and mathematical formulation.

3.1 Basic Reactor Units

As stated in section 2.5.1, the choice of the ideal reactors is a critical step in all reactor synthesis techniques. In choosing the type of base reactor units, the two things to be considered are the extremes of the mixing conditions that can exist in the EFG and the choice of representation of these conditions. The two reactors chosen as base reactor units for this study are the PFR and CSTR. The advantages of using this form of reactor representation have been reviewed under section 2.5.1. Hence, this discussion will focus on providing justifications for these two ideal reactors. The decision on the mixing conditions that can exist in the EFG is based on the work of Pedersen et al. (1997, 1998). In these studies, a horizontally oriented pulverised coal combustor was presented as a PFR with an internal recirculation stream. This recirculation leads to a deviation from ideal plug flow conditions i.e. the higher the recirculation the mixing in the reactor approaches a CSTR. Higman and van der Burgt (2003) proposed that the flow orientation of a gasifier determines the type of mixing that occurs in it. Hence, up-flow reactors such as Prenflo gasifiers can be modelled as CSTRs. It was also suggested by Bockelie et al. (2002) that gasifiers with tangential feeding exhibit well-mixed behaviour. This is due to the spiral flow pattern that is developed along the reactor line. This flow pattern creates a longer residence time allowing for adequate mixing. Similarly, Monaghan (2010) also showed that

down-flow EFGs with a high length to diameter ratio operate as PFRs. An example of such a reactor is the CSIRO gasifier. Hence, it was concluded that both CSTR and PFR mixing conditions can occur in an EFG.

3.2. Problem statement

The problem statement for the synthesis of the EFG is as follows.

Given:

(i) Coal of known composition and flowrate,

(ii) A set of reactions occurring in a gasifier and their kinetic data, and

(iii) The enthalpy and density of reacting species;

Determine:

(i) The optimal reactor network,

(ii) The volume of reactor units,

(iii) The optimal coal to steam ratio,

(iv) The optimal coal to oxygen ratio,

(v) The optimal operating temperature of the reactor, and

(vi) The feeding strategy.

3.3. Superstructure development

Based on the problem statement, the superstructure in Figure 3.1 is developed. The superstructure for the synthesis and design of the EFG comprises the reactor and distribution sections. The reactor section is made up of units in which changes in concentration occur. This study applies the concept of reactor compartments proposed by Mehta and Kokossis (1997, 1998). It is also similar to the concept of reactor modules used by Lakshmanan and Biegler

(1996) in the hybrid technique for reactor synthesis. A major departure of the representation in this study and that of Mehta and Kokossis (1997, 1998) is the use of a single reactor compartment to represent both reacting phases in the same reactor compartment. The heterogeneous system is treated as a pseudo-homogeneous system where both concentration and temperature gradients in an ideal reactor unit occur only in the axial direction. The components of the solid phase (char and ash) are treated as components in the entire reacting medium. The rate of reaction of the heterogeneous reactions is defined per volume of the entire reacting medium. This significantly reduces the complexity of the model making it amenable to gradient-based methods as opposed to the stochastic techniques used in the studies of Mehta and Kokossis (1997, 1998). Another difference between this study and that of Mehta and Kokossis (1997, 1998) is in the representation of the PFR. While in their study a PFR is modelled as several CSTRs in series, this study uses differential equations to model PFRs. The differential equations are then solved using appropriate discretization techniques during simulation and optimization. Figure 3.2 shows that each reactor compartment is made up of a CSTR and a PFR. CSTR and PFR are chosen as the basic reactor units because they represent the extremes of mixing in a chemical reactor. Any other intermediate mixing state can be achieved through an appropriate combination of these two reactors. The second component of the superstructure is the distribution section. This section of the superstructure is made up of mixers, splitters, bypass, and reuse/recycle streams.

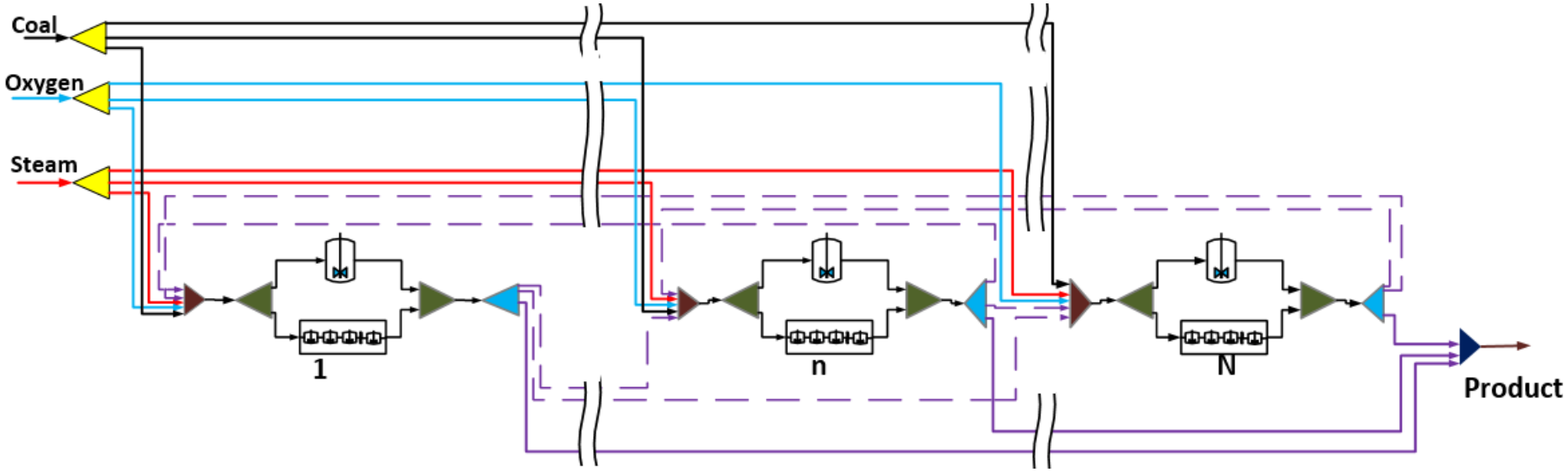

Figure 3.1. Superstructure for the synthesis and design of an entrained flow gasifier

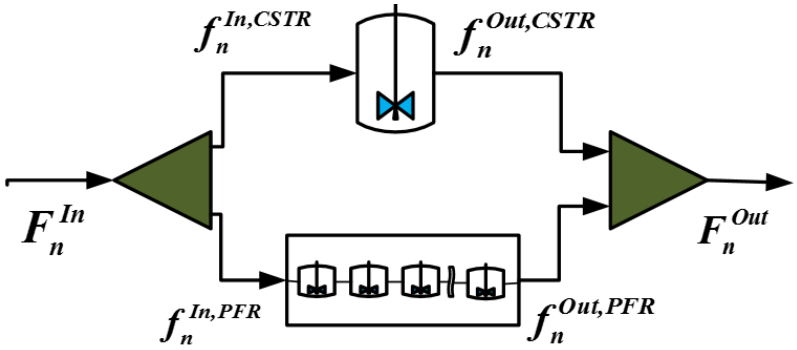

Figure 3.2. A reactor compartment

The main aim of the options provided by the distribution section is to produce an optimal inlet concentration for each reactor compartment. Figure 3.1 shows that there are feed sources namely coal, oxygen, steam, and one product stream. The superstructure offers the opportunity for each of the reactor compartments to receive an amount of the three feed sources. The remainder of the feed into a reactor compartment comes from reuse streams, from other reactor compartments. Figure 3.1 shows that each reactor compartment can contribute to the final product. These streams create series and parallel connections among the reactor compartments. The options provided by distribution and reactor sections lead to the design of a reactor with complex mixing and feed distribution systems. The final design is interpreted based on reactor theory. For example, if the final design includes two PFRs in series, it is represented as a single PFR since theoretically there is no difference between a single PFR and several PFRs in series if the total volume is the same.

3.4. Mathematical formulation

The Mathematical formulation comprises equations governing the reactor and the distribution sections of the superstructure. The reactor section of the superstructure explains the gasification process.

3.4.1 Gasifier/reactor model

The modelling of the gasifier is a very essential part of the gasifier synthesis procedure. The choice of the modelling approach depends on the purpose, desired accuracy, and robustness requirement of the developed model (Pérez-Fortes et al., 2009). This study uses a kinetic based-approach in the modelling of the basic reactor units. A kinetic model was chosen based on its ability to relate gasifier input parameters such as steam to coal ratio, oxygen to coal ratio, reactor volume, and type of reactor to output variables such as conversion, fuel-gas composition, and temperature profile. Kinetic models are particularly also suitable for preliminary designs. This section explains the equations for both the CSTR and PFR models.

3.4.1.1 Assumptions

The reactor equations are based on the following assumptions:

(i) Pyrolysis, heterogeneous and homogeneous reactions are the only reactions occurring in the gasifier

(ii) The pyrolysis of coal is spontaneous, i.e. there is no need to include kinetics for the process.

(iii) There are no tars present in the gasifier. This is because the gasifier operates at a very high temperature (1400K to 2000 K), and therefore, the tars will crack or thermally decompose to form light gases

(iv) Reactors operate under steady-state, i.e., there is no accumulation in the reactor.

(v) There is no variation of concentration in the radial direction of the gasifier.

(vi) There is no radial variation in gasifier operating temperature.

(vii) The entrained-flow system is very dilute in the solid phase; hence, inter-particle interactions are negligible.

(viii) The ash in the coal is inert.

(ix) The solid and gaseous phases are in thermal equilibrium, i.e. both phases have the same temperature.

(x) Heat loss from a reactor is 2% of the coal heating value (Giuffrida et al., 2011).

3.4.1.2 Pyrolysis model

The main purpose of pyrolysis is the conversion of feed to combustible gases and char. This study applies a modified version of the pyrolysis model proposed by Merrick (1983). The model uses both proximal and ultimate coal data to predict the products of pyrolysis. The model assumes that 10 products result from the pyrolysis of the coal. The products of pyrolysis are char, carbon dioxide, carbon monoxide, methane, ethane, ethene, water, ammonia, hydrogen,

and hydrogen sulphide (Lee et al., 2014). The Merrick model is based on the volatile matter and fixed carbon in the coal. The model includes five elemental balances on carbon, hydrogen, nitrogen, oxygen, and sulphur, 4 semi-empirical equations used to specify the yields of carbon monoxide, carbon dioxide, methane, and ethane, and 2 equations used to specify the yield of char. It must be stated that the volatile matter fractions of the coals used in deriving the Merrick model ranged from 16.3% to 37.7% (Merrick,1983) hence applying the model outside this range may lead to inaccuracies.

Equation (3.1) is an empirical formula relating the mass fraction of the gaseous pyrolysis product, w_{Gas}^{Pyro}, to the mass fraction of the volatile matter in the coal feed, w_{VM}^{Coal}, and gasifier operating pressure, $P_{Gasifier}$. The mass fraction of the gaseous pyrolysis product has a parabolic relationship with the mass fraction of the volatile matter. Equation (3.2) gives the yield of the char after pyrolysis.

$$w_{Gas}^{Pyro} = \frac{w_{VM}^{Coal} - 0.35\left(w_{VM}^{Coal}\right)^2}{P_{Gasifier}^{0.13}} \tag{3.1}$$

$$w_{char}^{Pyro} + w_{Gas}^{Pyro} = 1 \tag{3.2}$$

Equations (3.3) to (3.7) are elemental balances relating the product of pyrolysis, w_i^{Pyro}, to the ultimate analysis of the coal, w_j^{Coal}.

$$w_C^{Coal} = w_{Char}^{Pyro} + \frac{12}{44} w_{CO_2}^{Pyro} + \frac{12}{28} w_{CO}^{Pyro} + \frac{12}{16} w_{CH_4}^{Pyro} + \frac{24}{28} w_{C_2H_4}^{Pyro} + \frac{24}{30} w_{C_2H_6}^{Pyro} \tag{3.3}$$

$$w_O^{Coal} = \frac{32}{44} w_{CO_2}^{Pyro} + \frac{16}{28} w_{CO}^{Pyro} + \frac{16}{18} w_{H_2O}^{Pyro} \tag{3.4}$$

$$w_H^{Coal} = w_{H_2}^{Pyro} + \frac{2}{18} w_{H_2O}^{Pyro} + \frac{4}{28} w_{C_2H_4}^{Pyro} + \frac{6}{30} w_{C_2H_6}^{Pyro} + \frac{4}{16} w_{CH_4}^{Pyro} + \frac{3}{17} w_{NH_3}^{Pyro} + \frac{3}{34} w_{H_2S}^{Pyro} \tag{3.5}$$

$$w_S^{Coal} = \frac{32}{44} w_{H_2S}^{Pyro} \tag{3.6}$$

$$w_N^{Coal} = \frac{14}{17} w_{NH_3}^{Pyro} \tag{3.7}$$

To be able to solve the system of equations, the degree of freedom must be zero. The Merrick framework achieves this by providing additional equations predicting the yield of methane, ethane, carbon dioxide, and carbon monoxide from empirical equations. Equations (3.8) and (3.9) give the percentage of atomic/elemental oxygen in the coal feed that is converted to carbon monoxide and carbon dioxide respectively. Equations (3.10) and (3.11) give the percentages of hydrogen in the coal feed that leads to the formation of methane and ethane respectively (Lee et al., 2014).

$$\frac{18.5}{100} w_O^{Coal} = \frac{16}{28} w_{CO}^{Pyro} \tag{3.8}$$

$$\frac{11}{100} w_O^{Coal} = \frac{32}{44} w_{CO_2}^{Pyro} \tag{3.9}$$

$$\frac{32.7}{100} w_H^{Coal} = \frac{4}{16} w_{CH_4}^{Pyro} \tag{3.10}$$

$$\frac{4.4}{100} w_H^{Coal} = w_{C_2H_6}^{Pyro} \tag{3.11}$$

3.4.1.3 Reactor design equations

These equations are mass and energy balances for the CSTR and PFR. Equation (3.12) states that the mass flowrate of a component out of a CSTR, $f_{i,CSTR}^{out}$, equals the algebraic sum of the mass flowrate into the CSTR, $f_{i,CSTR}^{in}$, and the net consumption or generation rate of the component. Equation (3.13) is the mass balance of the PFR, which is the differential form of

Equation (3.12) due to the dependence of the mass flow, $f_{i,PFR}$, and the reaction rate, r_j, on the normalized volume, ξ.

$$f_{i,CSTR}^{Out} = f_{i,CSTR}^{In} + Mw_i \times V_{CSTR} \sum_{j=1}^{|J|} v_{ij} r_j, \forall i \in I \tag{3.12}$$

$$\frac{df_{i,PFR}}{d\xi} = Mw_i \times V_{PFR} \sum_{j=1}^{|J|} v_{ij} r_j(\xi), \forall i \in I \tag{3.13}$$

Equation (3.14) states that the net enthalpy change across the CSTR equals the net heat generated by the reactions when corrected for heat losses. In Equation (3.15), the net enthalpy change across the CSTR is computed. Equation (3.16) is the differential form of Equation (3.14), where the enthalpy of the stream is a function of the normalized volume. Equation (3.17) computes the enthalpy of the stream in the PFR.

$$H^{Out} - H^{In} + Q_{Loss} = V_{CSTR} \sum_{j=1}^{|J|} \left(-\Delta h_j^{rxn} r_j\right) \tag{3.14}$$

$$H^{out} - H^{in} = \left(f_{gas,CSTR}^{out} h_{gas,CSTR}^{out} - f_{gas,CSTR}^{in} h_{gas,CSTR}^{in}\right) + \left(f_{\text{solid},CSTR}^{out} h_{\text{solid},CSTR}^{out} - f_{\text{solid},CSTR}^{in} h_{\text{solid},CSTR}^{in}\right) \tag{3.15}$$

$$\frac{dH(\xi)}{d\xi} + Q_{Loss} = V_{PFR} \sum_{j=1}^{|J|} \left(-\Delta h_j^{rxn} r_j(\xi)\right) \tag{3.16}$$

$$H = f_{gas} h_{gas} + f_{solid} h_{solid} \tag{3.17}$$

The properties of the gas phase are calculated using the multi-flash property estimator and are a function of temperature, pressure, and composition of the gas. Equation (3.18) computes the enthalpy of the char (Eisermann et al., 1980). Equation (3.19) computes the enthalpy of ash (Lee et al., 2014). The reactor temperature T is measured in Kelvins.

$$h_{Char} = \int_{T_{Ref}}^{T} \left[-218 + 3.807T - \left(1.758 \times 10^{-3}\right) T^2\right] dT \tag{3.18}$$

$$h_{Ash} = \int_{T_{Ref}}^{T} [754 + 0.586T] dT \tag{3.19}$$

3.4.1.4 Reaction kinetic equations

It is assumed that seven homogeneous and four heterogeneous reactions occur in the gasifier (Lee et al., 2014). The homogeneous reactions are steam reforming of methane, hydrocarbon, carbon monoxide, and hydrogen combustion, and the water gas shift reaction.

$CH_4 + H_2O \rightarrow CO + 3H_2$ reaction 1

$CH_4 + 0.5O_2 \rightarrow CO + 2H_2$ reaction 2

$C_2H_4 + O_2 \rightarrow 2CO + 2H_2$ reaction 3

$C_2H_6 + O_2 \rightarrow 2CO + 3H_2$ reaction 4

$H_2 + 0.5O_2 \rightarrow H_2O$ reaction 5

$CO + 0.5O_2 \rightarrow CO_2$ reaction 6

$CO + H_2O \leftrightarrow CO_2 + H_2$ reaction 7

The homogeneous reaction rates are calculated using simple power-law equations. The rate equations for the homogeneous reaction(s) can be found in Table 3.1.

The heterogeneous reactions occurring in the gasifier are char combustion, steam gasification of char, the Boudouard reaction, and the hydrogasification of char as specified in the reactions below. The rate of heterogeneous reaction, r_d, is a function of the kinetic constant, k_d, char conversion, X_{Char}, the particle pore structural parameter, ψ_d, the reaction order, δ_d, the partial pressure, P_d, of the gasification species and the char concentration, C_{Char} (Kajitani et al., 2002; Lee et al., 2014).

$$r_d = k_d (1 - X_{Char}) C_{Char} \sqrt{1 - \psi_d \ln(1 - X_{Char})} P_d^{\delta_d} \tag{3.20}$$

The kinetic data for the heterogeneous reactions are given in Table 3.2. The rate constant for the heterogeneous reaction is also calculated using the Arrhenius equation.

Table 3.1. Homogeneous reactions used in the reactor model

Reaction equation **(kmol/m^{3}s)**	**Rate constant** **(kmol/m^3)$^{1-(\alpha+\beta+\gamma)}$**	**References**
$r_1 = k_1 C_{CH_4} C_{H_2O}$	$k_1 = 3\times10^8 \exp(\frac{-125600}{RT})$	Lee et al. (2014)
$r_2 = k_2 \left(C_{CH_4}\right)^{0.5} \left(C_{O_2}\right)^{1.25}$	$k_2 = 4.47\times10^{11} \exp(\frac{-125600}{RT})$	Jones and Lindstedt (1988)
$r_3 = k_3 C_{C_2H_4} \left(C_{O_2}\right)^{1.25}$	$k_3 = 4.26\times10^{11} \exp(\frac{-125600}{RT})$	Jones and Lindstedt (1988)
$r_4 = k_4 C_{C_2H_6} \left(C_{O_2}\right)^{1.25}$	$k_4 = 4.26\times10^{11} \exp(\frac{-125600}{RT})$	Jones and Lindstedt (1988)
$r_5 = k_5 C_{H_2} C_{O_2}$	$k_5 = 1\times10^{11} \exp(\frac{-42000}{RT})$	Lee et al. (2014)
$r_6 = k_6 C_{CO} \left(C_{O_2}\right)^{0.25} \left(C_{H_2O}\right)^{0.5}$	$k_6 = 2.26\times10^{12} \exp(\frac{-167000}{RT})$	Westbrook and Dryer (1981)
$r_7 = k_7 \left[C_{CO} C_{H_2O} - \frac{C_{CO_2} C_{H_2}}{k_{Equi}} \right]$	$k_7 = 2.87\times10^3 \exp(\frac{-125600}{RT})$ $k_{equi} = 0.0265 \exp(\frac{33012}{RT})$	Lee et al. (2014)

$$C + \frac{1}{\phi} O_2 = \left(2 - \frac{2}{\phi}\right) CO + \left(\frac{2}{\phi} - 1\right) CO_2$$ reaction 8

$C+H_2O \rightarrow CO+H_2$ reaction 9

$C+CO_2 \rightarrow 2CO$ reaction 10

$C+2H_2 \rightarrow CH_4$ reaction 11

.

Table 3.2. Heterogeneous reactions used in the reactor model

	Rate constant ($Pa^{-\delta}$)	δ	References
r_8	$k_8 = 2.363\times10^{-1}\exp(\frac{-130000}{R_U T})$	0.68	Lee et al. (2014)
r_9	$k_9 = 2.34\times10^{1}\exp(\frac{-214000}{R_U T})$	0.86	Lee et al. (2014)
r_{10}	$k_{10} = 1.127\times10^{-1}\exp(\frac{-140000}{R_U T})$	0.84	Lee et al. (2014)
r_{11}	$k_{11} = 5.692\times10^{-3}\exp(\frac{-138000}{R_U T})$	0.50	Lee et al. (2014)

3.4.2. Distribution section equations

The equations in this section account for the options in the distribution section of the superstructure. The equations take the form of an overall mass balance of streams and component balance of individual reacting species.

Equation (3.21) states that the mass flowrate of the feed into a reactor compartment, F_n^{In}, is the sum of the mass flowrates of the fresh feed, i.e. f_n^{Coal}, $f_n^{O_2}$ and $f_n^{H_2O}$, and the reuse streams, $f_{n',n}^{R,In}$, from the other reactor compartments.

Equation (3.22) states that the mass flowrate out of a reactor compartment, F_n^{out}, equals the sum of the mass flow of the fuel-gas product, $f_n^{P,out}$, and the mass flowrate to the other reactor compartments, $f_{n,n'}^{R,Out}$.

$$F_n^{In} = f_n^{Coal} + f_n^{O_2} + f_n^{H_2O} + \sum_{n'=1}^{|N|} f_{n',n}^{R,In}, \forall n' \in N, n \in N, n' \neq n \quad (3.21)$$

$$F_n^{out} = f_n^{P,out} + \sum_{n'=1}^{|N|} f_{n,n'}^{R,out}, \forall n' \in N, n \in N, n' \neq n \quad (3.22)$$

Equation (3.23) states that the mass flowrate of the stream into a reactor compartment, F_n^{in}, equals the sum of the mass flowrates into the CSTR, $f_{n,CSTR}^{in}$, and the PFR, $f_{n,PFR}^{in}$, of that compartment. Equation (3.24) states that the mass flowrate out of a reactor compartment, F_n^{out} is a sum of the mass flowrate of the streams out of the CSTR, $f_{n,CSTR}^{out}$ and PFR, $f_{n,PFR}^{out}$, of that reactor compartment.

$$F_n^{in} = f_{n,CSTR}^{in} + f_{n,PFR}^{in}, \forall n \in N \tag{3.23}$$

$$F_n^{out} = f_{n,CSTR}^{out} + f_{n,PFR}^{out}, \forall n \in N \tag{3.24}$$

Equation (3.25) states that the mass flowrate of the fuel-gas, F^{P}, equals the sum of the flowrate from the reactor compartments that contributed to the formation of the fuel-gas, $f_n^{P,out}$.

$$F^{\mathrm{P}} = \sum_{n=1}^{|N|} f_n^{P,out}, \forall n \in N \tag{3.25}$$

Equation (3.26) states that the mass fraction of the feed into a reactor compartment, $w_{F,i,n}^{in}$, is equal to the mass fraction of the feed into the CSTR, $w_{CSTR,i,n}^{in}$, and PFR, $w_{PFR,i,n}^{in}$, of that reactor compartment. Equation (3.27) states that the mass fraction of product out of a reactor compartment, $w_{F,i,n}^{out}$, equals the mass fraction of the stream from that compartment to the fuel-gas product, $w_{i,n}^{P,out}$, and the mass fraction of the reuse stream, $w_{i,n}^{R,out}$. Equation (3.28) states that the mass flowrate of component, *i*, in the product fuel-gas equals the sum of the mass flowrate of that component in all the streams that form the fuel-gas.

$$w_{F,i,n}^{in} = w_{CSTR,i,n}^{in} = w_{PFR,i,n}^{in} \forall i \in I, n \in N \tag{3.26}$$

$$w_{F,i,n}^{out} = w_{i,n}^{P,out} = w_{i,n}^{R,out} \forall i \in I, n \in N \tag{3.27}$$

$$w_i^{\mathrm{P}} F^{\mathrm{P}} = \sum_{n=1}^{|N|} w_{i,n}^{P,out} f_n^{P,out}, \forall i \in I, n \in N \tag{3.28}$$

Equation (3.29) states that the mass flowrate of a component leaving the compartment, as a product is the sum of the mass of that component in the CSTR and PFR product streams of that compartment.

$$w_{F,i,n}^{out} F_n^{out} = w_{CSTR,i,n}^{out} f_{CSTR,n}^{out} + w_{PFR,i,n}^{out} f_{PFR,n}^{out} \forall i \in I, n \in N \tag{3.29}$$

Equations (3.29) and (3.30) ensure that a reactor only receives feed when it exists.

$$0 \leq f_{CSTR,n}^{in} \leq y_{CSTR,n} f_{n,CSTR}^{U} \tag{3.29}$$

$$0 \leq f_{PFR,n}^{in} \leq y_{PFR,n} f_{n,PFR}^{U} \tag{3.30}$$

3.4.3 Modelling approach

This study adopts a modular approach in the modelling of an EFG. This involves developing fully functional generic sub-models for pyrolysis, property estimation, kinetics, CSTR, and PFR models. Based on the task at hand, the aforementioned sub-models are integrated into a single model. For the integrated model to function, there must be an interaction between the sub-models. From Figure 3.3, it can be seen that there is a 2-way interaction between the Multiflash property estimator and the kinetic and the reactor sub-models. The Multiflash property estimator receives, temperature, pressure, and composition from the reactor submodel and supplies enthalpy and density to the reactor sub-model. Similarly, the kinetic sub-model receives temperature, pressure, and concentration data from the reactor sub-model. The kinetic model supplies data on the reaction rate of the individual components to the reactor sub-model. The modular approach makes it easy to identify errors in modelling since smaller models can be diagnosed. The advantage of the modular approach is that a single model can be used for different simulations and optimizations. Another advantage is each of the submodels can be

changed with an alternative one. For example, the Merrick model is the pyrolysis model of choice in this study but can be replaced with another pyrolysis model.

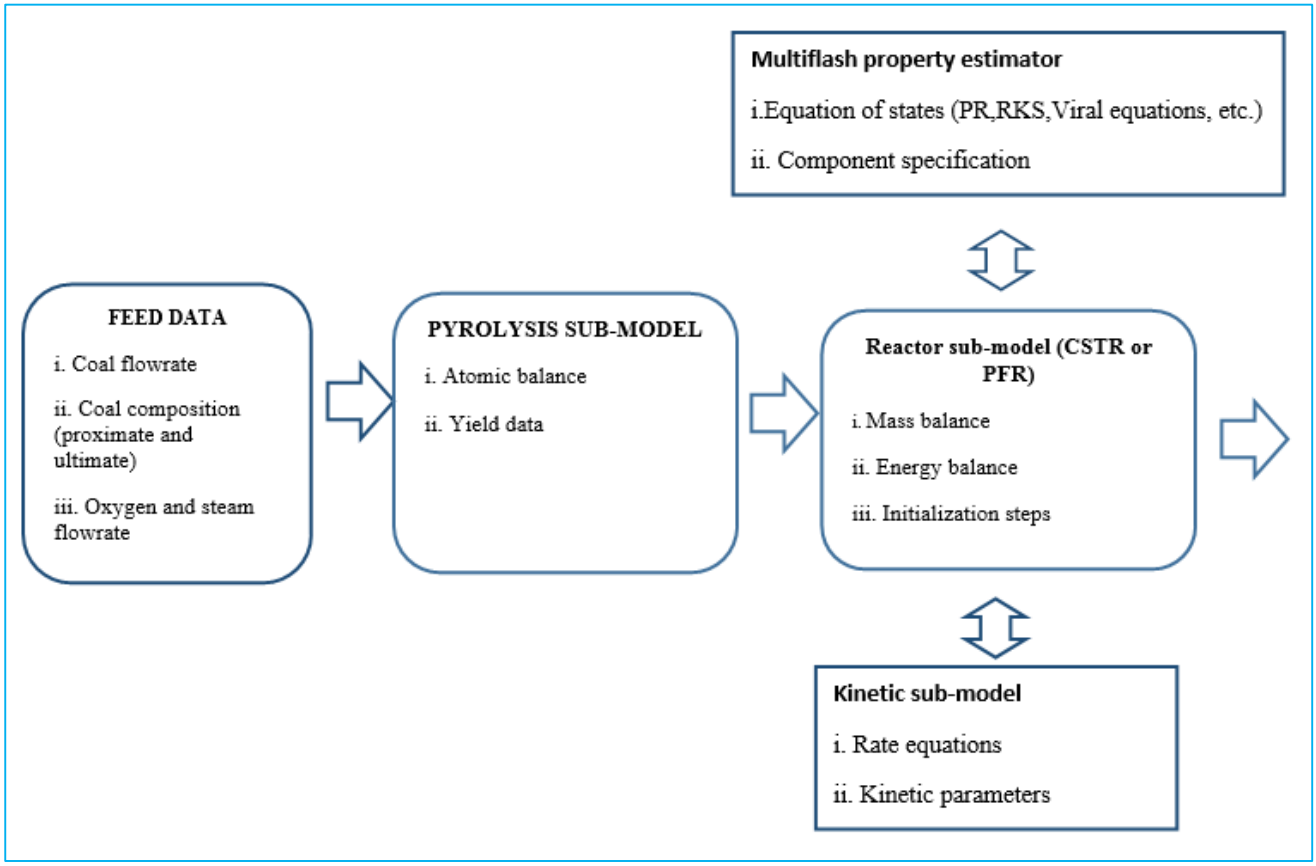

Figure 3.3. Structure of the developed reactor model

3.5 Modelling platforms

This study employs two main modelling software namely the general process modelling systems (gPROMS) and the Multiflash software packages.

3.5.1 *g*PROMS

The modelling, simulation, and optimization were performed on the gPROMS software package. gPROMS is a state-of-the-art modelling and optimization platform. The platform can carry out simulations, optimizations, and parameter estimation. The advantages of the modelling platform include the ability to handle differential-algebraic equations and dynamic models. Another advantage of the gPROMS platform is its ability to incorporate foreign

software such as Microsoft Excel and Matlab. Through the foreign object function of the modelling platform, thermodynamic property estimators such as Multiflash and Aspen properties can be integrated into the simulation process. This study uses the Multiflash property estimator.

The gPROMS software consists of some building blocks known as entities. The entities used in this study are Variable Types, Models, Processes, Saved Variable Sets, Optimisations, and Miscellaneous Files (PSE, 2013a). Figure 3.4 shows all the entities used in one of the optimizations performed in this study. There are other entities in the gPROMS platform not used in this study.

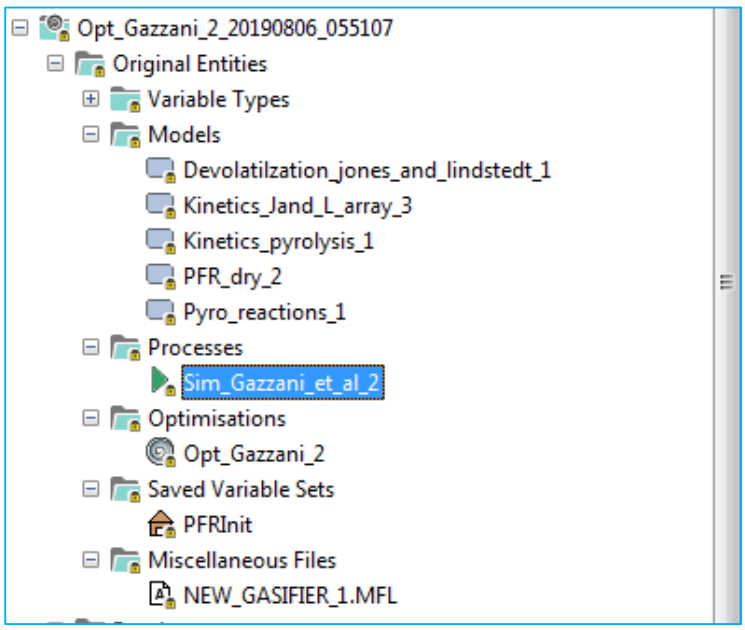

Figure 3.4. gPROMS entities

3.5.1.1 Variable Types entity

The ‘variable types’ entity is used in defining all the generic variable types to be used in the model. Each generic variable is described by a range and default value. The choice of the default value for a variable is essential in the convergence of a simulation. Figure 3.5 shows a

sample of the variable types used in this study. The software also allows the specification of units of measurement for each variable used.

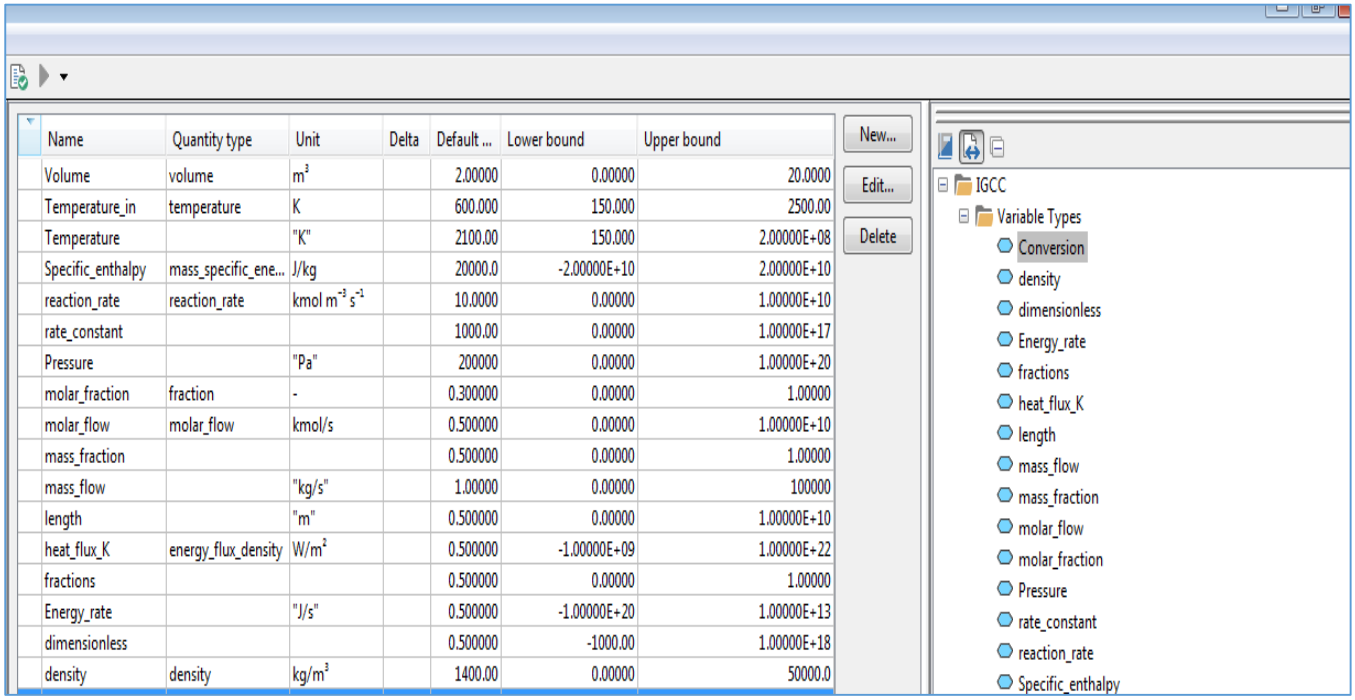

Figure 3.5. The variable type entity

3.5.1.2 Models entity

The ‘Models’ entity is used in developing all sub-models and the integrated model. In this entity, specific variables, which are a subset of the generic variable type, are declared. For example, the total flowrate of the fuel-gas and the flowrate of carbon monoxide are all subsets of the generic variable ‘mass_flow’ in Figure 3.5. The ‘model’ entity contains all the mathematical equations explained in section 3.4 and the initialization procedure for the solution of the mathematical model. The gPROMS platform allows the use of a previously developed model when developing a new model. Such a previously developed model serves as a sub-model performing specified functions. It is also possible to specify all the parameters needed under Models entity.

3.5.1.3 Saved Variables Sets

The ‘Saved Variables Sets’ entity is used to store the values of variables from a previous solution. These values are used in the initialization for future simulations under similar conditions. This eliminates the need for an initialization process during that simulation.

3.5.1.4 Miscellaneous files

The ‘Miscellaneous files’ entity is used in introducing the functions of files foreign to the gPROMS platform. Acceptable formats of the foreign files are attached under the ‘Miscellaneous files’ entity. From Figure 3.4, we can see that a Multiflash file known as ‘NEW_GASIFIER_1.MFL’ was attached under this entity. Using the appropriate gPROMS language under the ‘Processes’ and ‘Model’ entity, the aforementioned Multiflash file is used in the prediction of the thermodynamic properties of the gases and liquids.

3.5.1.5 Processes entity

The ‘Processes entity’ is used in simulating a single model or several models simultaneously. A simulation involves solving a problem with a zero degree of freedom. Simulation is done either for the validation of a gasifier model or as a pre-requisite for optimization of a superstructure. In the ‘processes’ entity, all parameters not specified in the ‘model’ entity, are specified. The ‘processes’ entity also contains the ‘solution parameters’ function (Figure 3.6) which specifies the solvers to be used in simulation and optimizations, and also the tolerances.

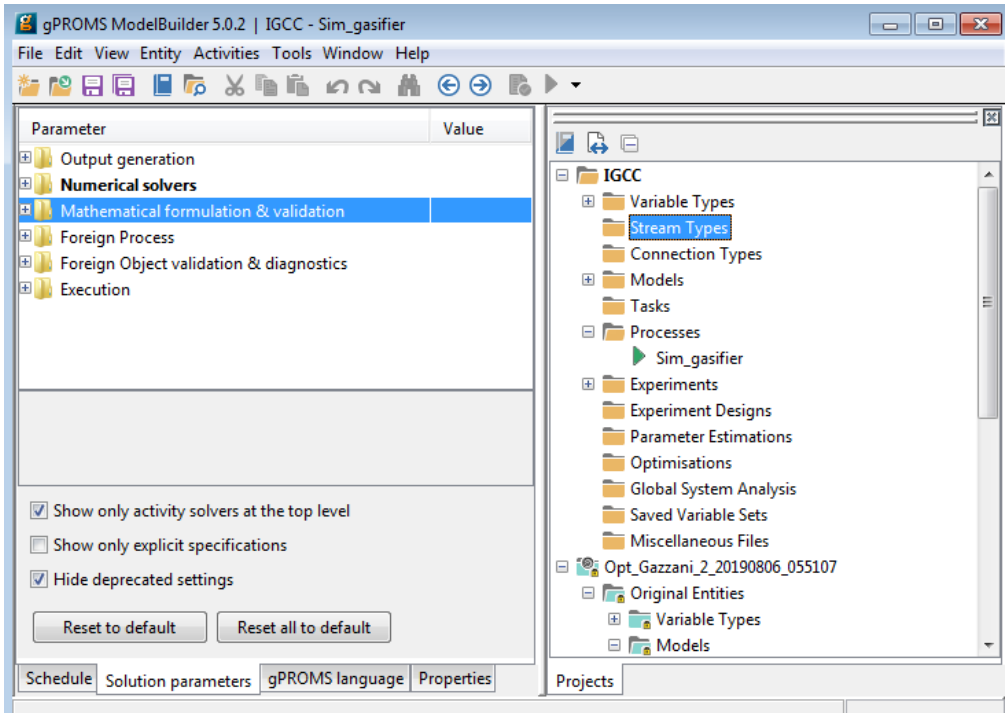

Figure 3.6. A diagram showing the choice of solution parameters for a process

3.5.1.6 Optimisations entity

The 'Optimisations' entity is used in the optimization of the superstructure or standalone gasifier. Each optimization is based on a prior simulation. To be able to perform a successful optimization, the simulation process on which it is based must be specified. This is preceded by the specification of the objective function of the optimization (Figure 3.7). The optimisation entity also has a controls tab where the optimization variables and their ranges are specified (Figure 3.8). Other tabs of the optimization include the constraints and the gPROMS language. The constraints tab is used in specifying optimizations constraints such as logical constraints and other process constraints. The specifications made in the aforementioned tabs lead to the writing of the gPROMS code (PSE, 2013 c).

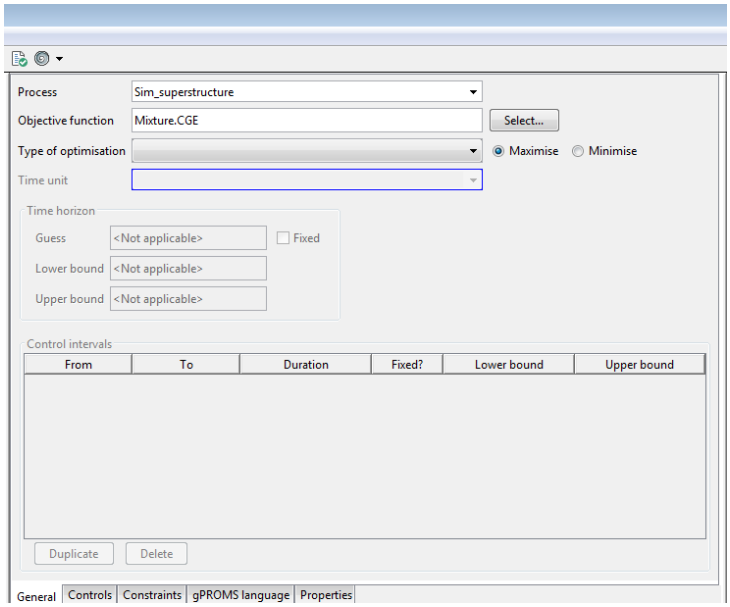

Figure 3.7. An optimization entity

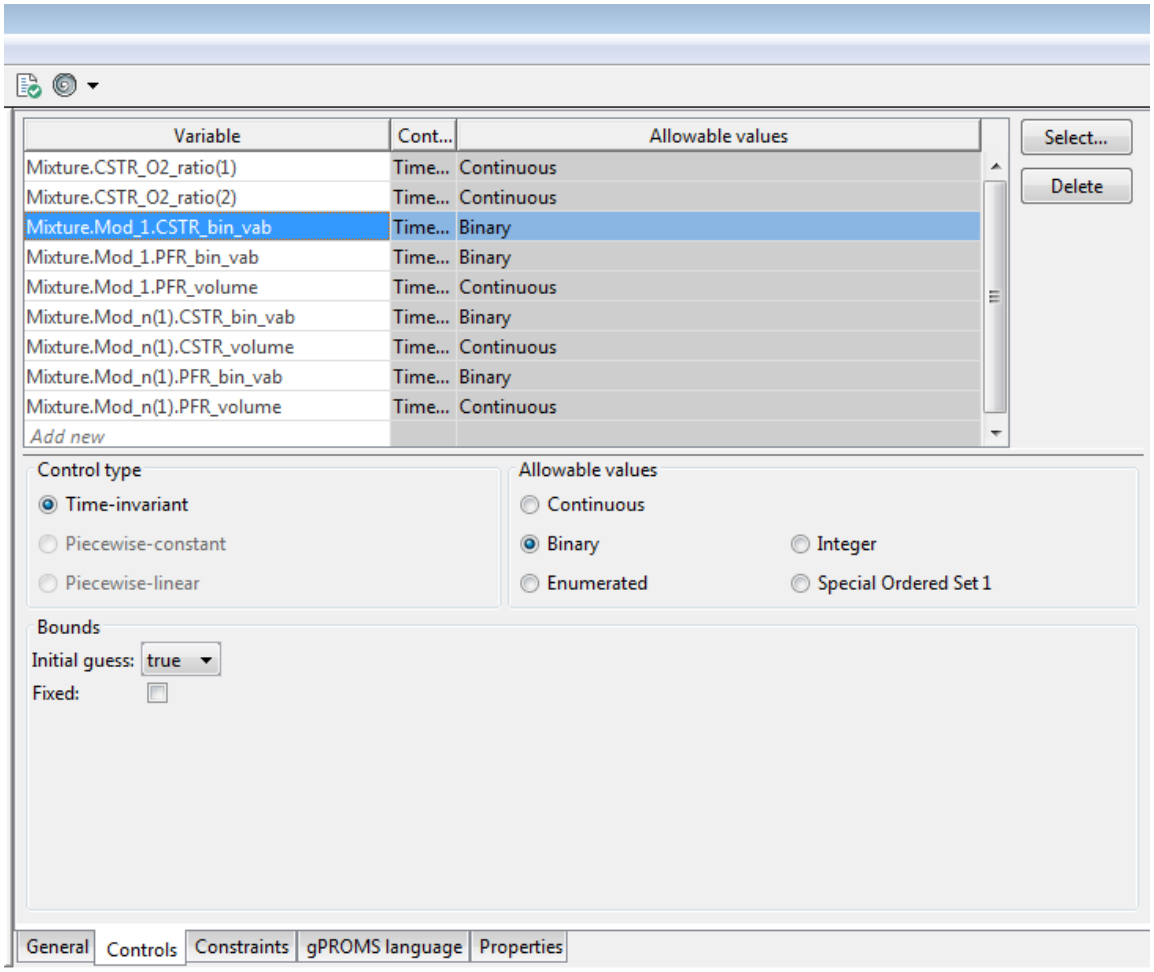

Figure 3.8. Optimization variables for gasifier model

3.5.1.7 Initialization and simulation

The developed model consists of a complex interaction of conservative equations, rates laws, reactor design equations, and inputs from external software. This makes a successful simulation operation difficult to attain without a good initial guess. This problem is exacerbated by low concentrations of carbon monoxide, hydrogen, and hydrocarbons after pyrolysis while having high reaction rates. This usually leads to near zero or negative concentrations, which prevent the simulations from converging. This challenge is addressed using the initialization function of the gPROMS platform. This comprises a set of simplifications and changes to the detailed model. These changes guarantee that the model will solve it initially. These changes are then reverted in a specified order so that the original problem can be solved. Anytime a simplification is reverted, the solution obtained in the previous step serves as the starting point for the new problem. Figure 3.9 shows an example of the initialization used in solving the gasifier model.

```
INITIALISATION_PROCEDURE Init Default
Start
Reactions            :=off;
Alpha                :=0;
EnergyBalance        :=isothermal;

End
Next Jump_To Revert Reactions; End
End
Next
  Jump_To Revert Alpha;  End
End
Next
  Jump_to Revert EnergyBalance; End
End
```

Figure 3.9. An initialisation procedure for the solution of a gasifier model

3.5.1.8 Optimization

After a successful simulation, an optimization is performed to determine the optimal EFG design and conditions. Figure 3.10 shows an example of a typical gPROMS interface for the synthesis of an optimal EFG. From Figure 3.10, it is observed that the variables are both continuous and integer. It can also be seen that for each variable (e.g. volume), the modelling platform requires an initial guess, a lower bound, and an upper bound. After all decision variables and constraints are stated, the software is allowed to run until an optimal objective function value is obtained. Based on the values of the continuous and binary variables an optimal EGC configuration is deduced.

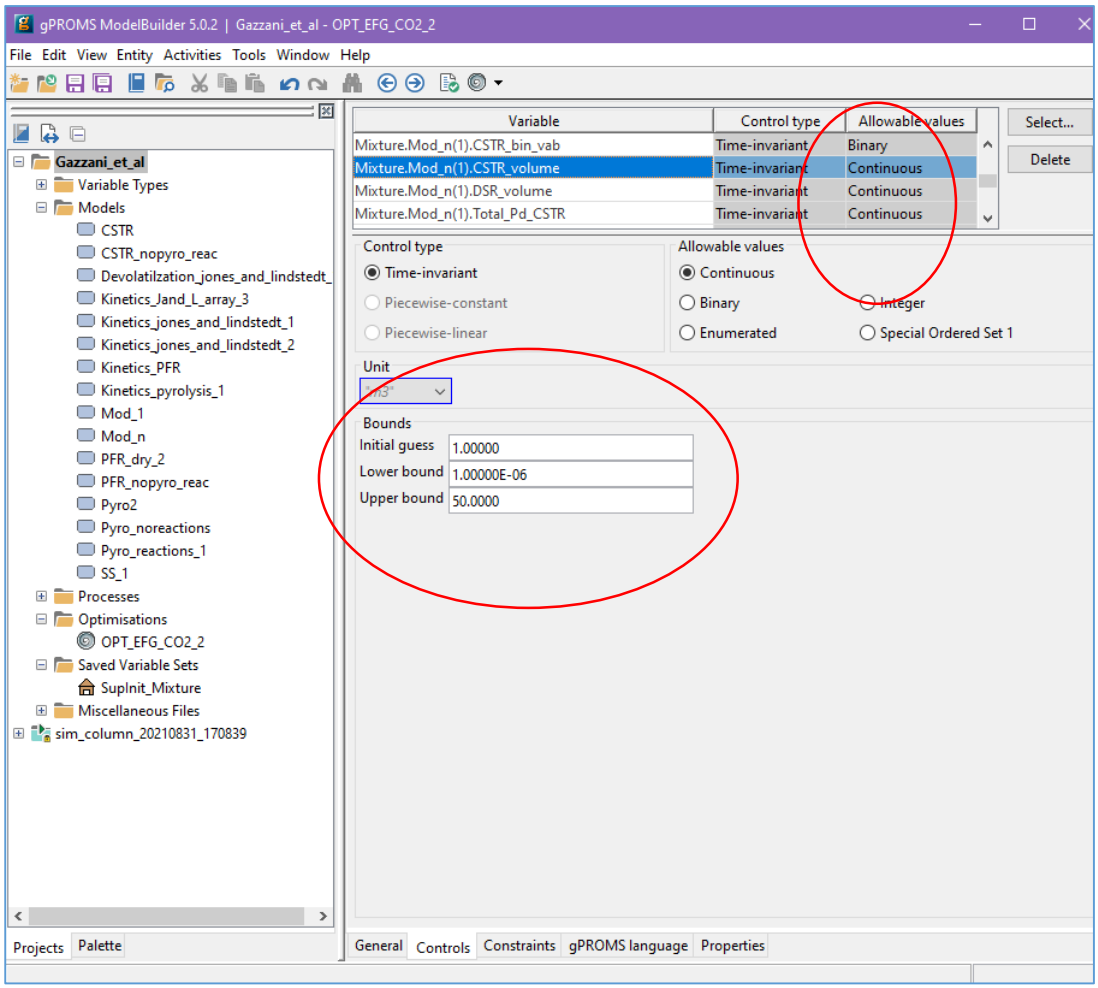

Figure 3.10. An interface showing the use of the gPROMS platform to synthesize and design an optimal EFG

3.5.1.9Choice of solvers

The process required the choice of a discretization technique for the conversion of differential equations to equivalent algebraic forms. The backward finite difference method (BFDM) was chosen as the discretization technique. The solvers for the linear and non-linear equations are 'MA48' and the block decomposition non-linear solver. The optimization requires the choice of decision variables and inequality constraints. In addition to the simulation solvers, the gPROMS platform uses the 'outer approximation extended relaxation augmented penalty' (OAERAP) algorithm in solving the problem. The algorithm decomposes the optimization problem into nonlinear programming (NLP) and mixed integer linear programming (MILP) sub-problems. The OAERAP algorithm requires the choice of both MILP and NLP sub-solvers. 'Lp_solve' and sequential quadratic programming (SQP) are specified as the solvers for the MILP and MLP sub-problems respectively.

3.5.2 Multiflash

An important aspect of the model development is the estimation of the gas phase properties. Some studies (Chen et al., 2000; Wantanabe and Otaka, 2006; Lee et al., 2010; Kasule et al., 2012) used ideal gas law and constant heat capacities in the simulation of gas properties. Ideal gas laws give accurate predictions at high temperatures and low pressures (~ 1 Bar). However, the EFG operates at much higher pressures (< 18 Bar). This necessitates the need for a more accurate property estimator. Multiflash is a powerful and versatile software for the estimation of thermodynamic properties of fluid and phases in equilibrium. The software can be used for all the thermodynamic and transport properties needed for engineering studies and comprehensive fluid characterisation model tuning for petroleum fluids. The software can also be used for flash calculations to determine the phases present at specified conditions and their

type, composition, and amounts. Additional functions of the software include the simulation of complete phase envelopes, showing phase boundaries and critical points, and modelling solids formation, including pure solids, halide scales, hydrates, and waxes. The software can operate as stand-alone software but it also integrates well with other software such as gPROMS and 'Cape-Open Cape-Open' (COCO) software platform (Infochem, 2014). Figure 3.11 shows the graphical user interface for Multiflash used as the physical property package to determine the thermodynamic properties of all the components in the gasifier except for char and ash.

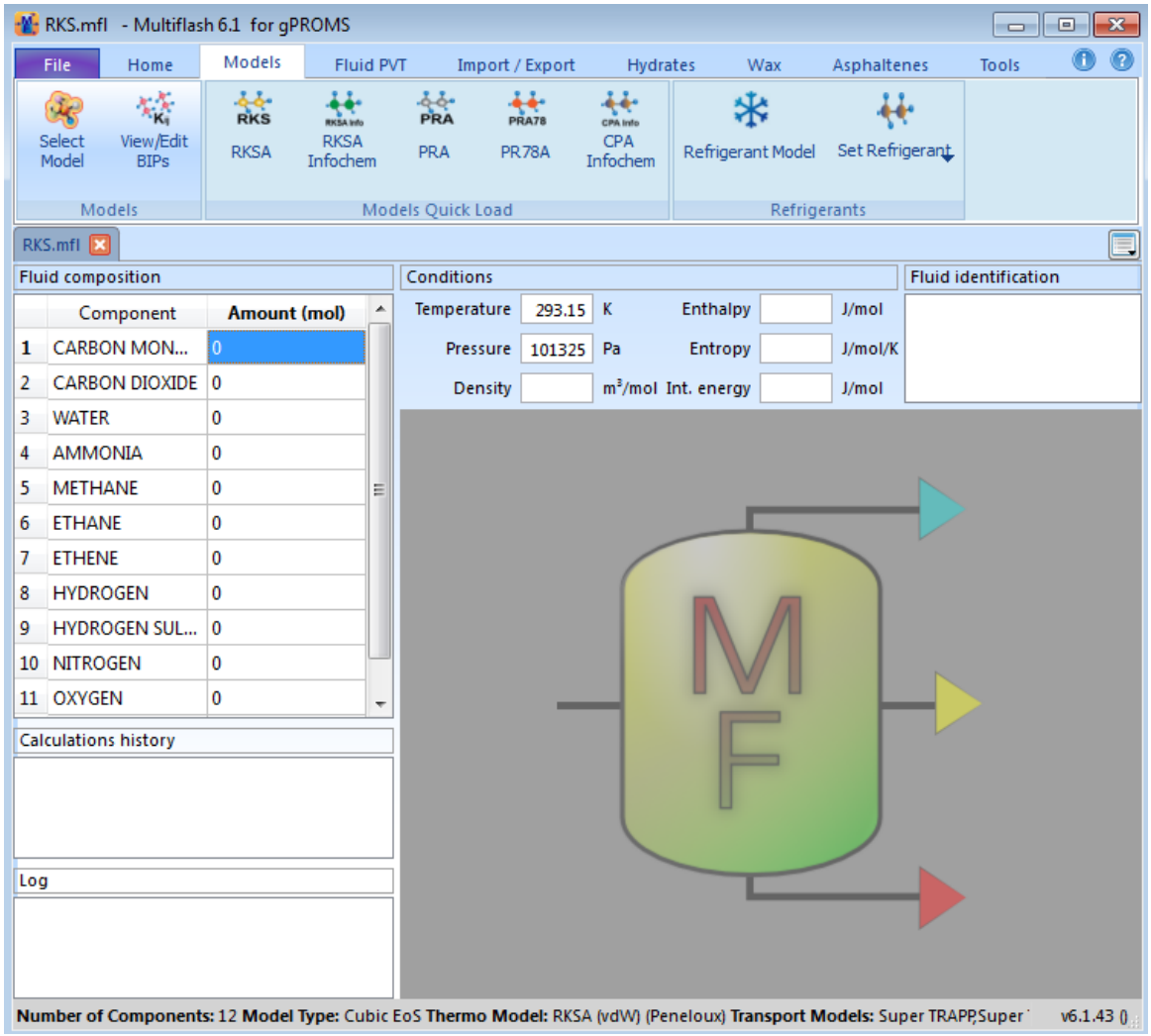

Figure 3.11. The graphical user interface of Multiflash for gPROMS

Although the software allows for the choice of numerous equation of states (EOS) such as viral equations, non-random two-liquid (NRTL) model, Soave-Redlich-Kwong (SRK), and the Peng

Robinson (PR) EOS. PR and SRK are the most successful EOS, due to their ability to accurately predict the properties of several gases over a wide range of temperatures and pressures (Ghanbari et al., 2017). The major limitation in the SRK EOS is that the critical compressibility factor takes on the unrealistic universal critical compressibility of 0.333 for all substances. Consequently, the molar volumes are typically overestimated, i.e., densities are underestimated. Another limitation of the SRK EOS was the poor liquid density prediction (Ramdharee et al, 2013). Hence this study chose the PR EOS.

3.6 Peng Robinson Equation

The Peng-Robinson (PR) equation of state was developed to handle both vapour and liquid properties near equilibrium conditions. The development of this equation was focused on natural gas systems (Ramdharee et al, 2013). Although the model incorporated a commercial software that accepts pressure and temperature and gaseous composition, to compute the gas properties, the basic equations explaining the relationship between the variables will be discussed briefly. The relationship between the most common gaseous properties is illustrated by equations (3.31) to (3.35). Equation (3.31) relates the gas pressure, P, to the temperature, T, the gas constant, R, the molar volume,v, energy parameter, a, and the co-volume,b. Equation (3.32) shows the relation between, the energy parameter and α, where Pc and Tc are critical pressure and temperature respectively. Equations (3.3) and (3.34) are used to calculate α which is a function of temperature and the acentric factor,ω. (Ramdharee et al, 2013; Saffari and Zahedi, 2013)

$$P = \frac{RT}{(v-b)} - \frac{a(T)}{(v(v+b)+b(b-v))} \qquad 3.31$$

$$a(T) = 0.45724\frac{\left(R^2T_C^2\right)}{P_C}\alpha(T) \qquad 3.32$$

$$\alpha = \left[1 + S\left(1 - \frac{T}{T_C}\right)\right]^2 \qquad 3.33$$

$$S = 0.3764 + 1.54266\omega - 0.26992\omega^2 \qquad 3.34$$

$$b = 0.07780 \times \frac{RT_C}{P_C} \qquad 3.35$$

3.7 Summary

A novel mathematical modelling technique for the synthesis of an optimal EFG has been developed and explained. The process employed includes superstructure development and mathematical formulation. The superstructure provides numerous options for mixing at different stages in an EFG. This is represented by the choice of a PFR or a CSTR. The superstructure also has a comprehensive distribution network which allows any feed to be delivered at any position along the length of the gasifier. These networks also allow final or intermediate products to be withdrawn from any point along the length of the gasifier. These options provided by the superstructure allow non-conventional designs to be generated. This chapter also provided both a mathematical description of options provided by the superstructure and an illustration of how the resulting mathematical framework can be solved using a computer-based modelling and optimization platform.

References

Bhatia, S. K., Perlmutter, D. D., 1980. A Random Pore Model for Fluid-Solid Reactions: 1. Isothermal, Kinetic Control. *AIChE,* 26(3), pp. 379-385.

Bhatia, S. K., Perlmutter, P. D., 1981. A Random Pore Model for Fluid-Solid Reactions: II. Diffusion and Transport Effects. *AIChE Journal*, 27(2), pp. 247-254.

Bhatia, S. K., Vartak, B. J., 1996. Reaction of Microporous Solids: The Discrete Random Pore Model. *Carbon*, 34(11), pp. 1383-1391.

Bockelie, M.J., Denison, M.K., Chen, Z., Linjewile, T., Senior, C.L., Sarofim, A.F. Holt, N., 2002. CFD modelling for Entrained Flow Gasifiers. Proceedings of the Gasification Technologies Conference 2002, San Francisco, CA, Oct.28-30, 2002(e).

Chen, C., Horio, M., Kojima, T., 2000. Numerical Simulation of Entrained Flow Coal Gasifiers. Part I: Modelling of Coal Gasification in an Entrained Flow Gasifier. *Chemical Engineering Science,* 55, pp. 3861-3874.

Eisermann W., Johnson P., Conger W.L., 1980. Estimating Thermodynamic Properties of Coal, Char, Tar and Ash. *Fuel Processing Technology*, 3, pp.39-53

Fogler, H. S., 2016. Elements of Chemical Reaction Engineering. Prentice-Hall International, Inc. Fifth Edition. pp. 280-310, 493-598

Ghanbari, M., Ahmadi, M., Asghar Lashanizadegan, A. 2017. A comparison between Peng-Robinson and Soave-Redlich-Kwong cubic equations of state from modification perspective, Cryogenics, 84, pp. 13-19.

Higman, C., van der Burgt, M., 2003. Gasification: Elsevier Science, pp 120-124.

Infochem, 2014. User Guide for Multiflash for Windows (Version 4.4)

Ju, Y., Lee, C.H., 2017. Evaluation of the Energy Efficiency of the Shell Coal Gasification Process. *Energy Conversion and Management*, 143, pp. 123–136.

Jones, W. P., Lindstedt, R. P., 1988. Global Reaction Schemes for Hydrocarbon Combustion. *Combustion and Flame*, 73, pp. 233-249.

Kasule, J. S., Turton, R., Bhattacharyya, D., Zitney, S. E., 2012. Mathematical Modelling of a Single-stage, Down-firing, Entrained-flow Gasifier. *Industrial and Engineering chemistry research*, 51, pp. 6429-6440.

Kajitani, S., Hara, S., Matsuda, H., 2002. Gasification Rate Analysis of Coal Char with a Pressurized Drop Tube Furnace. *Fuel*, 81, pp. 539-546.

Lakshmanan, A., Biegler, L. T., 1996. Synthesis of Optimal Chemical Reactor Networks. *Ind. Eng. Chem*. Res., 35, pp. 1344-1353.

Lee, H., Choi, S., Paek, M., 2010. A Simple Process Modelling for a Dry-feeding Entrained Bed Coal Gasifier. *Proc.IMechE Part A: J Power and Energy*, 225, pp. 74-84.

Lee, H.H., Lee, J.C., Joo, Y.J., Oh M., Lee C.H., 2014. Dynamic Modelling of Shell Entrained Flow Gasifier in an Integrated Gasification Combined Cycle Process. *Applied Energy*, 131. pp. 425–440

Levenspiel, O., Chemical Reaction Engineering, Third Edition, John Wiley and Sons, 1999

Mehta, V. L., Kokossis, A., 1997. Development of Novel Multiphase Reactors Using a Systematic Design Framework. *Computers chem. Engng*, 21, pp. S325-S330

Mehta, V. L., Kokossis, A., 1998. New Generation Tools for Multiphase Reaction Systems: A Validated Systematic Methodology for Novelty and Design Automation. *Computers chem. Engng*, pp. S119-S126

Merrick, D., 1983. Mathematical Models of the Thermal Decomposition of Coal. *Fuel,* 62, pp. 534-539.

Monaghan, R. F. D., Ghoniem, A. F., 2012. A Dynamic Reduced Order Model for Simulating Entrained Flow Gasifiers: Part I: Model Development and Description. *Fuel,* 91(1), pp. 61-80.

Monaghan, R. F. D., Ghoniem, A. F., 2012. A Dynamic Reduced Order Model for Simulating Entrained Flow Gasifiers: Part II: Model Validation and Sensitivity Analysis. *Fuel,* 94, pp.280-297.

Pedersen, L. S., Breithaptb, P., Dam-Johansen, K., Weber, R., 1997. Residence Time Distributions in Confined Swirling Flames. *Combustion Science and Technology,* 127, pp. 251-273.

Pedersen, L. S. Glarborg, P., Dam-Johansen, K., Hepburn, P. W., Hesselmann, G.,1998. A Chemical Engineering Model for Predicting NO Emissions and Burnout from Pulverised Coal Flames. *Combustion Science and Technology,* 132(1), pp. 251-314.

Pérez-Fortes, M., Bojarski, A. D., Velo, E. and Nouges, J. M., 2009. Conceptual Model and Evaluation of Generated Power and Emissions in an IGCC Plant. *Energy,* 34(10), pp. 1721-1732.

PSE., 2013. Model Developer Guide (Release version 3.7).

PSE., 2013. gPROMS Model Builder Guide (Release version 3.7).

PSE., 2013. Optimisation Guide (Release version 3.7).

Ramdharee, S. Muzenda, E. Belaid. M., 2013. A Review of the Equations of State and Their Applicability in Phase Equilibrium Modelling. *Int. Conf. Chem. Environ. Eng. (ICCEE 2013),* pp. 84-87

Saffari, H., Zahedi, A., 2013. A New Alpha-function for the Peng-Robinson Equation of State: Application to Natural Gas, *Chinese Journal of Chemical Engineering*, 21(10), pp. 1155-1161

Shi, S., Zitney, S.E., Shahnam, M., Syamlal, M., Rogers, 2006. W.A., Modelling Coal Gasification with CFD and the Discrete Phase Method, *Journal of the Energy Institute*, 79(4) pp. 217-221

Watanabe, H., Otaka, M., 2006. Numerical Simulation of Coal Gasification in Entrained Flow Coal Gasifier. *Fuel*, 85, pp. 1935–1943.

Westbrook, C. K., Dryer, F. L., 1981. Simplified Reaction Mechanisms for the Oxidation of Hydrocarbon. *Combustion Science and Technology*, 27, pp. 31-43.

4. SYNTHESIS OF REACTOR NETWORKS

This chapter primarily focuses on the use of the mathematical model developed in Chapter 3 for the synthesis and design of an optimal EFG. The first section of the chapter focuses on testing the robustness of the gasifier reactor models. This entails using either a standalone PFR or two CSTRs in series to simulate existing gasifiers. The PFR and CSTR used in the simulations are taken from the superstructure. In this section 4.1, four different EFGs are simulated using the CSTR and PFR models developed in section 3.4.1. For example, in section 4.1.1, the shell dry-fed gasifier was simulated. Lee et al. (2004) had simulated this gasifier using a standalone PFR. Hence the PFR model developed under section 3.4.1 was isolated and used in simulating the EFG. This will enable one to assess the ability of the PFR model developed in this study to sufficiently represent gasification under dry conditions. In section 4.1.2, a Prenflo gasifier is simulated. Perez-Fortes et al. (2009) simulated a Prenflo gasifier using two CSTRs in series. Hence this study used two CSTRs in series to simulate the Prenflo gasifier. This simulation tests the ability of the CSTR model to simulate dry-fed gasification. In section sections 4.1.3 and 4.1.4, the ability of the CSTR and PFR to adequately simulate gasification under slurry conditions is tested by selecting the right examples.

The second section focuses on the synthesis and design of an optimal EFG. This entails using the reactor superstructure to synthesize and design an optimal EFG.

4.1 Validation of CSTR and PFR models

In order to ensure the rigour of the CSTR and PFR models in the superstructure, it is validated by comparing simulation results to examples in literature. The input data needed for the validation of the gasifier reactor models is classified as either general for all the gasifiers or specific for the gasifier being simulated. The generic data includes kinetic data for the reactions

and thermodynamic data for the chemical species found in the gasifier. The kinetic data for homogeneous and heterogeneous reactions are given in Tables 3.1 and 3.2.

4.1.1 Simulation of dry-fed gasifiers

Dry-fed gasifiers involve the use of gases as the transporting medium for the coal feed. In this study, the reactor model developed is validated by simulating the output of a dry-fed gasifier with nitrogen as the transporting medium. The input data for the model is in Table 4.1. It must, however, be stated that for dry-fed gasifiers like Shell, the moisture content of the coal is controlled by drying it to 2% (Lee et al., 2014; Ju and Lee, 2017). Hence, the moisture content of the actual coal feed that goes into the gasifier is 2% and not as shown in Table 4.1. This drying also changes the mass fractions of the volatile matter (VM), fixed carbon (FC), and ash. The simulation of the PFR model is compared to both plant and simulated data by Lee et al. (2014).

4.1.1.1 Output data

Figure 4.1 shows the comparison of the results from the PFR model to the plant data (Lee et al., 2014b) and the study of Lee et al. (2014a). From Figure 4.1, the comparison shows a general agreement between the results from the PFR model developed in this study and both simulated and plant data. There is a much greater agreement between results from this model and the plant data. The major variation between the results from the developed reactor model and the work of Lee et al. (2014) is the mole fraction of hydrogen, which has a relative error of 14%. The major variation between the results from this study and the plant data is in the mole fraction of nitrogen.

Table 4.1. Input data for the simulation for nitrogen fed gasifiers

Proximate Analysis of coal		**Ultimate (daf) analysis of coal**	
$VM\ (\%)$	28	$C\ (\%)$	82
$FC\ (\%)$	52	$H\ (\%)$	5.1
$Ash\ (\%)$	15	$O\ (\%)$	10.24
$MC\ (\%)$	5	$N\ (\%)$	1.7
		$S\ (\%)$	0.9
Gasifier parameters			
β_{H_2O}	0.04	β_{O_2}	0.78
$V^{Max}\ (m^3)$	50	$P_{Gasifier}\ (Bar)$	45

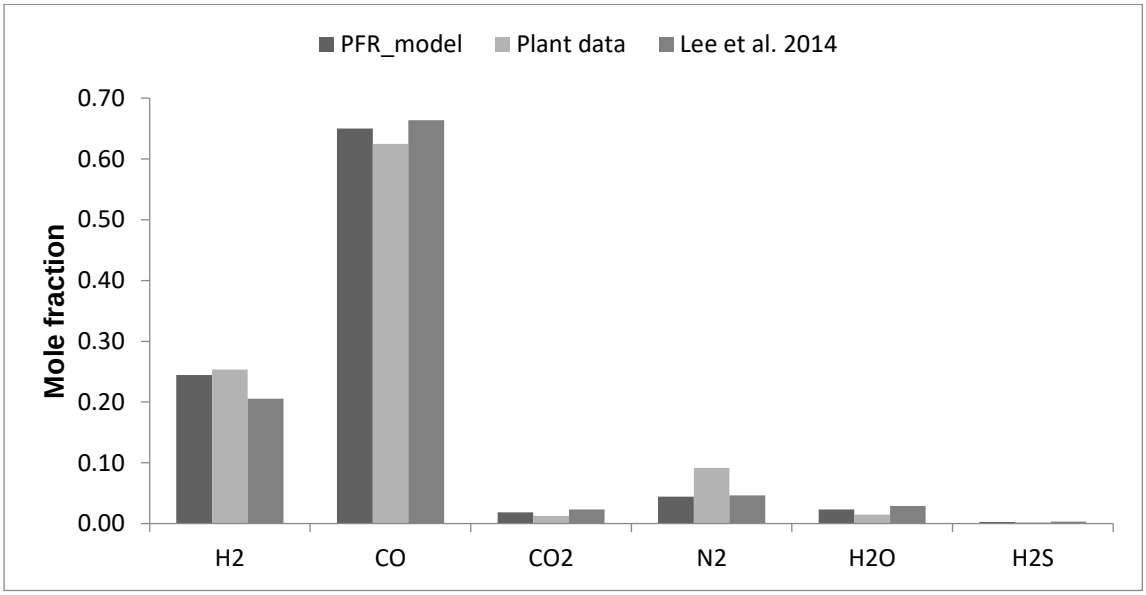

Figure 4.1. Comparison of simulated data with reference data

4.1.1.2 General model predictions

Figure 4.2 shows the temperature and the char conversion profile in the nitrogen-fed gasifier. The horizontal axis of the figure is the normalized volume of the gasifier. The temperature profile shows a significant increase in the temperature of the reactor within 10% of the reactor volume. This is due to the combustion reactions in the presence of oxygen. The temperature of the reactor after reaching the flame temperature experiences a gradual decrease. This is due to the endothermic gasification reaction. The exit temperature of the syngas is 1783 K (1510 ^{o}C). This is in the range of syngas temperature of commercial EFGs (Ju and Lee, 2017). The char conversion profile also displayed a sharp increase within 10% of the reactor volume. The remaining 90% of the reactor is responsible for a very limited amount of char conversion.

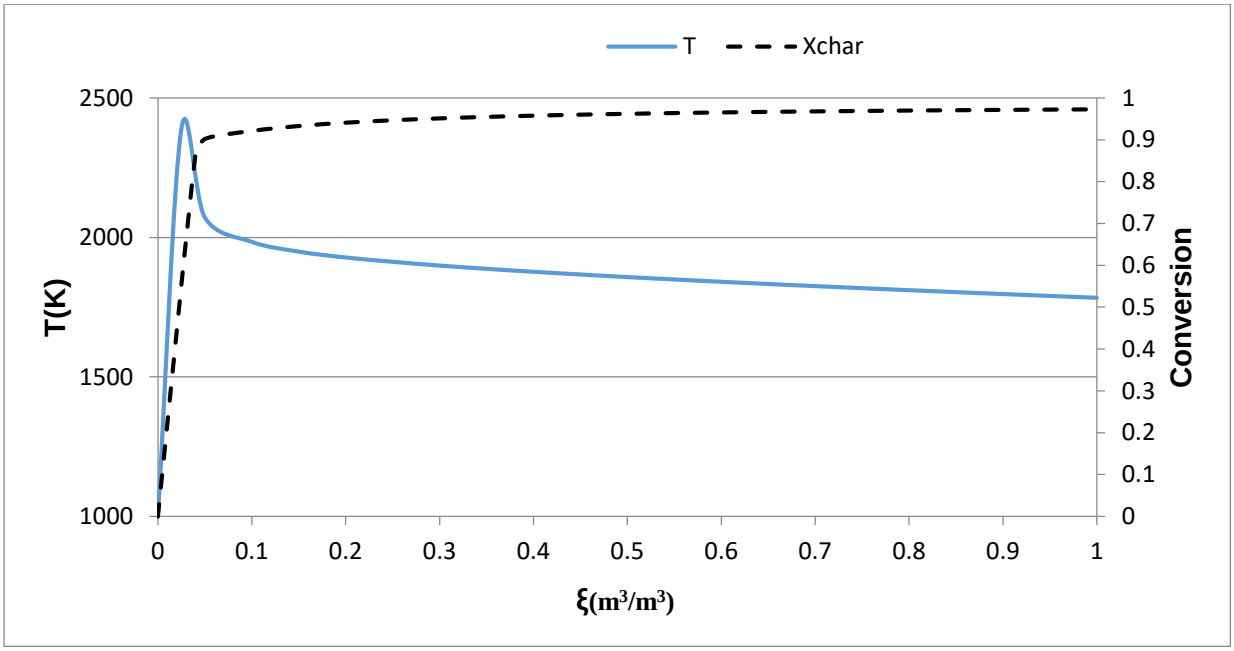

Figure 4.2. Temperature and conversion profile in the nitrogen Fed EFG

Figure 4.3 displays the evolution of the mole fraction of gaseous species in the nitrogen-fed EFG. It is observed that the amount of oxygen experiences a quick drop in the oxygen concentration. This is due to the rapid combustion of volatile gases and char. The quick drop in the amount of oxygen is the reason for the rapid temperature rise observed in the temperature

profile. The remainder of the gasifier volume is totally oxygen deficient. The results also show an initial increase in the mole fraction of CO_2 and H_2O due to initial combustion results, followed by a steady decrease in their amounts due to the Boudouard and steam gasification reactions. These reactions lead to the gradual decrease in reactor temperature observed in Figure 4.3 due to their endothermic nature. Since most of the reactions produce carbon monoxide and hydrogen, the fraction of carbon monoxide and hydrogen both show a steady increase in their concentration until their profile plateaus.

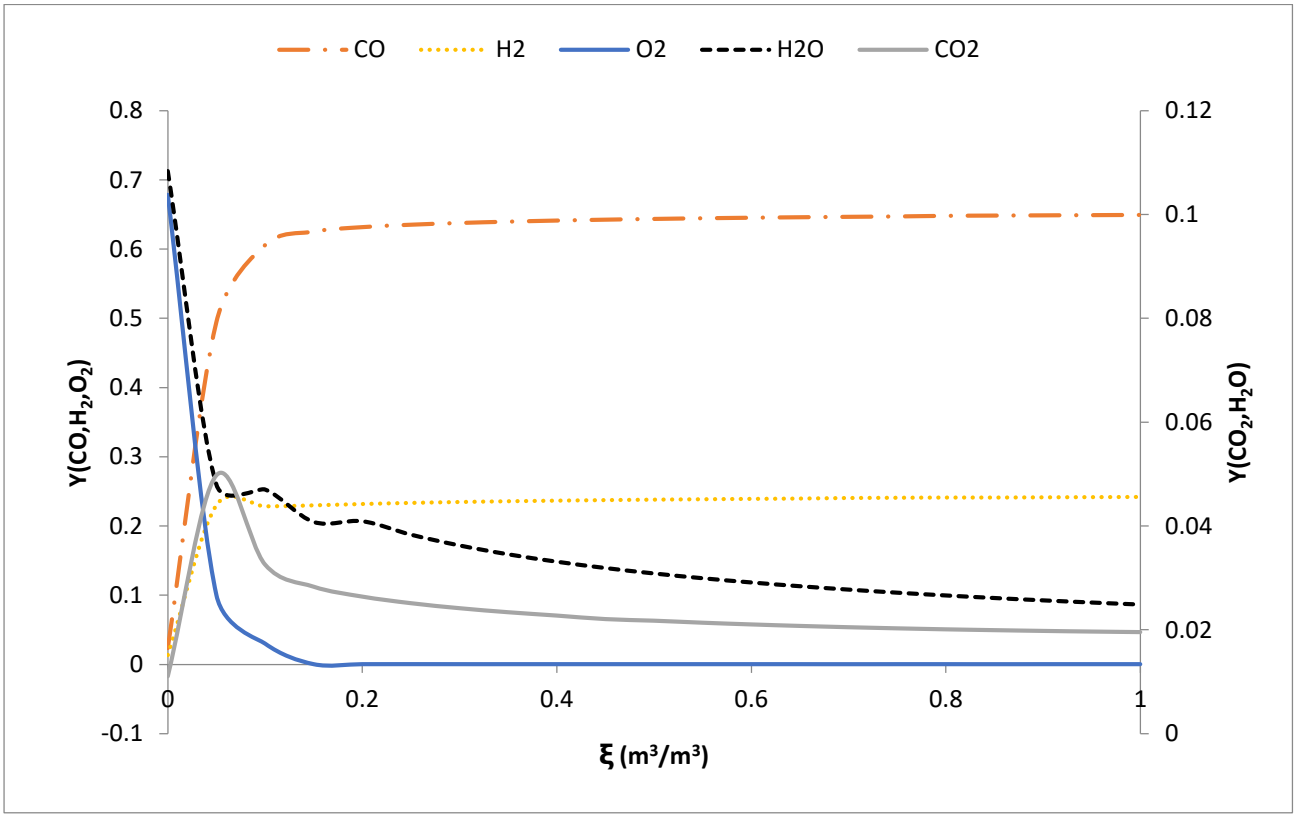

Figure 4.3. Mole fraction of gases in the nitrogen-fed EFG

4.1.2 Simulation of Elcogas-Prenflo gasifier

The Prenflo is the gasification technology employed at the world's largest solid feedstock-based gasifier at ELCOGAS's Puertollano IGCC plant in Spain (NETL). The design fuel for the gasifier is a mixture 50:50 by weight of low-grade coal and petroleum coke (Casero et al., 2017). This mixture is known as coal dust. The use of two different carbonaceous feed makes

the gasifier, a co-gasification reactor. There are studies (Uson et al., 2004; Valero and Uson, 2006) that have simulated the Prenflo gasifier with three or more feeds. However, this simulation focuses on the co-gasification of coal and petcoke. According to Casero et al. (2017), the operating conditions of the reactor are 0.68–0.72Nm^3 /kg for O^2/C and 0.1 kg/kg for steam/Coal. The composition of the feed mixture and the gasifier specifications can be found in Table 4.2. The oxidant composition of the Prenflo gasifier is 85% oxygen (Uson et al., 2004). It must be stated that the final moisture content of the mixture entering the gasifier is 2% and not 9.4% as shown in Table 4.2. This is standard practice for most dry-fed gasifiers (Lee et. Al., 2014). Hence, both proximate and ultimate analyses are recalculated based on a final drying moisture content of 2%. As it has been stated, the Prenflo gasifier operates as a CSTR (Higman and van Burgt, 2013). However, some studies have reported that two CSTRs in series followed by an equilibrium reactor can be used in the modelling of a Prenflo gasifier (Perez-Fortes et al., 2009). Hence, this study uses two CSTRs in series in simulating the Prenflo. This study does not include the equilibrium reactor since it is assumed that equilibrium is not achieved in the gasifier.

Table 4.2. Final fuel properties for the 50:50 (wt. %) mixture of coal and petcoke (Casero et al., 2017).

Proximate Analysis of feed		**Ultimate (Ar) analysis of feed**	
VM *(%)*	15.92	C (%)	59.21
FC *(%)*	54	H (%)	2.80
Ash *(%)*	20.68	O (%)	3.32
MC *(%)*	9.4	N (%)	1.36
		S *(%)*	3.21
Gasifier parameters			
β_{H_2O}	0.1	β_{O_2}	0.92
HHV (MJ/kg)	23.12	$P_{Gasifier}$ *(Bar)*	30

4.1.2.1 Simulation results

Figure 4.4 compares the results of the two-CSTR model extracted from the developed superstructure to the results from the Elcogas plant (Casero, 2007). There are two forms of Elcogas plant data namely design data and the averages of the actual plant data. From the results, it is observed that the developed model slightly over-predicts the composition of carbon monoxide. The difference between carbon monoxide predicted by the model and the design along with the actual plant data are 3.1% and 5.3% respectively. The developed model slightly

underpredicts the composition of hydrogen. The difference between hydrogen predicted by the model and the design and average plant data is 4.6% and 0.7% respectively. The biggest deviations between this model and Elcogas plant data are nitrogen and carbon dioxide. The lower composition of carbon dioxide is due to the overprediction of carbon monoxide, however, the discrepancies in the amount of nitrogen in the fuel-gas maybe be due to the lack of information on the amount of nitrogen used in transporting the coal dust feed. Table 4.3 summarizes other critical parameters from the simulation of the Prenflo gasifier.

Table 4.3. . Other gasifier parameters

Parameters	**Value**
CGE	83.57%
X_{Char}	99%
T_1^{Out}	1768.4^0C
T_2^{Out}	1738.5^0C

The model predicts a cold gas efficiency (CGE) of 83.5% and a carbon conversion of 99% both of which are in agreement with reported values (Cordis,1999). From Table 4.3, it can be seen that the temperatures of the two reactor chambers are very similar. This confirms the assertion by Higman and van de Burgt (2003) that the Prenflo acts as a single CSTR due to the very narrow temperature difference in the gasifier.

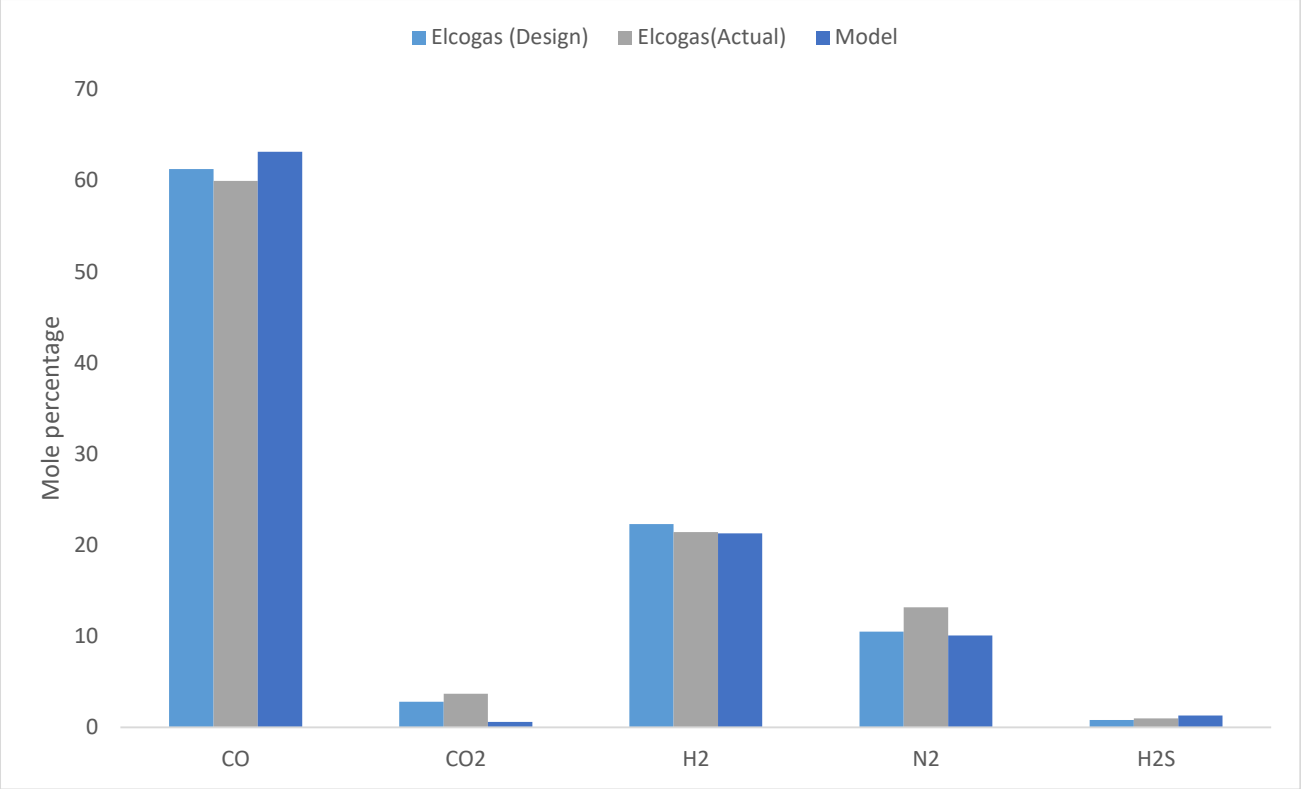

Figure 4.4. Comparison of model simulation with plant data

4.1.3 Simulation of a two-stage slurry-fed gasifier

The ability of the developed CSTR model to simulate a slurry-fed gasifier is tested by simulating a two-stage slurry-fed gasifier. A slurry-fed gasifier differs from a dry-fed gasifier based on the fluid used in transporting the coal feed. In the slurry-fed gasifier, water mixed with surfactants is used as the transporting medium for the coal feed. An example of a two-stage slurry-fed EFG is Conco-Philips or E-GAS™ gasifier. There is currently one IGCC plant using the E-Gas™ gasifier: the Wabash River IGCC plant in the USA (Majoumerd et al., 2014). The two-stage slurry-fed gasifier is modelled using two CSTRs in series. This is in agreement with the work of Lima et al. (2016) and Jillson et al. (2009) who described the two stages of the gasifier as a well-mixed reactor. The reference data for comparison with the simulation is taken from the work of Majoumerd et al (2014). The input data for the simulation is represented in Table 4.4. In addition to data represented in Table 4.4, 22% of the slurry is fed to the second

stage of the gasifier whiles the remaining 78% is fed to the first stage. The coal represented in Table 4.4 is bituminous.

Table 4.4. Input data for the simulation of a two-stage slurry-fed gasifier

Proximate Analysis of coal		**Ultimate (Ar) analysis of coal**	
VM (%)	27.00	C (%)	64.10
FC (%)	50.50	H (%)	5.02
Ash (%)	12.50	O (%)	16.09
Moisture (%)	10.00	N (%)	1.25
		S (%)	1.50
Gasifier parameters			
$w_{H_2O,Slurry}$	0.36	β_{O_2} (kg/s)	0.71
V_{TOTAL} (m^3)	23	$P_{Gasifier}$ (Bar)	43

4.1.3.1 Simulation results

Figure 4.5 compares the results of the two-CSTR model developed in this study and results from Majoumerd et al. (2014). From the results, it is observed that the developed model over-predicts the composition of carbon monoxide, carbon dioxide, and hydrogen whiles under-predicting the water content. The difference between carbon monoxide predicted by the model and the study of Majoumerd et al. (2014) is 6.7%. The difference between the hydrogen composition predicted by the model and the aforementioned study is 11.96%. The difference between the predicted carbon dioxide composition and that of Majoumerd et al. (2014) is 4.91%. It must also be stated that although the developed model predicted a negligible amount of hydrocarbons in the syngas product, the study of Majoumerd et al. (2014) predicted up to 3% of hydrocarbons.

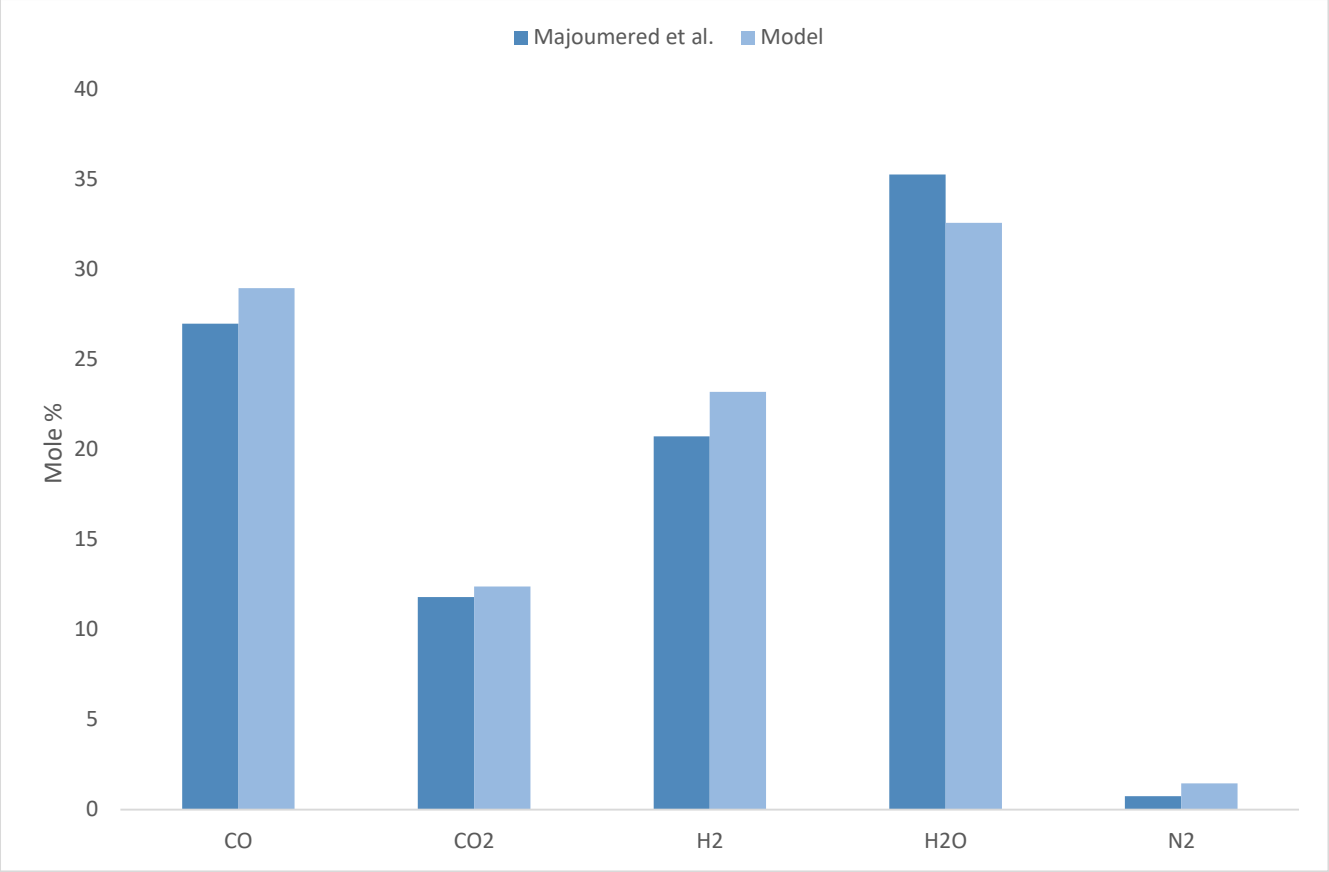

Figure 4.5. Comparison of model output with reference data

Table 4.5 shows that the model predicts a fuel-gas of LHV of 6.68MJ/kg and a carbon conversion of 93%

Table 4.5. Other gasifier parameters

Parameter	**Value**
Fuel-gas HHV	6.68 MJ/kg
X_{Char}	93%
T_1^{Out}	1628.2^0C
T_2^{Out}	1346.77^0C

4.1.4 Simulation of a one-stage slurry-fed gasifier

The PFR model developed is used in simulating the output of a one-stage slurry-fed gasifier. An example of such a gasifier is the Texaco or General Electric gasifier. The reference data for the validation is obtained from the work of Kasule et al. (2012). The work of Kasule et al. is a steady-state simulation of a PFR model with heuristic internal recirculation and plant data from Tampa Electrical Company (TECO). The coal used is Illinois no.6 type whose composition can be found in Table 4.6. The ratio of water to coal and ratio of oxygen to coal are 0.41 and 0.828 respectively. All ratios are stated on a mass basis. The operating pressure of the gasifier is 28 atm. Figure 6 shows the output of the PFR model in this study compared to the model of Kasule et al. (2012) and plant data from TECO.

Table 4.6. Input data for the simulation of a single-stage slurry-fed gasifier

Proximate Analysis of coal		**Ultimate (Ar) analysis of coal**	
VM (%)	34.99	C (%)	63.75
FC (%)	44.19	H (%)	4.50
Ash (%)	9.70	O (%)	6.88
Moisture (%)	11.12	N (%)	1.25
		S (%)	2.51
Gasifier parameters			
$w_{H_2O,slurry}$	0.3	β_{O_2}	0.83
V_{TOTAL} (m^3)	45	$P_{Gasifier}$ (Bar)	28

4.1.4.1 Output data

Figure 4.6 shows the comparison of the results from the PFR model to the study of Kasule et al. (2012). The concentration represented in figure 40 is on a dry basis. It is observed from Figure 39 that there is a fair agreement between the predicted data and the reference data. Comparing the output of the PFR model to that of Kasule et al. (2012), there is a relative error of 9.8% for CO predictions, 11.4% for CO_2 predictions, 2.5%, and H_2 predictions.

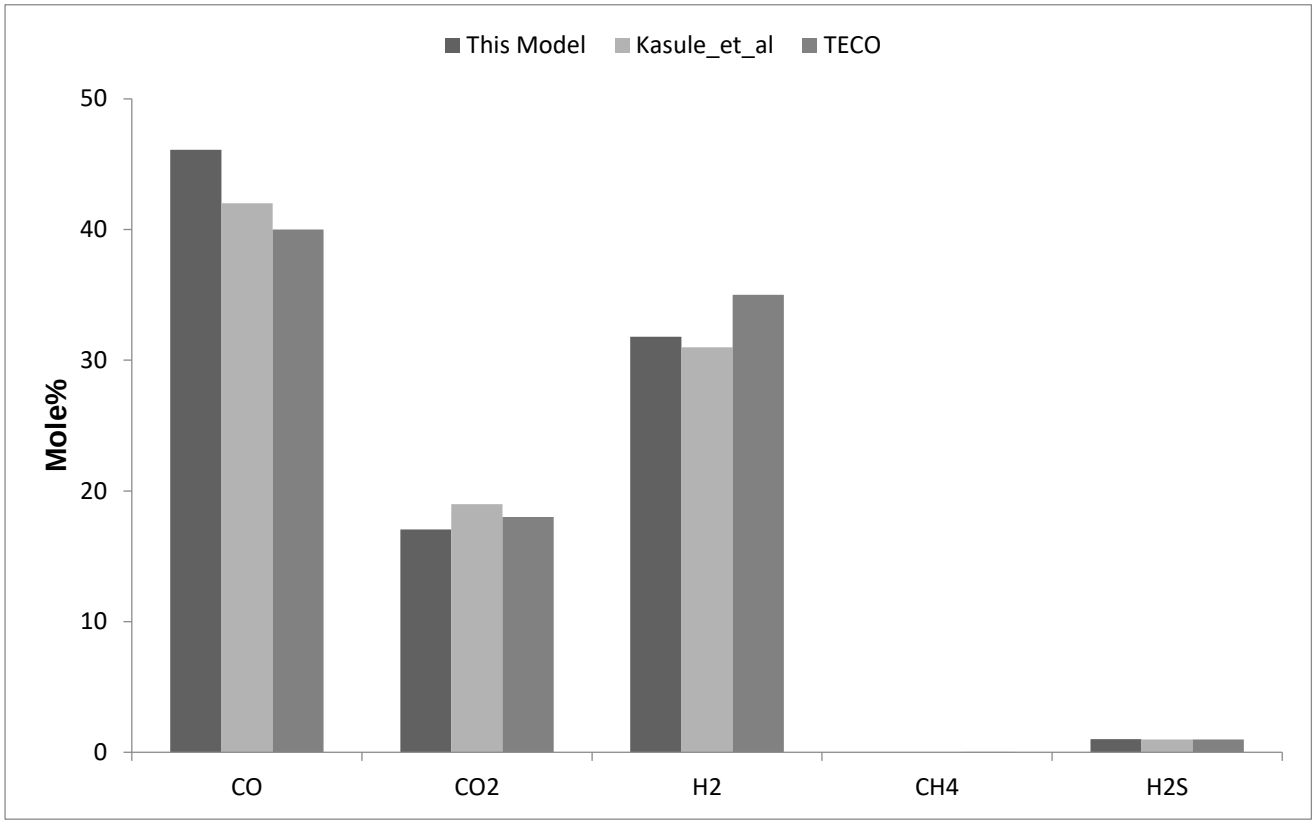

Figure 4.6. Comparison of model output with reference data

4.1.4.2 General model predictions

Figure 4.7 shows the temperature and conversion profile in the slurry-fed gasifier. The temperature profile shows a steep rise in the temperature of the early stages of the gasifier. As already said in the dry-fed gasifier, this is due to the combustion reactions in the presence of oxygen. This is followed by a gradual decrease in the reactor temperature. This is due to the

endothermic gasification reaction such as steam gasification, hydrogasification, and the Boudouard reaction. The exit temperature of the syngas is 1700 kelvin (1427 ^{o}C). Similar to the dry-fed gasifier, over 90% of the char conversion is also achieved within 10% of the reactor.

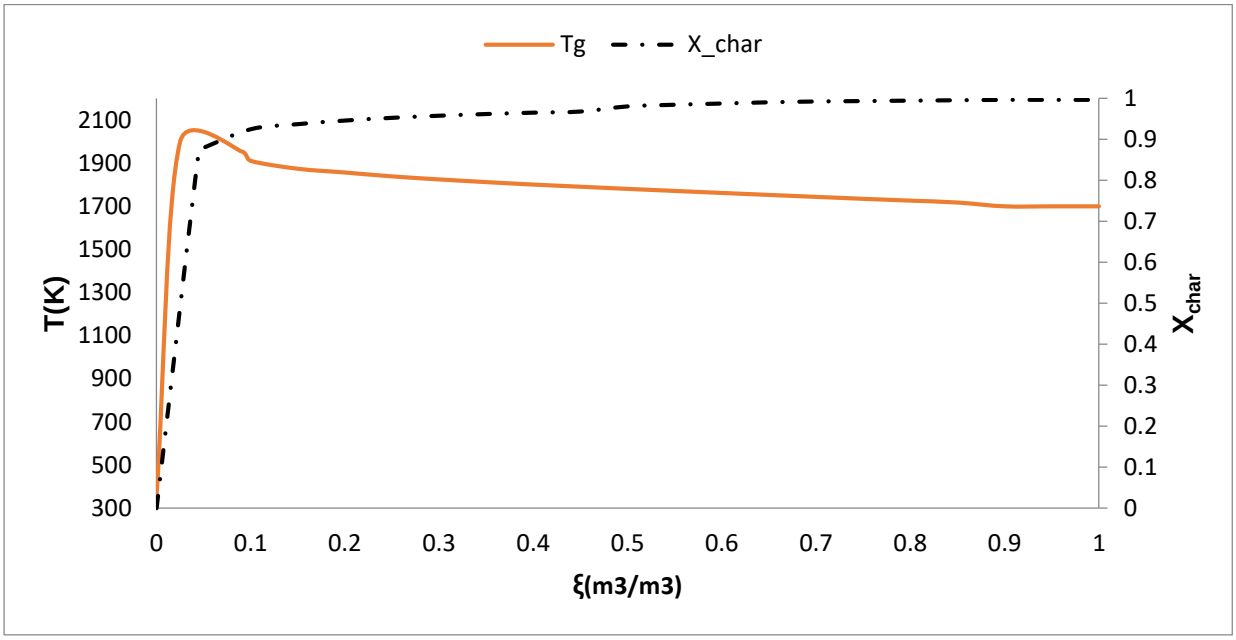

Figure 4.7. Temperature and conversion profile of a single-staged slurry-fed gasifier

Figure 4.8 displays the concentration profiles of the most significant species. It is observed that most of the oxygen is used within 10% of the reactor. This is due to the rapid combustion of volatile gases and char. The concentration profile of the carbon dioxide is plotted on a different scale to help to aid with its visibility. The combustion reactions occurring in the gasifier lead to an initial increase in the concentration of carbon dioxide in the gasifier. When the oxygen is depleted, the carbon dioxide concentration drops due to its consumption in the Boudouard reaction. After the observed drop in carbon dioxide concentration, there is a slow increase in the concentration of carbon dioxide throughout the gasifier volume. This is due to the effects of the water gas shift reaction. The hydrogen concentration profile shows an increased concentration throughout the gasifier. There is a steep increase in the initial parts of the reactor followed by a gradual increase in the hydrogen concentration. The water concentration

decreases throughout most of the gasifier. The concentration of carbon monoxide experiences a steep increase in the initial stages of the reactor and a slow decrease due to consumption by the water gas shift reaction.

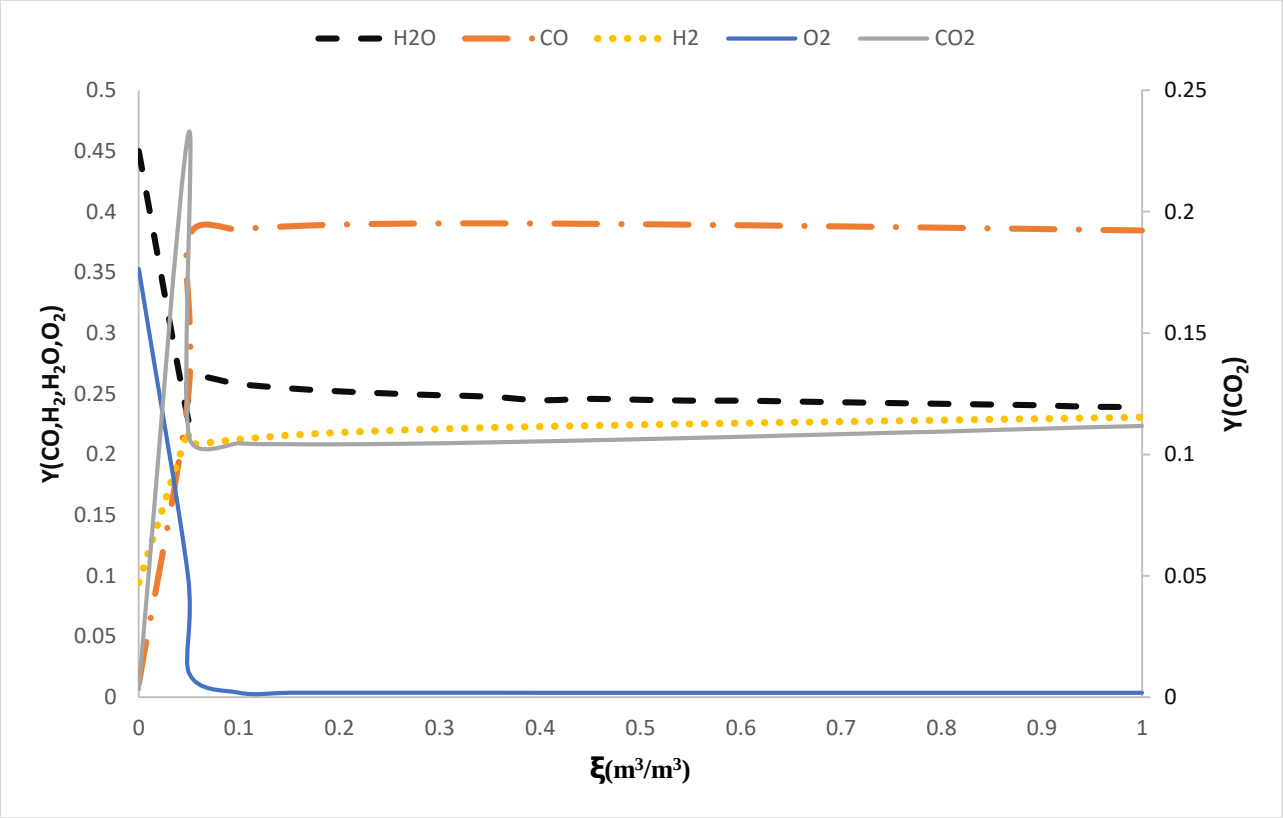

Figure 4.8. Concentration profiles in a single-staged slurry-fed gasifier

4.1.5 Discussion

The examples provided cover the different types of existing commercial and experimental EFGs. This study used either a standalone PFR or two CSTRs in series to satisfactorily predict gasification outcomes. This enables them to be used as the basic reactor units in the superstructure employed in the synthesis of an optimal gasifier.

4.2 Reactor synthesis

This section focuses on the use of the model based on the superstructure in the synthesis and design of an optimal gasifier for a single coal feed system. In each of the illustrative examples,

the new design obtained is compared to designs that already exist in literature. The models developed in this study are used to simulate the base case. This minimizes any discrepancies in the comparison between the base case and the optimal design that may result due to differences in assumptions between this study and the reference literature. The details of the synthesis problem are provided for each of the illustrative examples.

4.2.1 Synthesis of nitrogen fed gasifier

The first illustrative example involves the synthesis of an EFG with nitrogen gas as the transporting medium. The oxidizing agent used is pure oxygen. The objective function is the maximization of the CGE. The inputs for the optimization model can be found in Table 4.7.

The coal used is Pittsburgh no. 8. The base case or scenario 1 for this example is a conventional EFG design, which is a PFR (Lee et al., 2014; Ju and Lee, 2017). Scenario 2 for this example is a situation in which the oxygen to coal and the steam to coal ratios are varied under a fixed reactor configuration. All the feeds are also introduced at the inlet of the reactor. Scenario 3 is the optimal design, where both feed conditions and reactor configuration are treated as variables.

4.2.1.1 Results

The results of scenario 3 yield an optimal reactor network consisting of a CSTR followed by a PFR as indicated in Figure 5. The results show that a CSTR is needed when the feed is first introduced for the quick combustion reactions. These reactions usually require effective mixing which is provided by the CSTR. The PFR is also suitable for much slower reactions like Boudouard, steam gasification, and the water-gas shift. The size of the CSTR is $1m^3$ and the size of the PFR is 49 m^3. The nature of the reaction occurring in the different reactors accounts for different sizes. The results also show that feeding the steam to the second reactor is preferred.

Table 4.7. Input data for the synthesis of a dry nitrogen-fed gasifier

Proximate Analysis of coal		**Ultimate (daf) analysis of coal**	
VM (%)	35.82	*C* (%)	82.94
FC (%)	52.38	*H* (%)	5.63
Ash (%)	9.17	*O* (%)	7.05
MC (%)	2.63	*N* (%)	1.66
		S (%)	2.67
Coal heating properties			
HHV (MJ/kg)	30.5	T_{AF} (K)	1511
Gasifier parameters			
$F_{Max}^{H_2O}$ (kg/s)	5.0	$F_{Min}^{H_2O}$ (kg/s)	0
$F_{Max}^{O_2}$ (kg/s)	30	$F_{Min}^{O_2}$ (kg/s)	15
T_{Max} (K)	2400	T_{Min} (K)	1511
V_{Max} (m^3)	50	$P_{Gasifier}$ (bar)	45

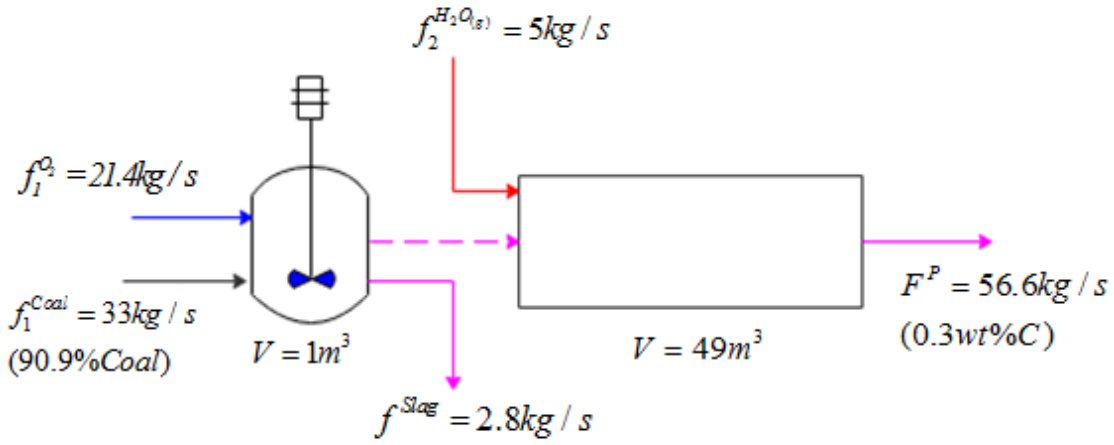

Figure 4.9. Optimal reactor design for a gasifier with nitrogen feeding

The efficiency of gasification is dependent on the amount of the coal converted to heat versus the amount of the coal converted to combustible syngas products such as carbon monoxide and hydrogen. When the percentage of coal converted to heat is very low, the temperature generated is not enough for the occurrence of gasification reactions. This leads to a low char conversion and CGE. Also, in the situation where the percentage of coal converted to heat is very high, it implies that the final product consists mostly of carbon dioxide and water leading to a low CGE. Hence, the role of reactor synthesis is to find the reaction path that creates conditions where there is an optimal balance between the conversion of coal to heat and syngas with combustible composition. The summary of the results obtained from the three scenarios is given in Table 4.8. The operating temperature of the gasifier is influenced by coal to oxygen and coal to steam ratio (Monaghan and Ghoniem, 2012). The results show that higher steam to coal ratio coupled with a decreased oxygen to coal ratio is the path that leads to a higher value of the objective function. Comparing scenarios 2 and 3, it is observed that the configuration of the reactor and the feed distribution also affect the performance of the gasifier.

As has been stated, all the steam is fed to the second reactor. The absence of steam in the first reactor implies that a very high reactor temperature is achieved at relatively low oxygen rates. This provides the energy needed for the gasification reactions occurring in the second reactor. The results show a lower fuel-gas exit temperature in the optimal design relative to the base case. This signifies a general reduction of combustion reactions and increased gasification reactions. For similar conversion rates, a lower fuel-gas temperature shows that most of the chemical energy in the coal has been converted into combustible products as opposed to sensible heat (Maurstad, 2005). This leads to a higher value of the objective function. The percentage improvement of the CGE is calculated relative to the base case. From Table 4.8, it is observed that while scenario 2 leads to 2.74% improvement, scenario 3 leads to a 6% improvement.

Table 4.8. Summary of optimization results for the synthesis of a dry nitrogen-fed reactor

	Base case	**Scenario 2**	**Scenario 3**
(a) Gasifier properties			
CGE (%)	81.6	83.9	86.5
%CGE improvement	-	2.74	6
X_{Char} (%)	99.5	99.1	99.1
Oxygen: Coal ratio	0.8	0.75	0.71
Steam: Coal ratio	0.04	0.17	0.17
(b) Other syngas properties			
HHV_{SG} (MW)	746.6	767.5	791.1
T^{Out} (K)	1956.9	1760.9	1749
F^{P} (kg/s)	55.42	57.93	56.6
Mw_{SG} (kg/kmol)	21.41	20.65	20.23

Table 4.9 shows the composition of the fuel-gas for the three scenarios. An analysis of the fuel-gas composition for the different scenarios shows that there is an increase in the hydrogen content for scenarios 3 and 2. This may be due to the effect of the water-gas shift reaction converting carbon monoxide and water to carbon dioxide and hydrogen, hence the reduction in the carbon monoxide composition for scenarios 2 and 3 when compared to the base case. Although the water gas shift reaction should lead to a reduction in the water composition in the final product that is not observed in scenarios 2 and 3. This is because of the high steam to coal ratio in both Scenarios 2 and 3. Comparing scenarios 2 and 3, it is observed that scenario 3 has a higher carbon monoxide and hydrogen composition. This is due to the slightly higher oxygen

to coal ratio for scenario 2, relative to scenario 3 (Table 4.8). This leads to the combustion of hydrogen and carbon monoxide, leading to an increase in the amount of water and carbon dioxide.

Table 4.9. . Product syngas composition for different scenarios for nitrogen-fed EFG

Gases	**Base case**	**Scenario 2**	**Scenario 3**
CO	65.52	58.49	59.92
H_2	24.84	27.52	29.77
H_2O	0.57	3.65	1.77
CO_2	0.30	2.01	0.90
C_2H_4	1.85	1.71	1.71
C_2H_6	0.42	0.39	0.39

4.2.2 Synthesis of carbon dioxide fed gasifier

The second illustrative example is the synthesis of an EFG with carbon dioxide as the transporting medium. The base case is taken from the study of Gazzani et al. (2013) where a reduced-order model (ROM) is used in the simulation of the EFG. This study uses a PFR for the simulation of the base case. Monaghan and Ghoniem (2012) stated that both ROM and a standalone PFR in the prediction of gasifier exit concentration could achieve comparative levels of accuracy. The input data for the base case can be found in Table 4.10. This example has three scenarios similar to example 1. It is worth noting that the coal is dried from a moisture concentration of 8% to 2%.

4.2.2.1 Results

Figure 4.10 shows that the optimal reactor sequence is two PFRs connected by a side stream. A PFR with a side stream has a mixing pattern that differs from a pure PFR. The optimal reactor design for this example is first PFR with a volume of 27.4 m^3 followed by another PFR of volume 21.6 m^3. The optimal design conditions involve the feeding of 46% of the total steam into the first reactor and the remainder into the second reactor.

Table 4.10. Input data for the synthesis of a dry carbon dioxide fed gasifier

Proximate Analysis of coal		**Ultimate (daf) analysis of coal**	
VM (%)	22.9	*C* (%)	66.52
FC (%)	54.9	*H* (%)	3.78
Ash (%)	14.15	*O* (%)	5.46
MC (%)	8	*N* (%)	1.56
		S (%)	0.52
Coal heating properties			
HHV (MJ/kg)	26.23	T_{AF} (K)	1511
Gasifier parameters			
$F_{Max}^{H_2O}$ (kg/s)	5.0	$F_{Min}^{H_2O}$ (kg/s)	0
$F_{Max}^{O_2}$ (kg/s)	30	$F_{Min}^{O_2}$ (kg/s)	15
T_{Max} (K)	2400	T_{Min} (K)	1511
V_{Max} (m^3)	50	$P_{Gasifier}$ (Bar)	45

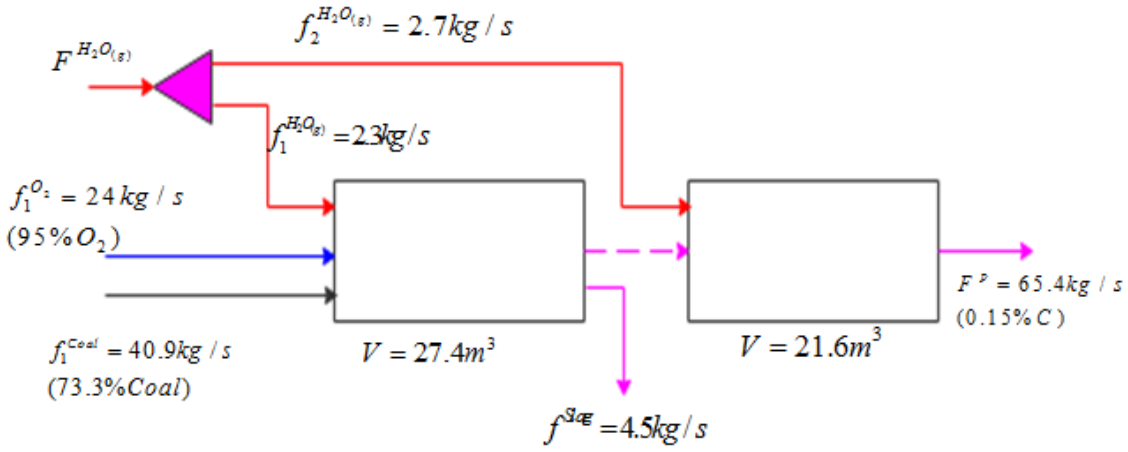

Figure 4.10. Optimal reactor design for a gasifier with carbon dioxide feeding

This shows that the amount of steam and oxygen used is key to the performance of the gasifier. From Table 4.11, it is observed that whereas scenario 2 leads to 4.1% improvement, scenario 3 leads to a 6.2% improvement. The increase in the objective function is due to reduced combustion reactions and an increase in gasification reactions. The main difference between the design obtained in scenarios 2 and 3 is how the steam is fed. While all the steam in scenario 2 is fed to the first reactor, scenario 2 has some of the steam fed to the second reactor. The variation in how the steam is fed, coupled with a reduction in the amount of oxygen used, leads to a different chemical environment hence a further improvement in the performance of the gasifier.

Table 4.12 shows the composition of the fuel-gas for the three scenarios. The carbon dioxide composition is high for all three scenarios compared to example 1. This is due to the use of carbon dioxide accompanying the coal feed. However, similar to example 1, the fuel-gas composition for the different scenarios shows that there is an increase in the hydrogen content for scenarios 3 and 2. This may be due to the water-gas shift reaction converting carbon monoxide and water to carbon dioxide and hydrogen. However, due to the high carbon dioxide

concentration through the gasifier, the effect of the water-gas shift reaction in a carbon dioxide-fed gasifier is different from the nitrogen-fed gasifier due to the shift in the equilibrium position.

Table 4.11. Summary of optimization results for the synthesis of dry carbon dioxide fed gasifier

	Base case	**Scenario 2**	**Scenario 3**
(a) Gasifier properties			
HHV_{SG} (MW)	696	724.18	738.75
% improvement	-	4.1	6.2
X_{Char} (%)	99.98	99.05	99.48
Oxygen: Coal ratio	0.83	0.81	0.80
Steam: Coal ratio	0.09	0.17	0.17
(b) Other syngas properties			
T^{Out} (K)	1833	1656	1679
F^{P} (kg/s)	65.8	65.9	65.41
Mw_{SG}	22.83	21.9	21.80

Table 4.12. Fuel-gas composition for three scenarios of a carbon dioxide-fed gasifier

Gases	**Base case**	**Scenario 2**	**Scenario 3**
CO	65.0	61.61	62.74
H_2	20.47	23.67	24.27
H_2O	6.89	6.82	6.22
CO_2	5.16	5.17	4.53

4.2.3 Synthesis of a slurry-fed gasifier

The third illustrative example involves the synthesis of a slurry-fed gasifier. The feed for this example is the Illinois number 6 type coal. The properties of this coal and the design parameters are found in Table 4.13.

Table 4.13. Input data for the synthesis of the slurry-fed gasifier

Proximate Analysis of coal		**Ultimate (Ar) analysis of coal**	
VM (%)	34.99	C (%)	63.75
FC (%)	44.19	H (%)	4.50
Ash (%)	9.70	O (%)	6.88
Moisture (%)	11.12	N (%)	1.25
		S (%)	2.51
Gasifier parameters			
$F_{Max}^{O_2}$ (kg/s)	30	$F_{Min}^{O_2}$ (kg/s)	15
θ_{Max}^{Coal}	0.3	θ_{Min}^{Coal}	0
T_{Max} (K)	2800	T_{Min} (K)	1511
V^{Max} (m^3)	45	*Pr* (bar)	28

This example also considers three scenarios. The first scenario or the base case is a standalone PFR with predetermined oxygen to coal ratios (Kasule et al., 2012). The second scenario is a gasifier with varying oxygen to coal ratio and secondary coal ratio in a pre-determined reactor configuration. The secondary coal ratio is defined as the ratio of coal fed to a secondary feed inlet to the ratio of total coal feed. Lang et al. (2011) first introduced the method demonstrated in scenario 2. In the aforementioned study, a two-stage gasifier is modelled using a Reduced Order computational fluid dynamics model. However, it has been demonstrated in literature

(Jillson et al., 2009; Lima et al., 2016) that a two-stage slurry gasifier can be modelled with two CSTRs in series. This study uses two CSTRs to model a two-stage slurry gasifier. For scenario 3, the developed superstructure is applied. The objective function for this optimization is the lower heating value of the syngas.

4.2.3.1 Results

Figure 4.11 shows that the optimal design configuration for the synthesis of the slurry-fed gasifier is a PFR with a side stream followed by a CSTR. The optimal design includes a 13.8 m^3 PFR reactor followed by a 20m^3 CSTR. The PFR has a secondary feed stream introduced at a volume of 5.2 m^3. The introduction of the secondary feed leads to improved gasification efficiency (Maurstad, 2005). This is due to the gasification reactions that occur when the newly introduced coal reacts with the high moisture and carbon dioxide content in the product syngas from the first PFR. scenarios 2 and 3 operate under similar principles and are therefore more efficient than scenario 1. The secondary coal ratio obtained for scenario 2 is similar to the value of 0.297 reported by Lang et al. (2011) for a two-stage slurry gasifier with the same feed.

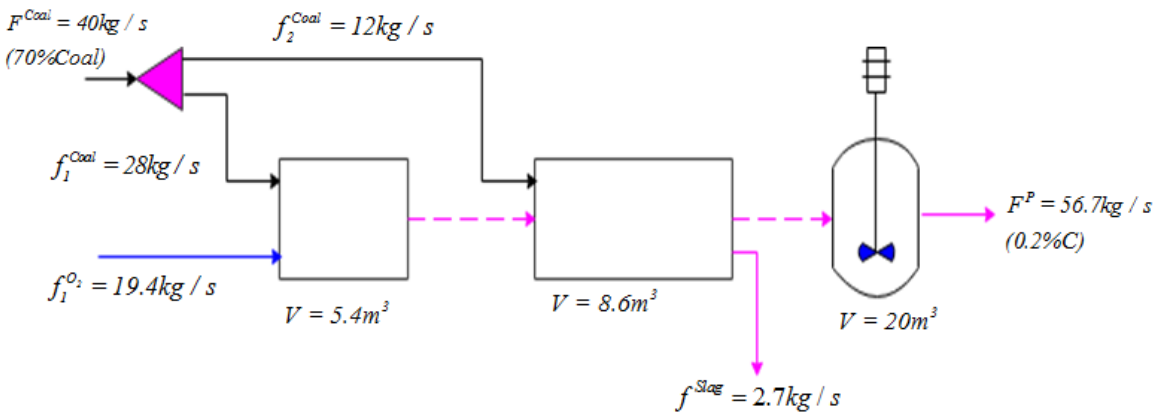

Figure 4.11. Optimal reactor design for the synthesis of a slurry fed gasifier

Table 4.14 summarizes the results of the three scenarios for this study. From Table 4.14, it is observed that while scenario 2 leads to a 4.4% improvement in the objective function, scenario

3 leads to a 13.3% improvement. This shows that the reactor configuration has a significant effect on the performance of a slurry-fed gasifier. It can be observed that scenario 3 has a higher secondary coal ratio as compared to scenario 2.

Table 4.15 shows the composition of the product fuel-gas for the three scenarios. The slurry-fed gasifier has higher amounts of water and carbon dioxide in its product compared to dry-fed ones. This is due to the high amount of water used in transporting the coal feed.

Unlike the two previous examples, the fuel-gas for scenarios 2 and 3 have a higher carbon monoxide and hydrogen composition compared to the base case. This cannot be attributed to the effect of the water-gas shift reaction. The increase in both carbon monoxide and hydrogen content of the product in scenarios 2 and 3 is due to the effect of steam gasification and the Boudouard reaction. The presence of additional char in the gasifier leads to these reactions.

Table 4.14. Summary of optimization results for the synthesis of a slurry-fed gasifier

	Base case	**Scenario 2**	**Scenario 3**
(a)Gasifier properties			
LHV(MW)	511.6	534	579.6
% improvement		4.4	13.3
X_{Char} (%)	99.7	97.3	99.6
Oxygen: Coal	0.83	0.75	0.69
θ^{Coal}		0.29	0.30
(b) Other syngas properties			
T^{Out} (K)	1776.8	1635	1606
F^{P} (kg/s)	60.1	57.9	56.7
Mw_{SG}	21.35	20.62	20

Table 4. 1. Fuel-gas composition for different scenarios of a slurry-fed gasifier

Species	Base case	Scenario 2	Scenario 3
CO	37.7	38.7	40.6
H_2	23.6	25.2	29.0
H_2O	23.3	21.7	17.5
CO_2	11.7	10.0	8.7
C_2H_4	1	1.2	1.1
C_2H_6	0.3	0.3	0.3

4.3 Summary

The ability of the mathematical model developed in chapter three to generate EFG designs that lead to better gasifier performance has been demonstrated in this chapter. The results indicate that superstructure optimization leads to an improvement in gasifier performance and that a lower oxygen rate and high steam rate lead to optimal gasifier performance. Furthermore, the results show that feed staging can be beneficial to the CGE of an EFG. Before the model was implemented, the CSTR and PFR units in the superstructure were validated by using a standalone PFR or two CSTRs in series to simulate EFGs under both dry and slurry conditions. The ability of these units to satisfactorily predict previously published data provides reliability for the optimization results.

References

Casero, P., 2007. Puertollano IGCC Power Plant. Operational Experience and Current Developments. *International Freiberg Conference on IGCC and Xtl Technologies*

Casero, P., Coca, P., García-Peña, F., and Hervás, N., 2017. Case Study: ELCOGAS Puertollano IGCC power plant, Spain. In: Wang, T., Stiegel, G. Integrated Gasification Combined Cycle (IGCC) Technologies, *Woodhead Publishing*, pp. 753–775

Cordis. 1999. Coal Gasification-Waste Heat Utilization. Available online at https://cordis.europa.eu/project/id/LG.-00354-87 [Accessed 7th June 2020]

Gazzani M, Manzolini G, Macchi E, Ghoniem A.F., 2013. Reduced Order Modelling of the Shell–Prenflo Entrained Flow Gasifier. *Fuel*, 101, pp. 822–837

Higman, C., van der Burgt, M., 2003. Gasification: *Elsevier Science*, pp. 120-124.

Jillson K.R., Chapalamadugu V, Ydstie B.E., 2009. Inventory and Flow Control of the IGCC Process with CO2 Recycles. *J Proc Cont*. 19(9):1470–1485.

Ju, Y., Lee, C.H., 2017. Evaluation of the Energy Efficiency of the Shell Coal Gasification Process. *Energy Conversion and Management*, 143, pp. 123–136.

Kasule, J. S., Turton, R., Bhattacharyya, D., Zitney, S. E., 2012. Mathematical Modelling of a Single-stage, Down-firing, Entrained-flow Gasifier. *Industrial and Engineering chemistry research*, 51, pp. 6429-6440.

Lang Y. Zitney S.E. Biegler L.T., 2011. Optimization of IGCC Processes with Reduced Order CFD Models. *Computers and chemical engineering*, 35, pp 1705– 1717.

Lee, H.H., Lee, J.C., Joo, Y.J., Oh M., Lee C.H., 2014. Dynamic modelling of Shell Entrained Flow Gasifier in an Integrated Gasification Combined Cycle Process. *Applied Energy*, 131. pp. 425–440

Lee, J.C., Lee, H.H., Joo Y.J., Lee, C.H., Oh, M., 2014. Process Simulation and Thermodynamic Analysis of an IGCC (Integrated Gasification Combined Cycle) Plant with an Entrained Coal Gasifier. *Energy*, 64, 58-68

Lima, F. V., Daoutidis, P., Tsapatsis, M., 2016. Modelling, Optimization, and Cost Analysis of an IGCC Plant with a Membrane Reactor for Carbon Capture. *AIChE Journal*, 62(5), pp. 1568-1580.

Majoumerd, M. M., Raas, H., De, S. Assadi, M., 2014. Estimation of Performance Variation of Future Generation IGCC with Coal Quality and Gasification Process – Simulation Results of EU H_2-IGCC Project. *Applied Energy*, 113, p. 452–462.

Maurstad O, Herzog H, Bolland O, Beér J., 2006. Impact of Coal Quality and Gasifier Technology on IGCC Performance. *In: 8th international conference on greenhouse gas control technologies (GHGT8)*, Trondheim, Norway

Monaghan, R. F. D., Ghoniem, A. F., 2012. A Dynamic Reduced Order Model for Simulating Entrained Flow Gasifiers: Part I: Model development and Description. *Fuel*, 91(1), pp. 61-80.

Monaghan, R. F. D., Ghoniem, A. F., 2012. A Dynamic Reduced Order Model for Simulating Entrained Flow Gasifiers: Part II: Model Validation and Sensitivity Analysis. *Fuel*, 94, pp.280-297.

NETL. UHDE-Prenflo. [Online]. Available online at https://netl.doe.gov/research/coal/energy-systems/gasification/gasifipedia/uhde-prenflo [Accessed 7 June 2020]

Pérez-Fortes, M., Bojarski, A. D., Ferrer-Nadal, S., Kopanos G.M., Nougués J.M., Velo, E., Puigjaner, L., 2008. Enhanced Modelling and Integrated Simulation of Gasification and Purification Gas Units Targeted to Clean Power Production. 18th European Symposium on Computer-Aided Process Engineering – ESCAPE 18

Pérez-Fortes, M., Bojarski, A. D., Velo, E. and Nougués, J. M., 2009. Conceptual model and Evaluation of Generated Power and Emissions in an IGCC Plant. *Energy,* 34(10), pp. 1721-1732.

Valero, A., Uson S., 2006. Oxy-co-gasification of Coal and Biomass in an Integrated Gasification Combined Cycle (IGCC) Power Plant. *Energy*, 31, pp. 1643–1655.

Uson, S., Valero, A., Correas, L., Martínez, A. 2004. Co-Gasification of Coal and Biomass in an IGCC Power Plant: Gasifier Modelling. *Int. J. Thermodynamics*, 7 (4), pp.165-172

5. MODEL DEVELOPMENT FOR THE SYNTHESIS OF AN OPTIMAL IGCC FLOWSHEET

This chapter focuses on developing a mathematical model that can synthesize the optimal IGCC flowsheet. This includes determining the optimal gasifier design and also the optimal integration between the ASU and the gas turbine. This is achieved by embedding the reactor superstructure developed in Chapter 3 in an IGCC model. The stages in developing the full IGCC model include stating the problem statement, developing a superstructure, and formulating mathematical equations from the described superstructure. The chapter ends with the definition of the objective function, which is the net thermal efficiency of the IGCC process.

5.1. Problem statement

The problem statement for the synthesis of the EFG is as follows.

Given:

(i) Coal of known composition and flowrate

(ii) A set of reactions occurring in a gasifier and their kinetic data

(iii) The enthalpy and density of reacting species

(iv) Different process units and their interconnections in the IGCC process

(v) The operating temperature and pressure for the different process units

(vi) The efficiency of the compressors and turbines;

(vii) The source and target temperatures for various process streams

Determine:

(i) The optimal reactor network

(ii) The volume of reactor units

(iii) The optimal steam to coal ratio

(iv) The optimal coal to oxygen ratio

(v) The feeding strategy

(vi) Optimal nitrogen flowrate into the gas turbine

(vii) Optimal air extraction

5.2 Superstructure development

The superstructure representation on which the proposed model is developed is shown in Figure 5.1. The components of the superstructure include a superstructure for the synthesis and design of the gasifier, an ASU, the gas turbine, and the HRSG. The superstructure for the synthesis and design of a gasifier has thoroughly been explained in Chapter 3. The reactor superstructure determines the composition, flowrate, and temperature of the fuel-gas product. These outputs determine the power generated in the combined cycle. The heating value of the fuel-gas produced determines the power output of the gas turbine. The exit temperature of the fuel-gas affects the amount of steam generated by the HRSG, which in turn determines the power output of the steam side. The reactor superstructure also determines the steam and oxygen flow into the gasifier. The total oxygen flowrate into the gasifier determines the load on the ASU main air compressor (MAC) and the oxygen product compressor. This affects the total auxiliary power consumed, hence the efficiency of the IGCC plant (Giuffrida et al., 2011). The amount of steam used in the gasifier also determines the amount of steam available for power generation (Majoumerd et al., 2012). Other optimization options provided by the superstructure include the amount of nitrogen injected into the gas turbine as part of its feed. This has the potential of increasing the power output of the gas turbine (Maurstad, 2005; Emun et al., 2010; Majoumerd et al., 2012). However, the nitrogen from the ASU must be compressed before injection into the gas turbine. This increases the power consumption and can therefore reduce the net power generated by the IGCC leading to a decrease in the efficiency of the plant. Hence, the optimization decision is the degree of injection that could lead to an increase in the efficiency of the IGCC plant. Another decision variable in the superstructure is the degree of

air extraction from the gas turbine to the ASU. The MAC of the ASU has a lower efficiency than the compressor of the gas turbine (Maurstad, 2005). Hence, the extraction of air from the compressor of the gas turbine to the ASU reduces the net power consumption but can also lead to a decrease in the gas turbine power output (Anand et al., 1996; Lee et al., 2007; Wang et al., 2016). Hence, there is the need to find the optimal extraction of air from the gas turbine into the ASU.

In summary, the superstructure provides choices such as the reactor configuration of the gasifier, the oxygen and steam rate into the gasifier, the ASU operating pressure, the degree of air extraction from the gas turbine into the ASU, and the degree of nitrogen injection into the gas turbine. Although the effect of most of these variables on efficiency has been explored, no study has combined all these variables. Hence, this approach makes a major contribution to determining the optimal flowsheet for an IGCC process.

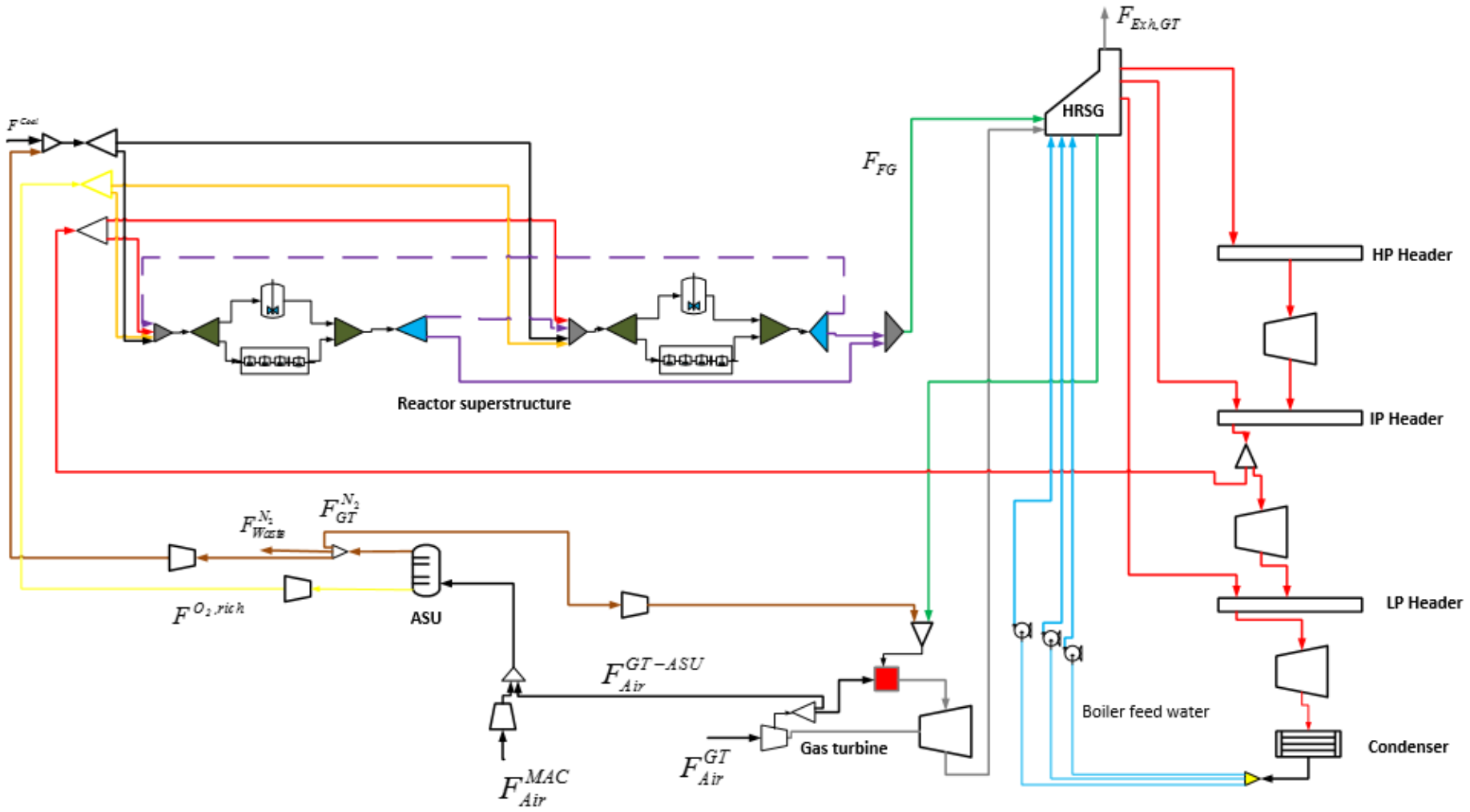

Figure 5.1. A superstructure for the optimal synthesis of an optimal IGCC plant

5.3 Mathematical formulation

This section explains the mathematical equations, describing the superstructure. The model equations describing the reactor superstructure are described in Chapter 3. This section will focus on explaining the model equations for the ASU, the gas turbine, and the HRSG.

5.3.1 ASU

This study employs a lumped model in the modelling of the unit. This model was used in the study of Jillson et al. (2009) and Lima et al. (2016). The ASU model assumes a one-stage flash operated isothermally at a temperature of 305 K. Air is assumed to contain only nitrogen and oxygen (Figure 5.2).

Equation (5.1) states that the total flowrate of the air into the ASU, F_{Air}^{ASU}, is equal to the sum of the oxygen-rich stream flowrate, $F^{O_2,rich}$, and nitrogen-rich stream flowrate, $F^{N_2,rich}$. Equation (5.2) is a component balance on nitrogen across the flash column.

$$F_{Air}^{ASU} = F^{N_2,rich} + F^{O_2,rich} \tag{5.1}$$

$$F_{Air}^{ASU} Y_{Air,N_2}^{ASU} = F^{N_2,rich} Y_{N_2}^{N_2,rich} + F^{O_2,rich} Y_{N_2}^{O_2,rich} \tag{5.2}$$

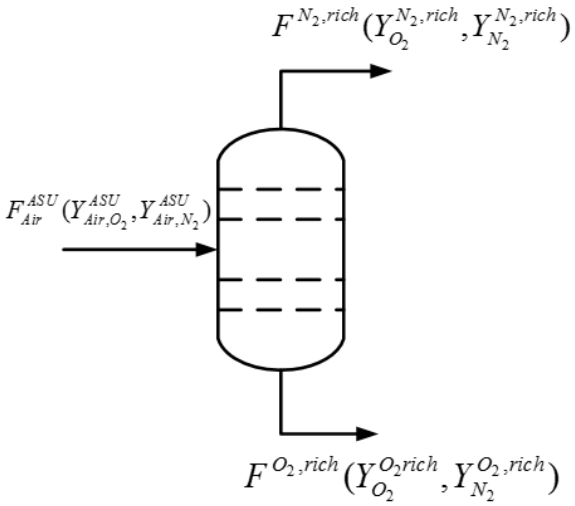

Figure 5.2. A simplified diagram of the cryogenic ASU

The composition of the oxygen-rich ($Y_{N_2}^{O_2,rich}, Y_{O_2}^{O_2,rich}$) and nitrogen-rich ($Y_{N_2}^{N_2,rich}, Y_{O_2}^{N_2,rich}$) streams are calculated using equations (5.3) and (5.4).

$$Y_{N_2}^{N_2,rich} = \frac{\alpha Y_{N_2}^{O_2,rich}}{\alpha Y_{N_2}^{O_2,rich} + Y_{O_2}^{O_2,rich}} \tag{5.3}$$

$$Y_{N_2}^{O_2,rich} + Y_{O_2}^{O_2,rich} = 1 \tag{5.4}$$

Where the relative volatility α equals 1881 (Jilson et al, 2009).

5.3.2 Integration between ASU and gas turbine

Figure 5.3 shows that the air to the ASU can be supplied in two ways. These are through the MAC of the ASU or from the compressor of the gas turbine. Therefore, equation (5.5) states that the total airflow into the ASU, F_{Air}^{ASU}, is equal to the sum of the air from the MAC, F_{Air}^{MAC} and the air from the gas turbine, F_{Air}^{GT-ASU}.

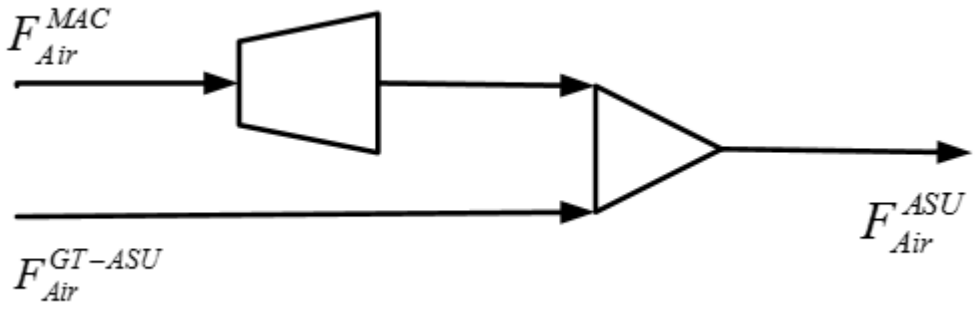

Figure 5.3. Air supply into the ASU

$$F_{Air}^{ASU} = F_{Air}^{MAC} + F_{Air}^{GT-ASU} \tag{5.5}$$

Equation (5.6) states that the air extraction ratio, θ_{Air}, equals the ratio of the air flowrate from the gas turbine, F_{Air}^{GT-ASU}, to the total air flowrate into the ASU, F_{Air}^{ASU}.

$$\theta_{Air} = \frac{F_{Air}^{GT-ASU}}{F_{Air}^{ASU}} \tag{5.6}$$

Figure 5.4 shows the options available to the nitrogen-rich stream produced by the ASU. These are it can be used to transport coal into the gasifier, $F_{Gasifier}^{N_2}$, injected into the gas turbine, $F_{GT}^{N_2}$, and/or disposed of as waste, $F_{Waste}^{N_2}$. Hence equation (5.7) states that the flowrate of the nitrogen-rich stream, $F^{N_2,rich}$, equals the sum of the three aforementioned streams. For slurry-fed gasifiers, $F_{Gasifier}^{N_2}$, is set to zero.

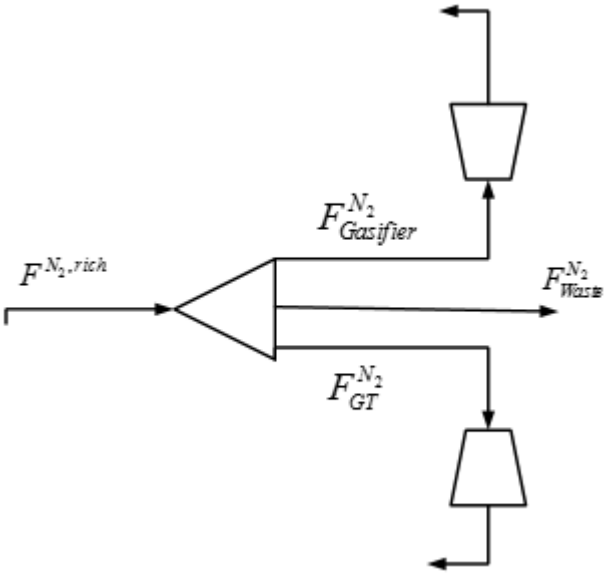

Figure 5.4. The balance on ASU nitrogen product

$$F^{N_2,rich} = F_{Gasifier}^{N_2} + F_{GT}^{N_2} + F_{Waste}^{N_2} \tag{5.7}$$

Equation (5.8) states that the ratio of the nitrogen injected, θ_{N_2}, equals the ratio of the flowrate of the nitrogen injected into the gas turbine, $F_{GT}^{N_2}$, to the sum of the flowrate of the disposed of nitrogen-rich stream, $F_{Waste}^{N_2}$, and the nitrogen injected into the gas turbine.

$$\theta_{N_2} = \frac{F_{GT}^{N_2}}{F_{GT}^{N_2} + F_{Waste}^{N_2}} \tag{5.8}$$

5.3.3 Compressors

There are several compressors in the IGCC plant, namely the MAC, the gas turbine compressors, the gasifier's oxygen, and nitrogen feed compressors, and the compressor for injected nitrogen. The equations developed under this section apply to all these compressors. This study uses standard thermodynamic equations to compute the power consumed by the compressors and the power generated by the expanders (Cengel and Boles, 2006; Moran and Shapiro, 2006). Equation (5.9) computes the exit temperature, $T_{Out,Isen}$, for isentropic compression from an inlet pressure, $P_{In,Comp}$, to an outlet pressure, $P_{Out,Comp}$. Equations (5.10) and (5.11) compute the isentropic power, $\dot{W}_{Isen,Comp}$ and the actual power, $\dot{W}_{Actual,Comp}$, consumed by a compressor of isentropic efficiency, $\eta_{Isen,Comp}$. Equation (5.12) computes the temperature of the stream exiting the compressor. All compressors were multi-staged and cooled.

$$\frac{T_{Out,Isen}}{T_{In}} = \left(\frac{P_{Out,Comp}}{P_{In,Comp}} \right)^{\frac{\gamma-1}{\gamma}} \tag{5.9}$$

$$\dot{W}_{Isen,Comp} = F_{Comp} \times Cp_{Comp} \times \left(T_{Out.Isen} - T_{In} \right) \tag{5.10}$$

$$\dot{W}_{Actual,Comp} = \frac{\dot{W}_{Isen,Comp}}{\eta_{Isen,Comp}} \tag{5.11}$$

$$\dot{W}_{Actual,Comp} = F_{Comp} \times Cp_{Comp} \times \left(T_{Out} - T_{In} \right) \tag{5.12}$$

5.3.4 Gas turbine

Figure 5.5 shows the gas turbine model used in this study. The components of the gas turbine include an air compressor, a combustion chamber, and an expander. Equation (5.12) states that the total airflow into the compressor of the gas turbine, F_{Air}^{GT}, equals the sum of the flowrate of the air into the combustion chamber, F_{Air}^{CC}, and the flow of the air extracted, F_{Air}^{GT-ASU}. Equation

(5.13) states that the flowrate of the combustion chamber exhaust, F_{CE}, equals the sum of the flowrates of the streams into the chamber. The streams into the chamber include the fuel-gas, F_{FG}, the injected nitrogen, $F_{GT}^{N_2}$, and the airflow into the combustion chamber, F_{Air}^{CC}. Equation (5.14) is a component balance of species entering the combustion chamber. Equation (5.15) computes the temperature of the combustion chamber. Each of the reactions occurring in the combustion chamber has an extent of reaction, $\in_m$, and a heat of reaction, $\Delta h_{Comb,\mathrm{m}}$.

$$F_{Air}^{GT} = F_{Air}^{Comb} + F_{Air}^{GT-ASU} \tag{5.12}$$

$$F_{Air}^{CC} + F_{FG} + F_{GT}^{N_2} = F_{CE} \tag{5.13}$$

$$F_{Air}^{CC} Y_{Air}^{i} + F_{FG} Y_{FG}^{i} + F_{GT}^{N_2} Y_{GT}^{N_2,i} + \sum_{m=1}^{M} \in_{m,i} = F_{CE} Y_{CE}^{i} \tag{5.14}$$

$$F_{Air}^{CC} h_{Air} + F_{FG} h_{FG} + F_{GT}^{N_2} h_{N_2} + \sum_{m=1}^{M} \in_m (-\Delta h_{Comb,\mathrm{m}}) = F_{\mathrm{CE}} Cp_{CE} \left(T_{Comb} - T_{\mathrm{Re}\,f} \right) \tag{5.15}$$

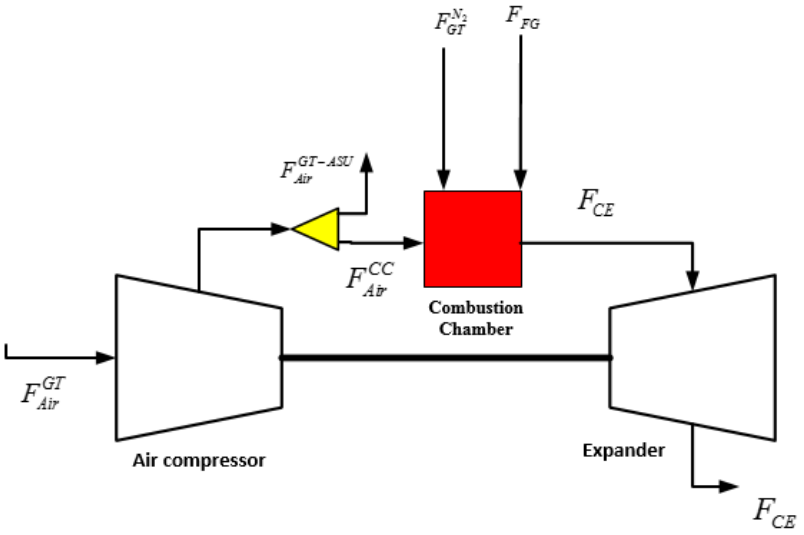

Figure 5.5. A simplified diagram of a gas turbine

Equation (5.16) computes the exit temperature, $T_{Out,Isen}$, for an isentropic expansion of the exhaust gas. Equations (5.17) and (5.18) compute the isentropic power, $\dot{W}_{Isen,Exp}$, and the actual power, $\dot{W}_{Acutal,\mathrm{Exp}}$, produced by an expander of isentropic efficiency, $\eta_{Isen,\mathrm{Exp}}$.

$$\frac{T_{Out,Isen}}{T_{In}} = \left(\frac{P_{Out,Exp}}{P_{In,Exp}} \right)^{\frac{\gamma-1}{\gamma}} \tag{5.16}$$

$$\dot{W}_{Isen,Exp} = F_{CE} \times Cp_{CE} \times \left(T_{In} - T_{Out.Isen} \right) \tag{5.17}$$

$$\dot{W}_{Acutal,\mathrm{Exp}} = \eta_{Isen,Exp} \dot{W}_{Isen,Exp} \tag{5.18}$$

The exit temperature of the exhaust gases, $T_{Out,Exp}$, is computed using equation (5.19).

$$\dot{W}_{Actual,Exp} = F_{CE} \times Cp_{CE} \times \left(T_{In,Exp} - T_{Out,\mathrm{Exp}} \right) \tag{5.19}$$

Equation (5.20) computes the net power output of the gas turbine.

$$\dot{W}_{Turbine} = \dot{W}_{Actaul,Exp} - \dot{W}_{Comp,GT} \tag{5.20}$$

5.3.5 Steam turbine

There are three steam turbines in the plant namely high, intermediate and low-pressure steam turbines. Equation (5.21) states the conservation of entropy, S, for a steam turbine undergoing isentropic expansion. The entropy of the steam is dependent on the temperature, T, pressure, P, and steam quality, x. If the steam is superheated, the entropy is just dependent on the temperature and pressure. Hence knowing the pressure of the exhaust stream, its temperature is calculated. Equations (5.22) and (5.23) compute the isentropic power $\dot{W}_{Isen,ST}$ and the actual power $\dot{W}_{Actual,ST}$ generated by a steam turbine of isentropic efficiency $\eta_{Isen,ST}$.

$$S_{In}(T_{In}, P_{In}, x_{In}) = S_{Out}(T_{Out}, P_{Out}, x_{Out}) \tag{5.21}$$

$$\dot{W}_{Isen,ST} = F_{H_2O_{(g)}} \times \left(h_{In} - h_{Out,Isen} \right) \tag{5.22}$$

$$\dot{W}_{Actual,ST} = \eta_{Isen,ST} \dot{W}_{Isen,ST} \tag{5.23}$$

The exit temperature of the steam leaving is computed using equation (5.24). This is because the exhaust steam enthalpy, h_{Out}, is a function of temperature, pressure, and quality (equation (5.25).

$$\dot{W}_{Actual,ST} = F_{H_2O_{(g)}}\left(h_{In} - h_{Out}\right) \tag{5.24}$$

$$h_{Out} = f(T_{Out}, Pr_{Out}, x_{Out}) \tag{5.25}$$

5.3.6 Heat recovery steam generator (HRSG)

Figure 5.6 shows the steam side of the IGCC plant. Figure 5.6 shows that the steam side has a three-pressure level HRSG. The configuration of the HRSG is taken from the work of Majoumerd et al. (2012). The HRSG is the heat exchanger network (HEN) used to recover heat in the steam side flowsheet. From Figure 5.6, the HRSG has two heat sources namely the raw fuel-gas and the gas turbine exhaust stream with flowrates F_{FG} and F_{CE} respectively. The raw fuel-gas is first used in generating high and intermediate pressure steams in the high and intermediate pressure evaporators (HP_EVAP and IP_EVAP) respectively. Equation (5.25) calculates the mass flowrate of the high and intermediate pressure steam from these pairings. Equations (5.26) and (5.27) enforce a pinch temperature of 10K. Equation (5.28) shows that the temperature into an evaporator, T_{Evap}^{In}, is the saturation temperature of the evaporator, T_{Evap}^{Sat} minus the approach temperature, T_{Evap}^{App}.

$$F_c\left(h_c^{Out} - h_c^{In}\right) = F_h\left(h_h^{In} - h_h^{Out}\right), \forall c \in C, h \in H \tag{5.25}$$

$$T_h^{In} - T_c^{Out} \geq 10, \forall c \in C, h \in H \tag{5.26}$$

$$T_h^{Out} - T_c^{In} \geq 10, \forall c \in C, h \in H \tag{5.27}$$

$$T_{Evap}^{In} = T_{Evap}^{Sat} - T_{Evap}^{App} \tag{5.28}$$

The remaining heat in the raw fuel-gas is used in heating the boiler feed water. The exhaust from the gas turbine is used for superheating in the high, intermediate, and low-pressure superheaters (HP_SH, IP_SH, and LP_SH). It is also used in the evaporator for low-pressure steam. The residual heat in the gas turbine exhaust stream is used together with raw fuel-gas in heating the boiler feed water. After the feed flow into the three pressure evaporators has been calculated, Equation (5.29) states that the total flow of water, F_{BFW}^{T}, equals the sum of the water flow into the high-pressure economiser, F_{BFW}^{HP}, the water flowrate into the intermediate-pressure economizer, and the flow into the low-pressure evaporator, F_{BFW}^{LP}.

$$F_{BFW}^{T} = F_{BFW}^{HP} + F_{BFW}^{IP} + F_{BFW}^{LP} \tag{5.29}$$

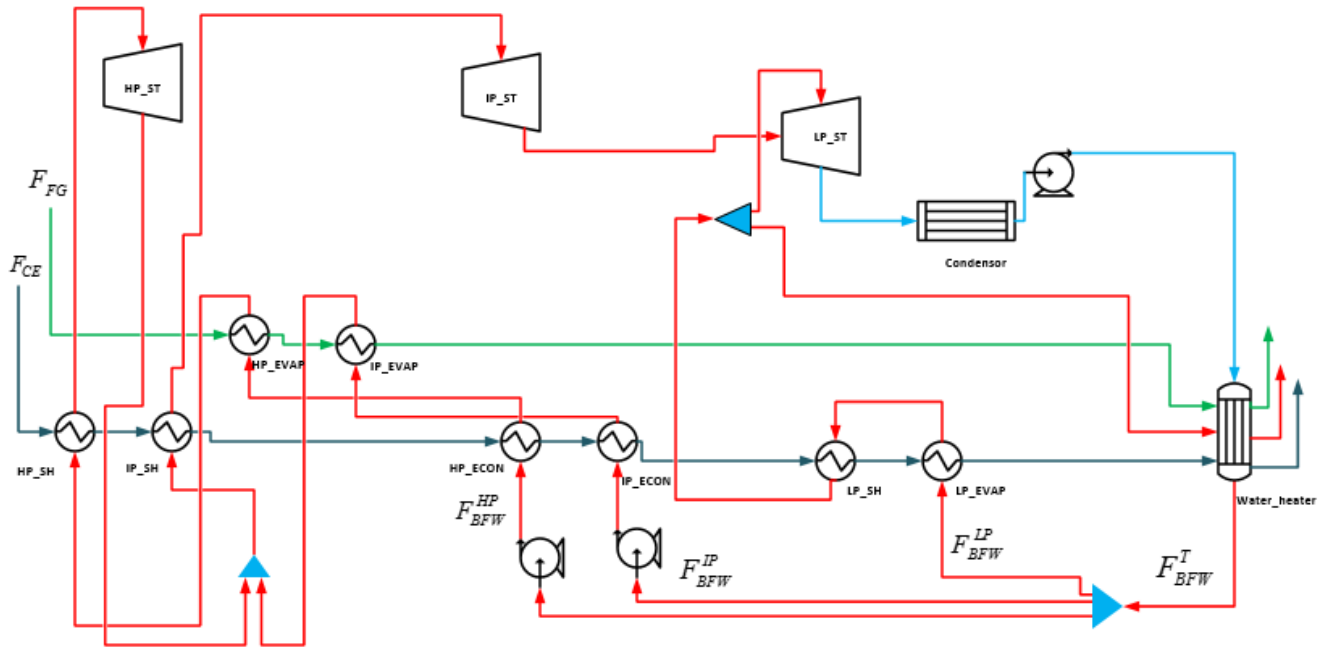

Figure 5.6. Heat exchanger network for the HRSG

Lastly, the mathematical equations developed for heat recovered by the HRSG compute the heat required by the water heater. Hence, there is a possibility that the residual energy of the fuel-gas and gas turbine exhaust stream is not sufficient to supply the energy required by the

water heater. This is resolved by extracting superheated low-pressure steam to supplement any residual heating requirement of the water heater (Campbell et al., 2010).

Equation (5.30) computes the pumping power, $\dot{W}_p^{Pump}$, for a pump, *p*, of efficiency, η_p^{Pump}, which increases the pressure of water of volumetric flowrate, $\dot{V}_p$, from an inlet pressure, P_p^{In}, to an outlet pressure, P_p^{Out}.

$$\dot{W}_p^{Pump} = \frac{\dot{V}_p \left(P_p^{Out} - P_p^{In} \right)}{\eta_p^{Pump}} \tag{5.30}$$

5.4 Objective function

The optimization problem presented in this study is focused on maximising the overall efficiency of the IGCC process (Lima et al., 2016).

Objective function:

$$MaxZ = \frac{\dot{W}_{GT} + \sum_{t=1}^{|T|} \dot{W}_{Actual,ST,t} + \sum_{b=1}^{|B|} \dot{W}_{Actual,Comp,b} - \sum_{p=1}^{|P|} \dot{W}_p}{F^{Coal} HHV^{Coal}} \tag{5.31}$$

5.5 Optimization

The final step is the use of the gPROMS platform to optimally synthesize the flowsheet of an IGCC process. The processes employed are as described under section 3.5. Figure 5.7 shows the gPROMS file used in the synthesis of the optimal IGCC flowsheet. It can be seen that except for the variable showing the variable for the air extraction and nitrogen injection, all the other variables are from the reactor superstructure. After all decision variables are specified, the software is run to obtain the optimum IGCC efficiency. The optimal IGCC flowsheet is deduced from both decision variables and calculated variables.

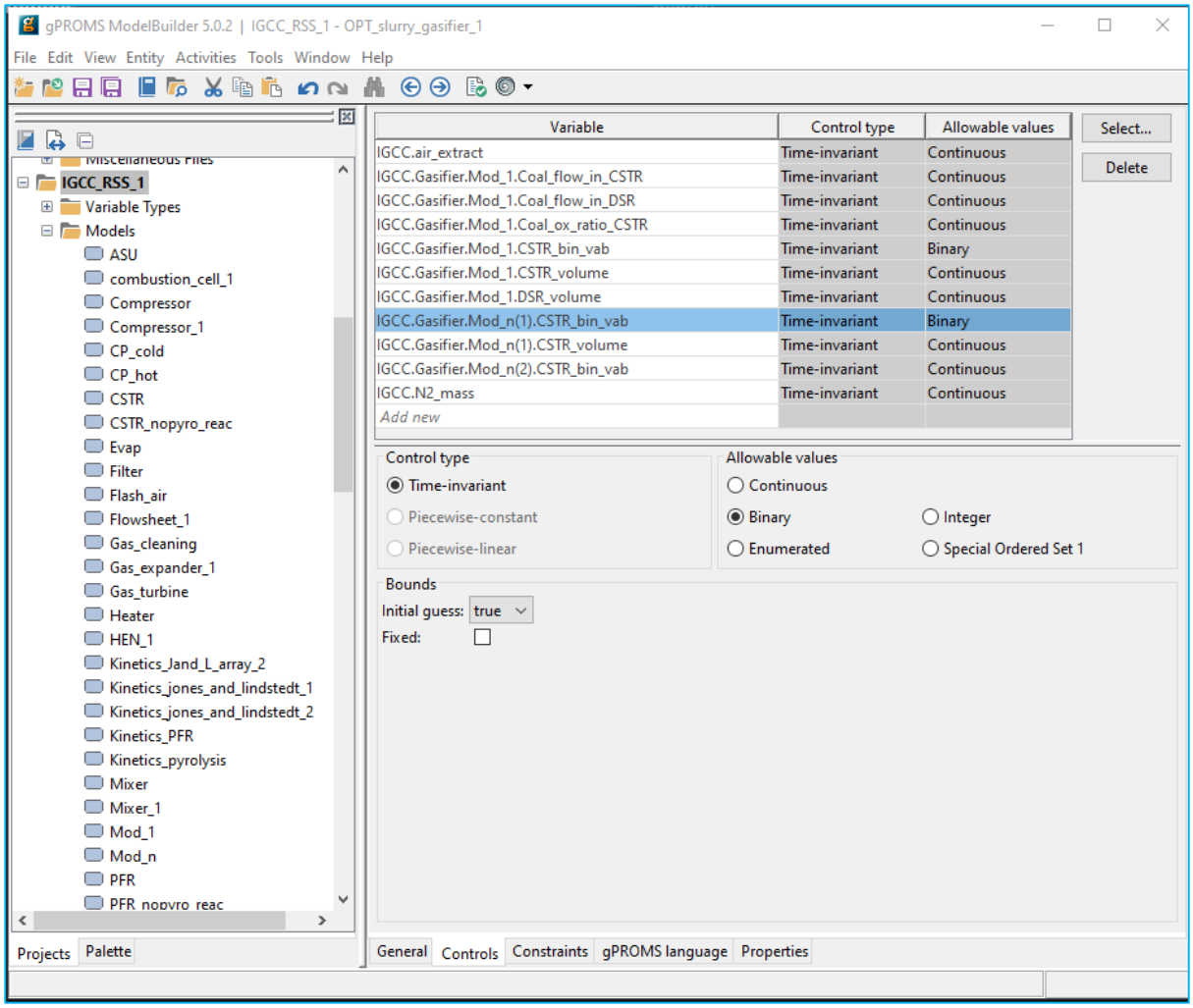

Figure 5.7. An interface showing the use of the gPROMS platform to synthesize an optimal IGCC flowsheet

5.6 Summary

A novel mathematical modelling technique for the synthesis of an optimal flowsheet of the gas-side of the IGCC process has been developed and explained. The approach involves integrating a gas turbine, an HRSG, steam turbine, and ASU with the reactor superstructure developed in chapter 3 to obtain a new superstructure. After the superstructure has been developed, mathematic equations describing it are formulated. The ability of the developed model to synthesize optimal IGCC flowsheets is demonstrated in the next chapter.

References

Anand, A. K., Cook, C. S., Corman, J. C., Smith, A. R., 1996. New Technology Trends for Improved IGCC System Performance. *Journal of Engineering for Gas Turbines and Power* 118, pp.732–736.

Campbell, P.E., McMullan, J.T., Williams B.C., 2000. Concept for a Competitive Coal-fired Integrated Gasification Combined Cycle Power Plant. *Fuel, 79*. pp. 1031–1040.

Cengel Y.A., Boles M.A., 2006. Thermodynamics: An Engineering Approach. Tata McGraw Hill. Fifth edition.

Emun, F., Gadallaa, M., Majozi, T. and Boer, D., 2010. Integrated Gasification Combined Cycle (IGCC) Process Simulation and Optimization. *Computers and Chemical Engineering*, 34(3), pp. 331–338.

Frey, H. C., Zhu, Y., 2006. Improved System Integration for Integrated Gasification Combined Cycle (IGCC) Systems. *Environmental Science and Technology*, 40(5), pp. 1693–1699.

Giuffrida, A., Romano, C. R., Lozza, G., 2011. Thermodynamic Analysis of Air-blown Gasification for IGCC Applications. *Applied Energy*, 88, pp. 3949–3958.

Jillson K.R., Chapalamadugu V, Ydstie B.E., 2009. Inventory and Flow Control of the IGCC Process with CO2 Recycles. *J. Proc. Cont.* 19(9), pp.1470–1485.

Lang Y. Zitney S.E. Biegler L.T., 2011. Optimization of IGCC Processes with Reduced Order CFD models. *Computers and chemical engineering*, 35, pp 1705– 1717.

Lee, C., Lee, S. J. and Yun, Y., 2007. Effect of Air Separation Unit Integration on Integrated Gasification Combined Cycle Performance and NOx Emission Characteristics. *Korean Journal of Chemical Engineering*, 24(2), pp. 368-373.

Lima, F. V., Daoutidis, P., Tsapatsis, M., 2016. Modelling, Optimization, and Cost Analysis of an IGCC Plant with a Membrane Reactor for Carbon Capture. *AIChE Journal*, 62(5), pp. 1568-1580.

Majoumerd, M.M., De S., Assadi M., Breuhaus P., 2012. An EU Initiative for Future Generation of IGCC Power Plants using Hydrogen-rich Syngas: Simulation Results for the Baseline Configuration. *Applied Energy*, 99, pp. 280-290.

Maurstad, O. 2005. An Overview of Coal based Integrated Gasification Combined Cycle (IGCC) Technology; MIT LFEE 2005-002 WP; Massachusetts Institute of Technology: Cambridge, MA

Moran, M.J., Shapiro, S.N., 2006. Fundamentals of Engineering Thermodynamics. John Wiley & Sons Inc. Fifth Edition. pp 174-257

Wang, M., Liu, G., Hui, C. W., 2016. Simultaneous Optimization and Integration of Gas Turbine and Air. *Energy*, 116, pp. 1294-1301.

6. ILLUSTRATIVE EXAMPLES FOR THE SYNTHESIS OF IGCC FLOWSHEET

This section uses the developed model based on the superstructure to synthesise an optimal IGCC flowsheet for two illustrative examples. There are three scenarios in each example. The base case or scenario 1 for each is a simulation of a standard IGCC plant. The second scenario is the synthesis and design of the gasifier with the background IGCC process. This is to determine if the gains in the CGE of the gasifier have a direct impact on the efficiency of the entire plant. The third and final scenario is the determination of the optimal flowsheet path for the IGCC. This includes the optimal gasifier design as well as the optimal integration between the ASU and the gas turbine and the optimal syngas to air ratio in the gas turbine.

6.1 General data

Table 6.1 shows the input data common to both illustrative examples. These include inputs to the HRSG, steam turbines, the ASU column and compressor, and the gas turbine expander and compressors. The data includes the pressure levels of the steam turbine, the efficiencies of all the turbines, pumps, and compressors, the approach temperature of the evaporators, the number of compression stages, and the inlet and outlet pressures and temperatures. The table also shows that there is no integration between the ASU and gas turbine i.e., there is no flow of air from the gas turbine and the ASU and no flow of nitrogen from the ASU to the gas turbine. The data on the HRSG is taken from Majoumerd et al. (2012) while that of the ASU and gas turbine is taken from Wang et al. (2016).

Table 6.1. Input data for the simulation of the IGCC

Steam turbine		**Gas turbine compressor**	
$P_{HP}/P_{IP}/P_{LP}$ (bar)	140/45/4	P_{In} (Bar)	1.01
$\eta_{ST,HP}$ (%)	97	P_{Out} (Bar)	20.27
$\eta_{ST,IP}$ (%)	95	$n^{cs}_{GT\_Comp}$	5
$\eta_{ST,LP}$ (%)	95	η_{Isen,GT_Comp} (%)	90
ASU compressors		**HRSG**	
$T_{In,Air}$ (°C)	25	$T_{SH,HP}, T_{RH,IP}$ (°C)	500
$P_{In,Air}$ (Atm)	1	$T_{SH,LP}$ (°C)	300
F^{GT-ASU}_{Air} (kg/s)	0	T^{App}_{Evap} (°C)	5
$F^{N_2}_{GT}$ (kg/s)	0	ΔT_{Pinch}, (°C)	10
$\eta_{Isen,N_2}/\eta_{Isen,O_2}/\eta_{Isen,MAC}$ (%)	80/80/85	P_{Cond} (Bar)	0.40
$n^{cs}_{MAC}/n^{cs}_{O_2}/n^{cs}_{N_2}$	4/8/8	T^{In}_{WH} (°C)	25
		η_{Pump} (%)	85
ASU column		**Gas turbine expander**	
P_{Column} (Bar)	15.20	$P_{Out,}$ (Bar)	1.01
ΔP_{Column} (Bar)	2.03	P_{In} (Bar)	20.27
		T_{Out} (°C)	577

6.2 Synthesis of an optimal flowsheet of an IGCC plant with a dry-fed gasifier

This section describes the use of the developed model in the synthesis of an optimal IGCC power plant with a dry-fed gasifier. Such an IGCC plant is known to have the highest overall thermal efficiency. A full description of the IGCC can be found in the work of Majoumerd et al. (2012) and Campbell et al. (2010). However, the process is described briefly. The hot fuel-gas of temperature 1200 to 1600°C leaving the gasifier is cooled to 900°C by mixing particle-free fuel-gas of temperature 200 to 300 °C. The product fuel-gas from the quench tank is further

cooled by the generation of saturated high-pressure steam and intermediate-pressure steam. It is then passed through filters to remove all particulates. The raw fuel-gas is further cooled to 35^{o}C by heating the boiler feed water. The cooled fuel-gas is passed through an absorption column to remove hydrogen sulphide. The clean fuel-gas is sent to the combustor of the gas turbine where it is mixed with compressed air to generate electricity. The exhaust gas leaving the gas turbine is used in superheating both high and intermediate pressure steam. The residual heat in the gas turbine is used in generating low-pressure steam. Except for the steam extracted as feed to the gasifier, all the steam generated is used in generating electrical power. The objective function of this case study is the thermal efficiency of the plant is based on an LHV basis.

6.2.1 Simulation of the base case

To be able to simulate the base case, the additional data needed is the composition of the coal, the gasifier specification, and the specification of the heat sources. The specification of the gasifier is displayed in Table 6.2. The coal used in this study is Pittsburgh number 8 coal whose properties are taken from the study of Campbell et al. (2010). Table 6.2 also contains the heat source specifications for the HRSG, and are the fuel-gas and the gas turbine exhaust gas. These aforementioned flowrates can only be determined after the simulations.

6.2.1.1 Model output

Table 6.3 summarizes the major output of the IGCC plant. The model developed in this study predicts a net efficiency of 45.6%. Compared to the value of 46.3% reported in the study of Majoumerd et al. (2012), there is a difference of 1.5%. This shows a close agreement between the prediction of this model and the reference value. In addition to the overall efficiency, the power output of the steam turbines makes 37% of the gross power generated. This also compares favourably to the 40% reported in literature (Campbell et al., 2010; Majoumerd et

al., 2012). The ASU power consumption makes up the majority of the auxiliary power consumption. This is in agreement with the observation in literature. Table 6.3 also provides a summary of steam side data.

Table 6.2. Input for the simulation of the IGCC plant

Gasifier data			
Proximate Analysis of coal		**Ultimate (daf) analysis of coal**	
VM (%)	35.82	C (%)	82.94
FC (%)	52.38	H (%)	5.63
Ash (%)	9.17	O (%)	7.05
MC (%)	2.63	N (%)	1.66
		S (%)	2.67
Coal heating properties			
LHV (MJ/kg)	29.71	T_{AF} (K)	1511
Gasifier parameters			
$F_{Max}^{H_2O}$ (kg/s)	5.0	$F_{Max}^{O_2}$ (kg/s)	30
F^{Coal} (kg/s)	30	$V_{Gasifier}$ (m^3)	3
P (Bar)	45		
HRSG HEN data			
Stream	T_S (^oC)	T_T (^oC)	
Fuel-gas 1	900	239	
Fuel-gas 2	239	35	
Gas turbine exhaust	577	100	

Figure 6.1 presents a summary for the base case IGCC plant. The difference in flowrate between the gasifier inlet and outlet is the amount of slag generated in the gasifier. It must also be noted that the differences between the flowrate of the fuel-gas, $F_{FG,1}$, entering and exiting the evaporators of the HRSG equals flowrate of the particulate matter removed after cooling.

Table 6.3. The performance of the IGCC base case plant

IGCC plant outputs		**Steam side stream flowrates**	
Gas turbine power (MW)	277	$F_{Exh,GT}$ (kg/s)	589.8
Steam turbine power (MW)	164.6	F_{Air}^{GT} (kg/s)	537.1
Gross power generated (MW)	441.6	$F_{H_2O_{(g)}}^{HP}$ (kg/s)	90.4
ASU compression power demand (MW)	30.7	$F_{H_2O_{(g)}}^{IP}$ (kg/s)	7.8
Gasification power demand (MW)	2.9	$F_{H_2O_{(g)}}^{LP}$ (kg/s)	40.2
HRSG pumping power (MW)	1.4	F_{BFW} (kg/s)	138.4
Total auxiliary power demand (MW)	35		
Net power output (MW)	406.6		
Net IGCC efficiency (% LHV)	45.6		

Table 6.4. HRSG HEN data

Stream data				
Stream	F_S	T_S (°C)	T_T (°C)	Δh (MW)
Fuel-gas 1	115.25	900	239	97.70
Fuel-gas 2	54.59	239	35	49.46
Gas turbine exhaust	589.8	577	100	354.24

Finally, differences between the flowrate of the fuel-gas, $F_{FG,2}$, entering and exiting the economizers of the HRSG equals flowrate of the gaseous pollutants removed after cooling. Figure 6.1 also shows that the total flowrate of the steam entering the IP steam turbine equals the sum of the exhaust of the HP turbine and the IP steam generated. However, the figure does not show the reheating of the intermediate steam that occurs before it enters the IP steam turbine. From table 6.4, the total heat recovered by the steam from the streams equals 501.4

MW. This implies that a total steam turbine output power of 164.6 MW is equivalent to a net thermal efficiency of the steam turbine of 33%.

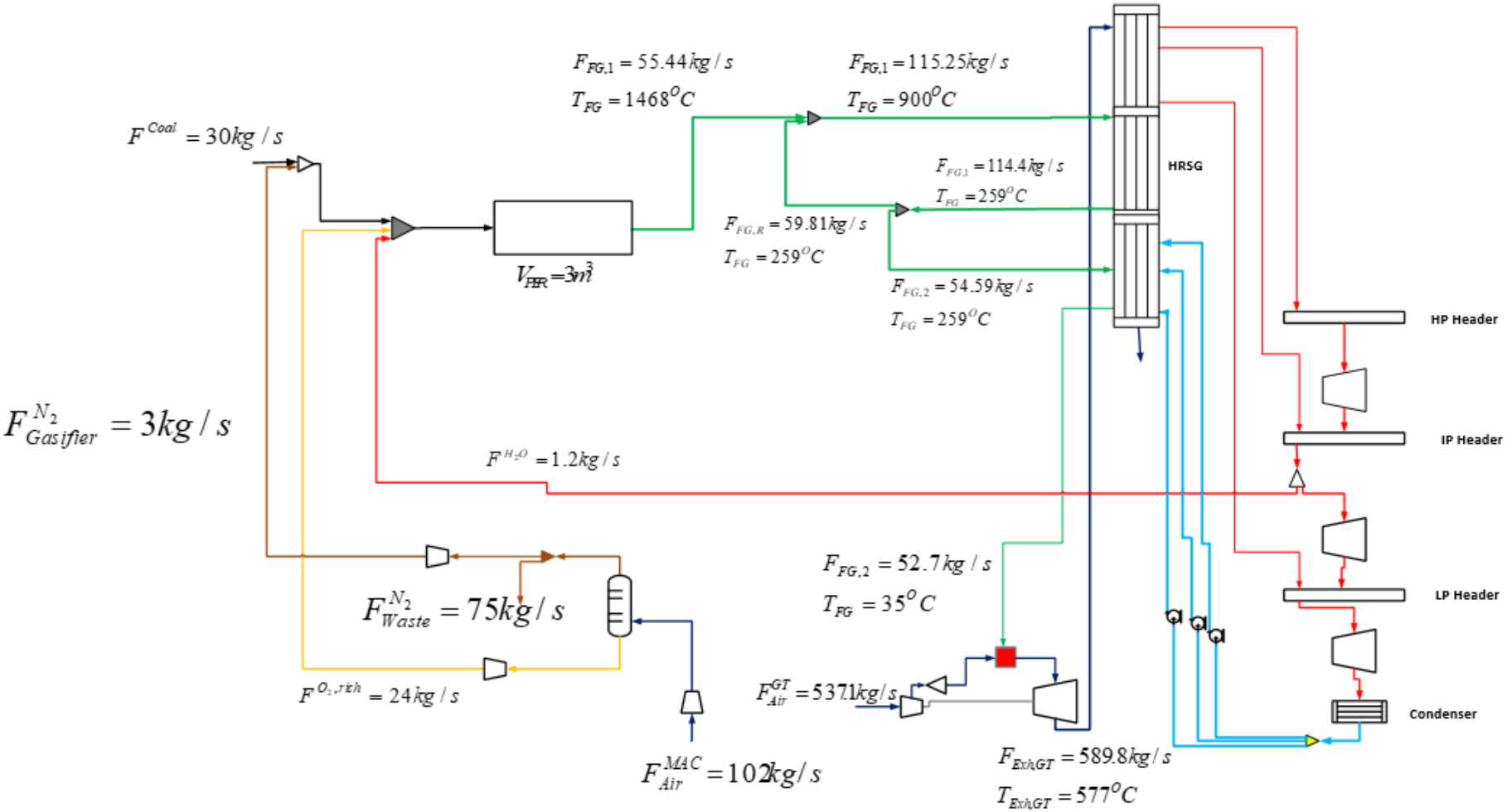

Figure 6.1. The flowsheet of a baseline IGCC plant with a dry-fed gasifier

6.2.2 Optimization of the IGCC process

After the simulation was completed, the optimal IGCC flowsheet is determined. Table 6.8 shows the optimization parameters considered. This includes the flow interval of the steam and oxygen. Table 6.5 shows the optimization parameters for the gasifier and ASU-gas turbine. The maximum air extraction ratio, $\theta_{Air,ASU}^{Max}$, is limited to 0.5. The percentage of ASU feed extracted from the compressor of the gas turbine is limited to 50% because a 100% supply of ASU air from the gas turbine will lead to start-up and operability issues.

Table 6.5. Optimization parameters for the synthesis of an IGCC plant with a dry-fed gasifier

Gasifier parameters			
$F_{Max}^{H_2O}$ (kg/s)	5.0	$F_{Min}^{H_2O}$ (kg/s)	0
$F_{Max}^{O_2}$ (kg/s)	30	$F_{Min}^{O_2}$ (kg/s)	15
T_{Max} (K)	2400	T_{Min} (K)	1511
V_{Max} (m^3)	50	Pr (bar)	45
ASU-gas turbine parameters			
$\theta_{N_2}^{Min}$	0	$\theta_{N_2}^{Max}$	1
$\theta_{Air,ASU}^{Min}$	0	$\theta_{Air,ASU}^{Max}$	0.5

6.2.3 Results

Table 6.6 summarizes the result of the optimization processes. The base case has already been described. scenario 2 represents the optimization of the thermal efficiency of the IGCC plant focusing only on the gasification variables. Scenario 3 focuses on both gasification parameters and the integration between the ASU and the gas turbine. From Table 6.6, it is observed that both scenarios 2 and 3 lead to an improvement of the IGCC performance. The main reason for

the improvements observed is the properties of the fuel-gas produced. The fuel-gas properties directly affect the amount of gas turbine power output and indirectly affect the steam turbines' power output. The increase in the heating value and flowrate of the fuel-gas leads to an increase in the gross power generated. Comparing scenarios 2 and 3, it is observed that the integration of the ASU and gas turbine leads to a further improvement in the efficiency of the IGCC plant. The effect of ASU-gas turbine integration on the efficiency of the IGCC has been well documented in literature (Frey and Zhu, 2006; Lee et al., 2007; Emun et al., 2010). However, in this study, it has been performed simultaneously with the optimization of the gasifier variables. From Table 6.6, it is observed that scenarios 2 and 3 have comparable gross power outputs but a higher variation in their net power outputs. The higher difference in the net power output is due to the lower ASU compression power in scenario 3. From Table 6.7, it is observed that scenarios 2 and 3 have similar oxygen flowrates. The reduced ASU compression power is due to 40% of the ASU air supply taken from the compressor of the gas turbine that is more efficient. The extraction of air from the compressor leads to a marginal decrease in the gas turbine power generated; however, this is not observed in scenario 3. This is because the nitrogen injected into the gas turbine replaces the loss in mass due to air extraction. From Table 6.7, it is observed that the oxygen to coal ratio for scenarios 2 and 3 are higher than that of the base case. This contrasts with what was observed when the objective function of the optimization is the CGE of the gasifier. The reason for this observation is that while the CGE of a gasifier is dependent on the composition and flowrate of the fuel-gas, the thermal efficiency of the IGCC plant depends on the composition, flowrate, and temperature of the fuel-gas. Hence, the high oxygen rate keeps the high temperature of the fuel-gas. From Table 6.7, it is observed that both scenarios 2 and 3 consume a higher amount of steam compared to the base case. High steam to coal ratio improves the gasifier performance (Ju and Lee, 2017). The increase in oxygen and steam flowrates leads to an increase in the fuel-gas flowrate.

Table 6.6. Summary of the optimization results for the synthesis of an optimal IGCC plant 1

	Base case	**Scenario 2**	**Scenario 3**
Net IGCC efficiency (% LHV)	45.6	48.7	50.6
% increase	-	6.79	10.96
Net power output (MW)	406.6	434.5	451.3
Gas turbine power (MW)	277	291.9	291.4
Steam turbine power (MW)	164.6	179.5	185
Gross power generated (MW)	441.6	471.4	476.3
ASU compression power demand (MW)	30.7	32.3	19.5
Gasification power demand (MW)	2.9	3	3
HRSG pumping power (MW)	1.4	1.6	1.6
Total auxiliary power demand	35	37	25

Table 6.7. Optimal gasifier and ASU-gas turbine parameters for an IGCC plant with a dry-fed gasifier

	Base case	**Scenario 2**	**Scenario 3**
(a) Gasifier properties			
Oxygen: Coal ratio	0.8	0.84	0.85
Steam: Coal ratio	0.04	0.12	0.14
$V_{Gasifier}$ (m^3)		9.15	6.03
(b) ASU-gas turbine			
θ_{N_2}	0	0	0.64
$\theta_{Air,ASU}$	0	0	0.40

This offsets any loss in syngas heating value caused by an increase in oxygen flowrate. Figures 6.2 and 6.3 show the optimal IGCC flowsheet for scenarios 2 and 3 respectively. Scenarios 2 and 3 have the same optimal gasifier design which is a CSTR of volume followed by a PFR. However, they do have different volumes. It must be stated that the HRSG in Figures 6.2 and 6.3 are identical to that of Figure 6.1. However, the diagram is simplified to prevent the crowding of the flowsheet. Figure 6.3 shows the optimal gasifier design for the IGCC plant is similar to the optimal of the standalone gasifier under Section 4.2.1 The major difference is that the optimal volume for the IGCC plant is smaller than the optimal volume of the standalone gasifier in Section 4.2.1. This is due to the reduced effect of the gasifier volume on the objective function as one moves from the standalone gasifier to an IGCC plant. This is due to the effect of other variables such as the operating pressures of the HRSG, the air flowrate into the gas turbine, and ASU-gas turbine integration. Even though the gasifier is the most critical unit in the IGCC plant (Lee et al., 2014), the individual variables, such as the exact volume of the gasifier, may have a less prominent effect on the efficiency of the overall plant. Hence, when the gasifier volume reaches a value where its effect on the thermal efficiency of the plant becomes negligible, the optimizer does not continue to increase the volume. This is observed in Table 6.7 where the gasifier volume total for scenario 2 is higher than that of scenario 3. This is because there are more optimization variables in scenario 3 than in scenario 2. The justification for process integration is the differences in the final designs for the three different scenarios, which are an optimised standalone gasifier, an optimised gasifier with an IGCC background, and an optimized gasifier with nitrogen injection and air extraction.

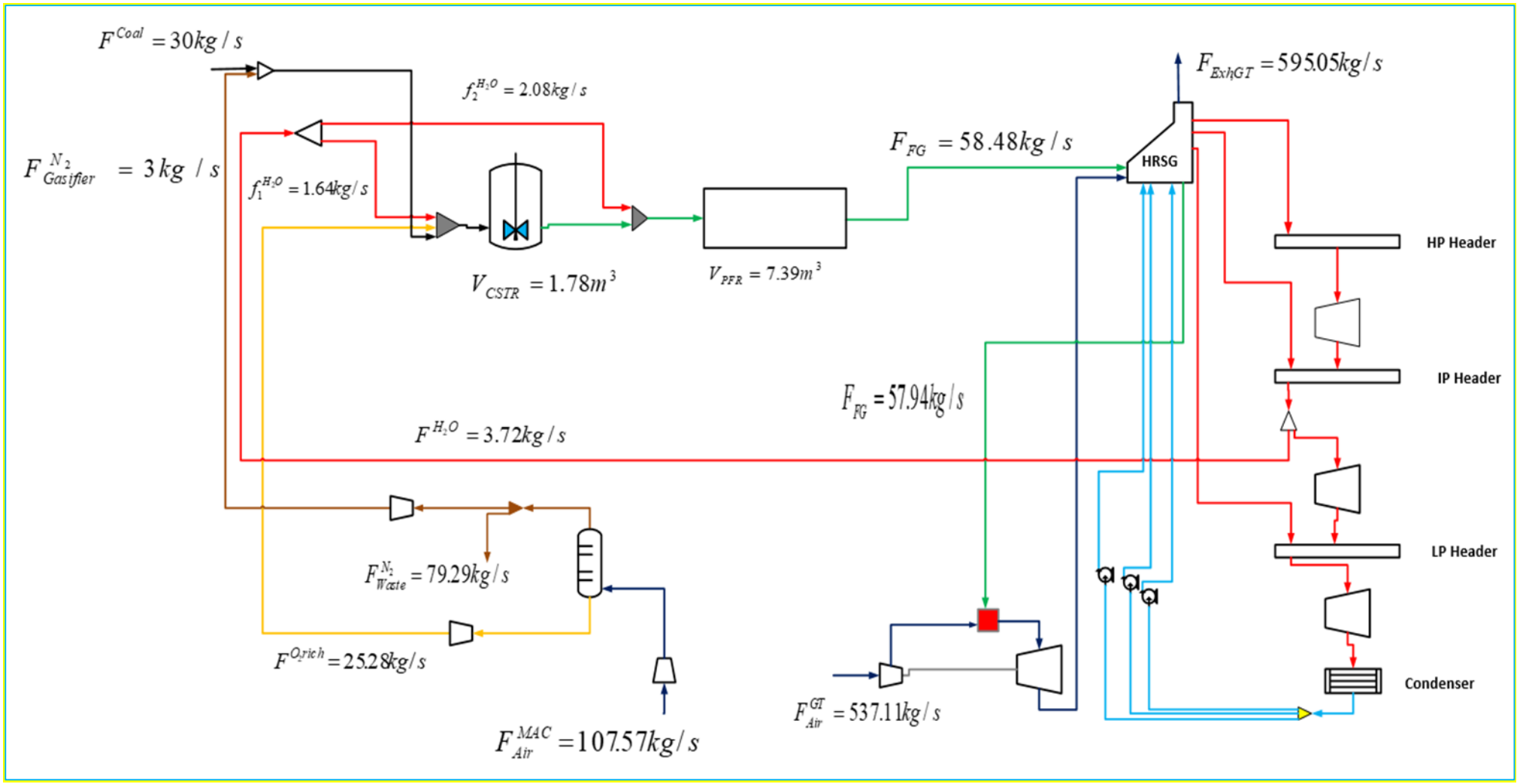

Figure 6.2. The optimal flowsheet of an IGCC plant with a dry-fed gasifier (scenario 2)

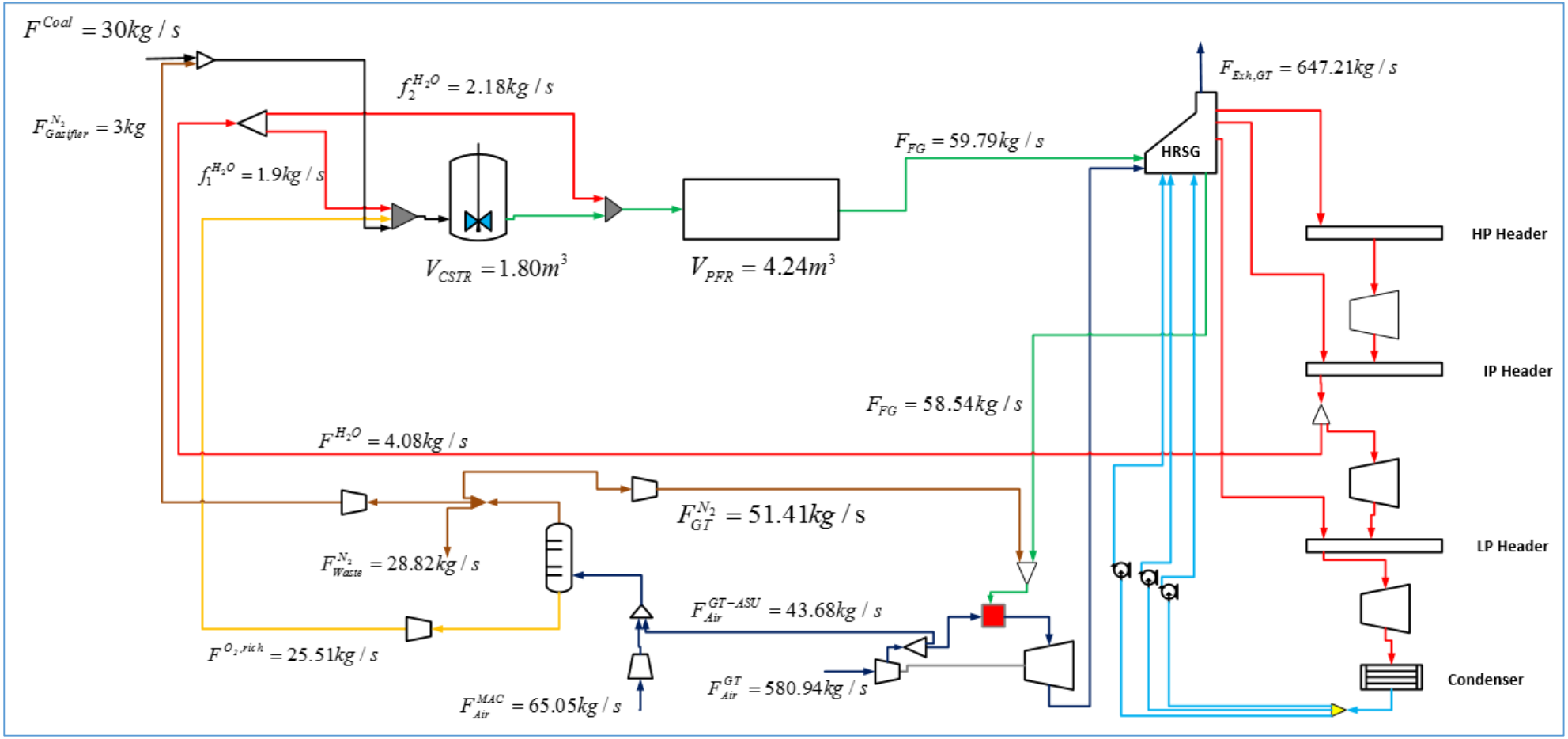

Figure 6.3. The optimal flowsheet of an IGCC plant with a dry-fed gasifier (scenario 3)

6.3 Synthesis of an optimal flowsheet of an IGCC plant with a slurry-fed gasifier

This section describes the use of the developed model in the synthesis of an optimal IGCC power plant with a slurry-fed gasifier. This plant is similar to the Tampa electric IGCC power plant (McDaniel, 2002; NETL, 2013). The main difference between this is that the Tampa plant uses a radiant heat exchanger while this example uses gas recycling to cool the fuel-gas exiting from the gasifier.

6.3.1. Simulation of the base case

The data used in the simulation of the base includes coal data, gasifier data, ASU and gas turbine data. Table 6.8 contains gasifier and coal data. The coal used is Illinois number 6 coal. The input data for the coal is taken from the study of Kasule et al. (2012); however, the HHV of the coal is taken from NETL. This case study uses the HHV of the coal instead of the LHV in the previous case study because the available information on the efficiency of the IGCC plant is on an HHV basis (NETL, 2013). The heat sources of the HRSG are the same as those stated in the previous case study.

6.3.1.1 Model output

Table 6.9 summarizes the major output of the IGCC plant with a slurry-fed gasifier. The model developed in this study predicts a net IGCC thermal efficiency of 39.6% for the base case. Compared to the value of 39% reported in the literature (NETL, 2013) for slurry-fed gasifier based-IGCC plants, there is a difference of 1.5%. This shows a close agreement between the prediction of this model and the reference value. In addition to the overall efficiency, the power output of the steam turbines makes 38% of the gross power generated. There is no breakdown data to compare in literature, but it is reasonable to assume that the energy split is similar to an IGCC plant with a dry-fed gasifier. The ASU power consumption makes up the majority of the

auxiliary power consumption, which is in agreement with the observation in literature. Based on these observations, the developed model represents an IGCC plant to a satisfactory level.

Table 6.8. Input data for gasifier

Proximate Analysis of coal		**Ultimate (daf) analysis of coal**	
VM (%)	34.99	*C* (%)	63.75
FC (%)	44.19	*H* (%)	4.50
Ash (%)	9.70	*O* (%)	6.88
MC (%)	11.12	*N* (%)	1.25
		S (%)	2.51
Coal heating properties			
HHV (MJ/kg)	27.1	T_{AF} (K)	1511
Gasifier parameters			
$w_{H_2O,Slurry}$ (slurry)	0.3	F^{O_2} (kg/s)	23.66
F^{Coal} (kg/s)	28	*P* (bar)	28

Figure 6.4 presents the flowsheet for the base case IGCC plant. The reasons for differences in flowrate between inlet and outlet streams for the various units have already been given under section 6.2.1.1 From Table 6.10, the total heat recovered by the steam from the streams equals 409.4 MW. This implies that a total steam turbine output power of 127.5 MW is equivalent to a net thermal efficiency of the steam turbine of 31%.

Table 6.9. Summary of the optimization results for the synthesis of an optimal IGCC plant 2

IGCC plant outputs		**HEN stream flowrates**	
Gas turbine power (MW)	207.5	F_{Air}^{GT} (kg/s)	400
Steam turbine power (MW)	127.5	$F_{H_2O_{(g)}}^{HP}$ (kg/s)	82.2
Gross power generated (MW)	335	$F_{H_2O_{(g)}}^{IP}$ (kg/s)	7.3
ASU compression power demand (MW)	30.3	$F_{H_2O_{(g)}}^{LP}$ (kg/s)	26
Gasification power demand (MW)	2.8	F_{BFW} (kg/s)	115.5
HRSG pumping power (MW)	1.5		
Total auxiliary power demand	34.6		
Net power output (MW)	300.4		
Net IGCC efficiency (% HHV)	39.6		

Table 6.10. HRSG HEN data

Stream data				
Stream	F_S (kg/s)	T_S (ºC)	T_T (ºC)	Δh (MW)
Fuel-gas 1	94.87	900	239	92.64
Fuel-gas 2	59.53	239	35	30.11
Gas turbine exhaust	458.51	577	100	286.65

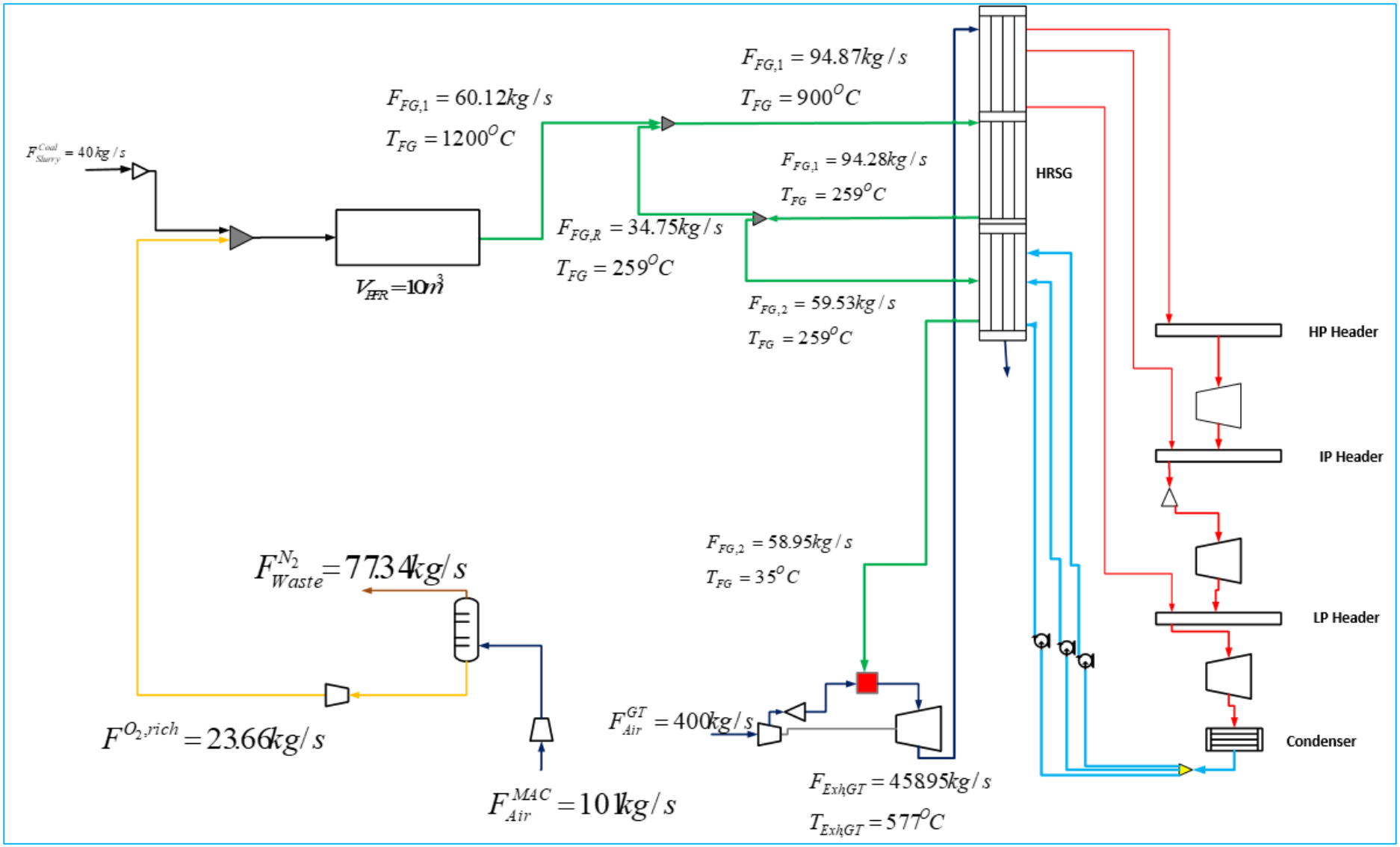

Figure 6.4. The flowsheet of a baseline IGCC plant with a slurry-fed gasifier

6.3.2. Optimization of IGCC with a slurry-fed gasifier

After the simulation of the slurry-fed IGCC plant, the optimal flowsheet is determined. The optimization parameters considered are shown in Table 6.11. This includes the flow interval of the steam and oxygen and the coal distribution ratio. Table 6.11 also shows the optimization parameters for the ASU-gas turbine parameters. These are similar to the parameters applied in the synthesis of the IGCC with a dry-fed gasifier.

Table 6.11. Optimization parameters for the synthesis of an IGCC plant with a slurry-fed gasifier

Gasifier parameters			
$F_{Max}^{O_2}$ (kg/s)	30	$F_{Min}^{O_2}$ (kg/s)	15
θ_{Max}^{Coal}	0.3	θ_{Min}^{Coal}	0
T_{Max} (K)	2400	T_{Min} (K)	1511
V_{Max} (m^3)	50	Pr (bar)	28
ASU-Gas turbine parameters			
$\theta_{N_2}^{Max}$	1	$\theta_{N_2}^{Min}$	0
$\theta_{Air,ASU}^{Max}$	0.5	$\theta_{Air,ASU}^{Min}$	0

6.3.3 Results

Table 6.12 summarizes the result of the optimization processes. The base case represents the simulation described. From Table 6.12, it is observed that both scenarios 2 and 3 lead to an improvement of the IGCC performance. The relative improvement for scenarios 2 and 3 relative to the base case are 11% and 15.8% respectively. From Table 6.13, it is observed that the oxygen to coal ratio for scenarios 2 and 3 are higher than that of the base case. This contrasts what was observed when the objective function for optimisation is the CGE of the gasifier.

Table 6.12. Summary of optimization results for the synthesis of an optimal IGCC plant 2

	Base case	**Scenario 2**	**Scenario 3**
Net IGCC efficiency (% HHV)	39.6	43.96	45.86
% increase	-	11	15.8
Net power output (MW)	300.4	333.6	348
Gas turbine power (MW)	207.5	214.9	213.3
Steam turbine power (MW)	127.5	154.6	157.9
Gross power generated (MW)	335	369.5	371.2
ASU compression power demand (MW)	30.30	31.10	18.36
Gasification power demand (MW)	2.80	2.90	2.90
HRSG pumping power (MW)	1.50	1.90	1.90
Total auxiliary power demand (MW)	34.6	35.90	23.16

The model favours a high flowrate and exit temperature of the fuel-gas. Figures 6.5 and 6.6 show the optimal IGCC flowsheet for scenarios 2 and 3 respectively. Scenarios 2 and 3 have the same optimal gasifier design, which is a PFR with a side stream; however, they have different volumes. Similar to the first case study, the optimal gasifier volume for the IGCC plant is less than the optimal volume of the standalone gasifier. The reason for this observation was discussed in section 6.2.2. The optimal ratio of the coal slurry feed to the second reactor is also lower for the gasifier design under the IGCC plant relative to the standalone gasifier

Table 6.13. Optimal gasifier and ASU-gas turbine parameters for an IGCC plant with a slurry-fed gasifier

	Base case	**Scenario 2**	**Scenario 3**
(a) Gasifier properties			
Oxygen: Coal ratio	0.85	0.87	0.87
θ^{Coal}	0.00	0.1	0.1
$V_{Gasifier}$ (m^3)		10.72	11.15
(b) ASU-gas turbine			
θ_{N_2}	0	0	0.58
$\theta_{Air,ASU}$	0	0	0.43

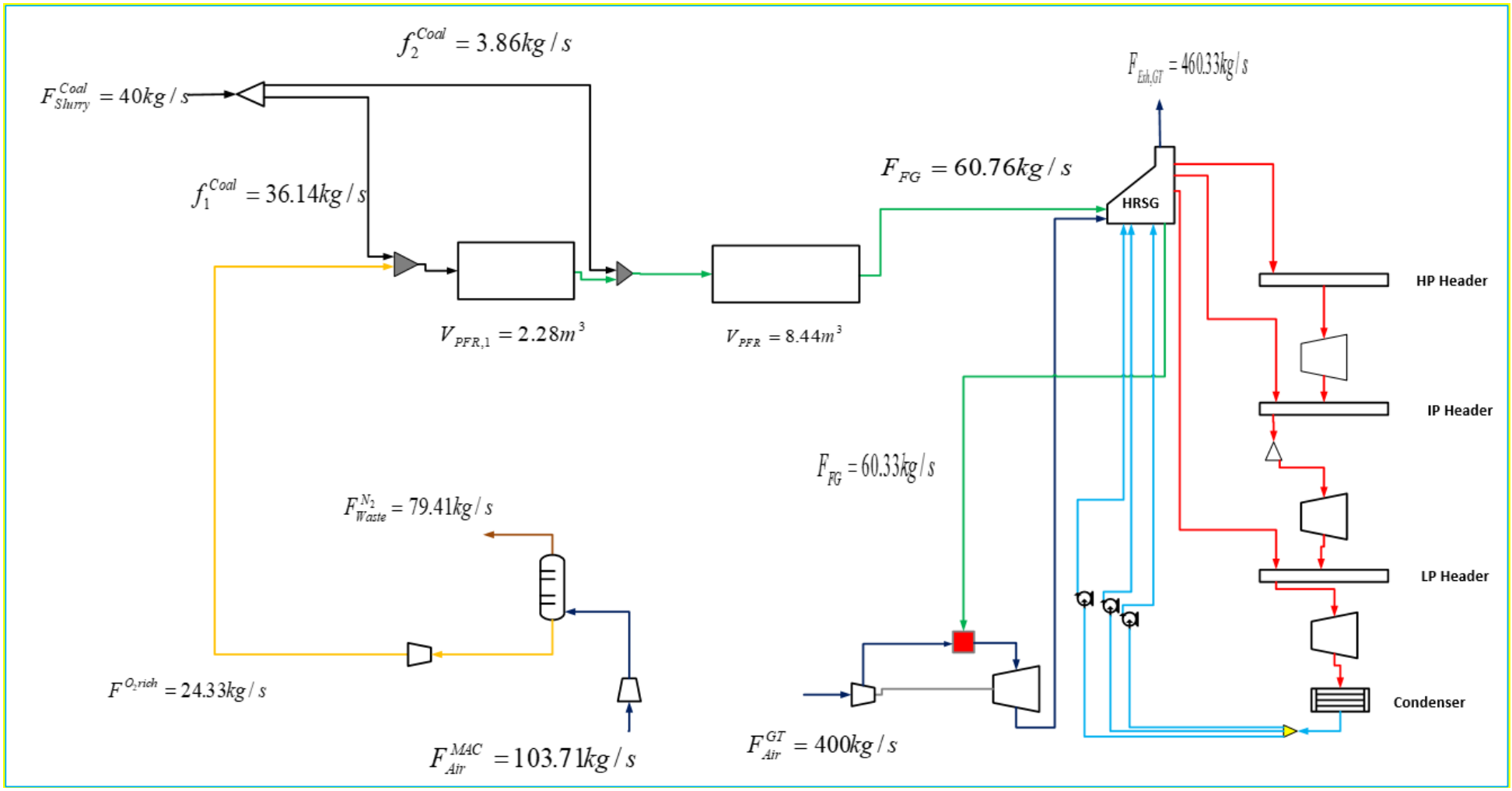

Figure 6.5. The optimal flowsheet of an IGCC plant with a slurry-fed gasifier (scenario 2)

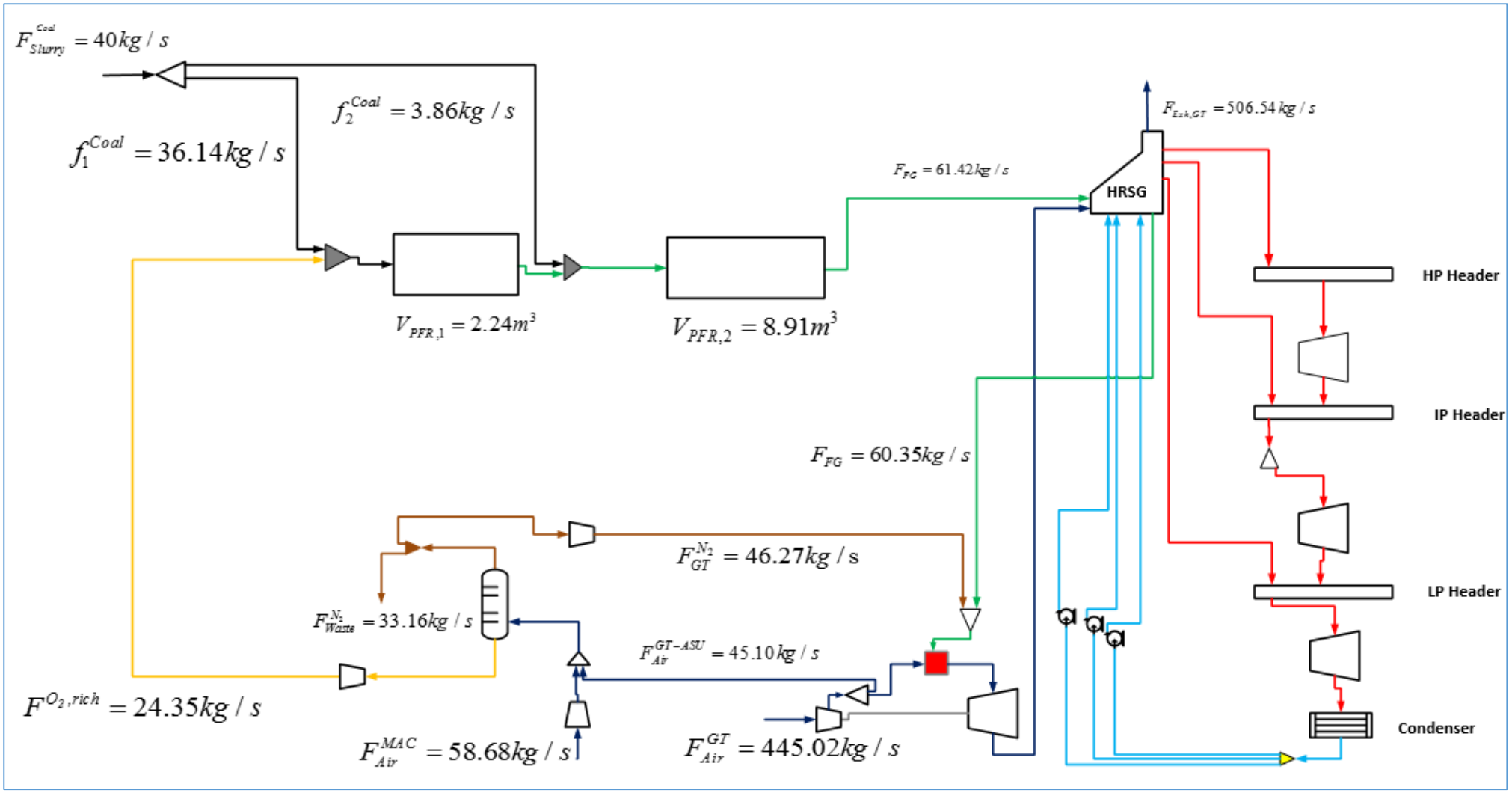

Figure 6.6. The optimal flowsheet of an IGCC plant with a slurry-fed gasifier (scenario 3)

6.4 Summary

In this chapter, the ability of the mathematical technique developed in chapter 5 to synthesize optimal IGCC flowsheet has been tested. The results show that both gasifier optimization and ASU-gas turbine integration have a positive effect on the efficiency of the IGCC plant. However, the optimization leads to gasifiers with larger volumes. This implies an increase in the capital cost of the plant.

References

Anand, A. K., Cook, C. S., Corman, J. C., Smith, A. R., 1996. New Technology Trends for Improved IGCC System Performance. *Journal of Engineering for Gas Turbines and Power*, 118, pp.732–736.

Campbell, P.E., McMullan, J.T., Williams B.C., 2000. Concept for a Competitive Coal-fired Integrated Gasification Combined Cycle Power Plant. *Fuel*, 79. pp. 1031–1040

Kasule, J. S., Turton, R., Bhattacharyya, D., Zitney, S. E., 2012. Mathematical Modelling of a Single-stage, Down-firing, Entrained-flow Gasifier. *Industrial and Engineering chemistry research*, 51, pp. 6429-6440.

Majoumerd, M.M., De S., Assadi M., Breuhaus P., 2012. An EU Initiative for Future Generation of IGCC Power Plants using Hydrogen-rich Syngas: Simulation Results for the Baseline Configuration. *Applied Energy*, 99, pp. 280-290.

Maurstad, O. 2005. An Overview of Coal based Integrated Gasification Combined Cycle (IGCC) Technology; MIT LFEE 2005-002 WP; Massachusetts Institute of Technology: Cambridge, MA

McDaniel, J., 2002. Tampa Electric Polk Power Station Integrated Gasification Combined Cycle Project. Final Technical Report. (Morgantown, WV: US Department of Energy Office of fossil energy, National Energy Technology Laboratory)

NETL. IGCC Efficiency/Performance. Available online at https://netl.doe.gov/research/Coal/energy-systems/gasification/gasifipedia/igcc-efficiency

NETL, 2013. Cost and Performance Baseline for Fossil Energy Plants Volume 1: Bituminous Coal and Natural Gas to Electricity. Available online at https://www.netl.doe.gov/sites/default/files/netl-file/BitBase_FinRep_Rev2.pdf [Accessed 1st October 2020]

NETL., 2019. Quality Guidelines for Energy System Studies: Detailed Coal Specification. Available online at https://netl.doe.gov/projects/files/QGESSDetailedCoalSpecifications_100119.pdf

Wang, M., Liu, G., Hui, C. W., 2016. Simultaneous optimization and integration of gas turbine and air. *Energy*, 116, pp. 1294-1301.

7. CONCLUSIONS AND RECOMMENDATIONS

7.1 Conclusions

The following conclusions are drawn from the study.

In the first section of this study, a novel optimization technique for the optimal synthesis of EFGs was developed. The technique included the extension of optimization variables in previous studies to include reactor configuration, reactor volume, and feed staging. The decision variables were evaluated using a superstructure made up of CSTRs and PFRs. In addition to this, the model differs from most of the earlier models due to the accurate modelling of gaseous properties such as enthalpy and density. There was also more compact modelling of the PFR compared to those previously used in most reactor synthesis studies.

The model which is based on the superstructure was applied to three examples taken from literature. The results from the optimization were compared to two scenarios. The base case or scenario 1 was a standalone PFR. Scenario 2 was fixed reactor configuration varying feed conditions.

The first example studied was the optimal synthesis and design of a dry, nitrogen-fed EFG with the CGE as the objective function. After the optimisation was performed, an improvement of 6% and 3.1%, relative to the base case and scenario 2 respectively was achieved. The second example under this section was the synthesis and design of a dry, carbon dioxide-fed gasifier. The objective function of this example was the higher heating value of the fuel-gas. The results showed an improvement of 6.2% and 2% in the objective function relative to the base case and scenario 2 respectively. The third and final example under this section was the synthesis and design of a slurry-fed gasifier. The objective function of this example was the lower heating value of the syngas. After the optimization was performed, there was a 13.3% and 8.5% improvement in the objective function relative to the base case and scenario 2 respectively.

In the second section of this study, the developed reactor superstructure model was integrated into an IGCC framework. The model based on the superstructure was applied to two examples namely an IGCC with a dry-fed gasifier and one with a slurry-fed gasifier. The objective function for both studies was the thermal efficiency of the IGCC. In each of these examples, 3 scenarios were explored. Scenario 1 is a baseline IGCC plant. Scenario 2 is an optimization of the gasifier with a background IGCC process. Scenario 3 is a superstructure that optimizes the gasifier design, the degree of nitrogen injection, and the extent of air extraction.

In the first example, improvements of 6.79% and 10.96% in the objective function relative to scenario 1 were achieved for scenarios 2 and 3, respectively. In the second example improvements of 11% and 15.8% in the objective function relative to scenario 1 were achieved for scenarios 2 and 3 respectively.

These results show that superstructure optimization leads to an efficiency increase of the IGCC plant.

7.2 Recommendations

The recommendations made are aimed at improving the generality of the results and to help in the application of the results emanating from this study to practical situations. Based on these goals, the following recommendations are made.

7.2.1 Developing coal specific kinetics

In this study, the same kinetic data were used for the different kinds of coal. It seems unrealistic that the char from different kinds of coal will have the same reactivity. It is recommended that although the same gasification model can be used for different coals, the differences in char reactivity can be accounted for by determining the reaction rate constants for the specific coal to be used. Since the output of the optimization process is hugely dependant on the kinetic data

used, it would be prudent to use accurate values if the purpose is to implement the results of the optimization. This would lead to more realistic designs.

7.2.2 Catering for the effect uncertainties on design

The use of kinetic data is the main source of uncertainties in the reactor synthesis model. These uncertainties result from the wide variation in the Arrhenius constant and the activation energy of the homogeneous reactions. Hence, it is recommended that a reactor synthesis technique is developed accounting for the uncertainty in the kinetic data.

7.2.3 Developing a detailed design technique

A thorough design of an EFG includes details such as reactor geometry, number and type of injectors, and the direction of flow. The technique presented in this study represents the first step in designing an optimal EFG. However, there must be a comprehensive technique, which builds on the preliminary optimal design. This technique must provide details on a final EFG such as length to diameter ratio, shape and orientation of reactor, three-dimensional temperature distribution, and slag development profile. This will provide a blueprint for the implementation of optimal design.

7.2.4 Performance of economic optimization

The two examples studied in chapter 6 showed that the development of an optimal IGCC flowsheet in scenario 3 leads to an increase of 10.96% and 15.8% in the objective function relative to scenario 1 for examples 1 and 2 respectively. However, in both case studies, the results showed that this improvement is achieved at the expense of increased gasifier volume. An increase in gasifier volume leads to an increased capital cost. Hence an optimization with the profit as the objective function is recommended.